Powering up Industry

Optimizing Heat Pump Deployment in the context of the Energy Transition

de Raad, B.W.

DOI
10.4233/uuid:2ab3c2ad-b5f0-45f7-b2a8-fed41152c647

Publication date
2025

Document Version
Final published version

Citation (APA)
de Raad, B. W. (2025). *Powering up Industry: Optimizing Heat Pump Deployment in the context of the Energy Transition.* [Dissertation (TU Delft), Delft University of Technology].
https://doi.org/10.4233/uuid:2ab3c2ad-b5f0-45f7-b2a8-fed41152c647

Important note
To cite this publication, please use the final published version (if applicable).
Please check the document version above.

POWERING UP INDUSTRY

OPTIMIZING HEAT PUMP DEPLOYMENT IN THE CONTEXT OF THE ENERGY TRANSITION

BRENDON DE RAAD

Powering up Industry
Optimizing Heat Pump Deployment in the context of the Energy Transition

Dissertation

for the purpose of obtaining the degree of doctor
at Delft University of Technology
by the authority of the Rector Magnificus,
prof. dr. ir. T.H.J.J. van der Hagen, Chair of the Board for Doctorates,
to be defended publicly on
Tuesday, 16 September 2025 at 12.30 o'clock

by

Brendon William DE RAAD

Master of Science in Sustainable Energy Technology,
Delft University of Technology, Netherlands
born in Rotterdam, Netherlands

This dissertation has been approved by the promotors.

Composition of the doctoral committee:

Rector Magnificus,	chairperson
prof. dr. ir. C.A. Ramirez Ramirez	Delft University of Technology, promotor
dr. ir. L. Stougie	Delft University of Technology, copromotor
dr. ir. M. van Lieshout	Rotterdam University of Applied Sciences, external advisor

Independent members:

prof. dr. ir. A.A. Kiss	Delft University of Technology
prof. dr. ir. S.A. Klein	Delft University of Technology
prof. dr. ir. D.M.J. Smeulders	Eindhoven University of Technology
dr. ir. B. Zühlsdorf	Danish Technological Institute
prof. dr. ir. W. de Jong	Delft University of Technology, reserve member

This research was partially funded by the Dutch Government Office for Enterprising (RVO) within the framework of the Mission-driven Research, Development, and Innovation funds (MOOI) under the project title: “The Heat is On” under the lead of the Dutch Institute for Sustainable Process Industry (ISPT).

Printed by: Mediacenter Rotterdam bv

Cover by: Mediacenter Rotterdam bv

ISBN 978-90-9040568-1

An electronic version of this dissertation is available at https://repository.tudelft.nl/

Summary

The European Union aims to reduce greenhouse gas (GHG) emissions with at least 55% by 2030 and become climate-neutral in 2050. Industrial companies play a key role in achieving these targets as they are responsible for about 30% of European GHG emissions. However, despite years of optimization, the energy-intensive industry lags behind other sectors in its decarbonization efforts. Approximately 60% of the industry's GHG emissions result from burning fossil fuels to heating requirements. Reducing heat-related emissions is therefore a promising route to decarbonize the industrial sector. Heat pumps that recycle waste heat back into the process offer a promising solution for decarbonizing industrial heat, as they increase energy efficiency and enable the switch to low-carbon energy carriers. However, the adoption of heat pumps in the industrial sector has been limited, particularly for applications above 100 °C, due to the complexity of identifying the process connections and economically viable heat pump solutions.

In this research, design methods are developed to support the deployment of heat pump solutions in a transitioning industrial sector. These methods assess the impact of both technical changes to the production process and the heat pump configuration, as well as changes in energy prices and technology cost on the techno-economic viability of an industrial heat pump. Consequently, the main research question is:

How to identify optimal techno-economic heat pump solutions for industrial processes in the context of the energy transition?

To answer this question, the following sub-questions have been formulated and answered:

Sub-question 1: How does the deployment sequence of a heat pump and other industrial CO_2 mitigation measures influence their combined CO_2 reduction potential?

Current decarbonization pathways often assume that interactions between mitigation measures are covered by conservative estimates and ballpark figures. However, bottom-up verification assessments indicate that this approach may be inadequate for heat integration measures.

In this work, the impact of the deployment sequence of CO_2-mitigation measures was explored by studying the heat integration in plausible future plant layouts of a biodiesel production process. These layouts were developed based on a literature review of relevant CO_2-mitigation measures with a Technology Readiness Level (TRL) of at least 8. Consistent energy and mass balances were constructed for each layout and used in a pinch analysis to estimate the performance of a heat pump. All possible sequence variations of the deployment were considered to assess their effects on the combined CO_2 reduction potential.

In the case study, the deployment sequence achieving the highest CO_2 reduction only reaches 58% of the expected combined reductions. Conversely, the same components in a different order result in an infeasible solution. Thus, the deployment sequence significantly impacts the combined CO_2 reduction potential of technologies when considering heat integration measures. The sequence can prevent other technologies from being effective, reduce the effectiveness of existing processes, or create new opportunities for future technologies.

Research question 2: How to identify CO_2-mitigation measures that improve the performance of an already installed heat pump?

Heat pumps can reduce heating requirements by recycling low-temperature surplus (waste) heat back into the process. This is effective when a heat pump operates across the pinch point, i.e. the intersection between the region with a net heat demand and a net heat surplus. However, changes to the process due to the deployment of other CO_2 mitigation measures might affect the location of the pinch point and therefore the performance of the heat pump.

The impact of process changes on the location of the pinch point and the performance of the heat pump was studied using Process Change Analysis. In this approach, heat pump connections were extracted from the rest of the (background) process to study how those streams relate. By combining Process Change Analysis with exergy analysis to form the Split-Exergy Grand Composite Curve, the impact of deploying CO_2-mitigation measures on the heat pump's work targets could be directly assessed.

The Split-Exergy Grand Composite Curve was applied to case studies of a biodiesel production plant and a vinyl chloride monomer purification process. The results show that the heat pump's performance in a biodiesel production plant is limited by its connections being above the pinch point of the background process. Replacing the wet water washing column with a membrane separation unit improves the plant-level coefficient of performance (COP) of the heat pump from 4.0 to 4.1, whilst reducing net heat requirements from 0.9 MW to 0.3 MW. Demonstrating the effectiveness of the Split-Exergy Grand Composite Curve in identifying CO_2 reduction measures and improving the performance of an already installed heat pump.

Research question 3: How to identify the optimal techno-economic heat pump configuration in case of high temperature lifts?

Literatures mentions over 70 different heat pump configurations that aim to minimize the irreversibilities that cause the subcritical single-stage (SS) cycle to become uneconomical at higher temperature lifts. In this study, both energy and exergy-based methods are used to identify the most cost effective option for a steam-generating heat pump. The benchmark of approaches shows that the results of the exergy analysis steered towards economically viable design improvements, whereas these did not logically follow from the energy analysis.

The potential for improvement depends on the required sink temperature and the temperature lift. Mappings of decline rates in exergy efficiency on a component-level were made to explain these differences and compare heat pumps on a cycle-level. Advanced exergy analysis showed that the component-level exergy destruction became increasingly endogenous with higher temperatures and temperature lifts.

At moderately high heat sink temperatures (i.e., 100-130 °C) highly efficient cycles like the two-stage compression and a flash vessel cycle are preferred over less efficient closed cycles, despite their high investment cost. However, when a heat source meets the minimal pressure requirement for an open cycle i.e., a mechanical vapor recompressor (MVR), the reduction in capital expenses outweighs the efficiency gains. When the heat source cannot directly be used to produce steam, but heat is required at high sink temperatures (i.e., > 130 °C), an MVR on top of an single stage subcritical cycle producing steam at 80 °C shows a marginally better economic performance than the closed cycle with two-stage compression and a flash vessel, under the assumed equipment cost and energy prices. However, the optimal configuration is sensitive to these cost assumptions and the temperature at which another heat pump configuration is preferred easily changes. Yet, exergy-based cost minimization together with the exergy destruction curves provide an effective tool to assess trade-offs between reductions in

operational cost from energy efficiency measures and the cost of additional investments.

Research question 4: How do energy prices and investment costs affect the deployment of heat pumps and other power-to-heat and storage technologies in the electrification of utility systems?

Heat pumps can be combined with other power-to-heat and storage technologies to maximize economic benefits from fluctuating renewable energy sources. A mixed integer linear programming model with direct electricity-to-heat conversion, indirect electricity-to-heat conversion via hydrogen, and electrification by upgrading waste heat and thermal and electrical storage technologies is used to minimize the total annual cost of a utility system for a process with highly volatile demand.

The results of the model show that electrification of existing utility systems is economically viable under the considered energy and equipment prices, though highly sensitive to their values. The results show that high and stable electricity prices favor the installation of heat pumps, while high price variance and lower electricity prices make electric boilers and thermal energy storage more attractive.

Overall, energy prices and other cost estimates play a crucial role in the sizing and operation of heat pumps and other power-to-heat and storage technologies. However, the modeling approach presented allows the qualification of economic tipping points.

Concluding, the following three steps are needed for the identification of the optimal techno-economic heat pump solution in an industrial process in the context of the energy transition:

Step 1: Assess the Relation to Other Process Changes Examine how the deployment sequence of heat pumps and other CO_2-reduction technologies either enhance or hinder their combined effectiveness. Use Process Change Analysis and the Split-Exergy Grand Composite Curve to visualize the relationship between the pinch of the background process and the heat pump connections, as well as the heat pump's minimal work requirements.

Step 2: Optimize Heat Pump Configuration Use exergy-based cost minimization to identify necessary improvements based on the cost of exergy destruction by specific components. Trends in component and cycle-level exergy destruction can be used to identify interesting configurations for a specified source and sink temperature and advanced exergy analysis can be used to further detail the origin of losses.

Step 3: Consider fluctuating energy prices and technology cost Determine the optimal sizing and operation of heat pumps and other power-to-heat technologies under the influence of fluctuating energy prices and assess the robustness of the identified utility system to changes in the technology cost.

Future research should focus on developing a fourth step that aids in identifying the optimal level of process integration for a heat pump when taking into account fluctuating energy prices, grid transport capacity, grid emission factors, and part-load efficiencies in order to explore the role of low-cost heat pumps as a peak technology.

Contents

1. Introduction

Immediate action is required to mitigate the impacts of climate change [1]. The enhanced greenhouse effect, driven by anthropogenic greenhouse gas (GHG) emissions, had increased the global average atmospheric temperature in 2023 by 1.48 °C since the 1850-1900 preindustrial level [2]. This increase has already caused significant damage to health, livelihoods, food security, water supply, human security, and economic growth [1]. To limit further harm, GHG emissions have to be reduced significantly [1]. In response, the European Union adopted a set of policies to cut European GHG emissions by at least 55% by 2030 and aims to become the first climate-neutral continent in 2050 [3]. Industry plays a crucial role in achieving these targets, as it accounted for about 30% of European GHG emissions in 2022, with CO_2 making up for 75% of emissions [4, 5]. Therefore, industrial companies must invest in CO_2-mitigating technologies to comply with regulations while maintaining their economic viability.

This introduction outlines the need for CO_2 emission reduction in the industrial sector and explains our focus on industrial heat pumps to achieve this goal. Section 1.1 discusses current CO_2 emissions from industry, the role of heating requirements, the potential of heat pumps to reduce these emissions, and the necessary steps to achieve these reductions. Section 1.2 presents the research objectives and questions of this thesis. Section 1.3 details the research approach and section 1.4 provides an outline of the dissertation.

1 Background and motivation

Industrial GHG emissions are largely caused by energy-intensive processes such as crude oil refining, steam cracking, ammonia production, and the manufacturing of materials like cement, bricks, glass, and paper [6]. Despite years of optimization, the energy-intensive industry lags behind other sectors in decarbonization efforts [7]. This is in part due to its large variety of processes [8, 9]. However, close to 80% of the industry's GHG emissions restult from burning fossil fuels to meet power (~25%) and heating (~75%) requirements, as presented in Fig. 1 [6, 10]. Reducing heat-related emissions is therefore a crucial route to decarbonizing the industrial sector [11].

Heat is required by industrial systems to increase their thermal and internal energy to enable process operations. An increase in internal energy changes the system's dynamics on the molecular and sub-molecular levels [12]. These changes alter the physical properties of a substance due to, for example, a phase change or a reaction with other substances [13]. The disordered microscopic nature of thermal energy is randomly distributed throughout a substance, which sets it apart from macroscopic forms of energy, like kinetic or potential energy, where on a macroscopic level the entire system behaves compared to one reference frame. The disorderedness of thermal energy, i.e. entropy, means that not all energy is available on a macroscopic level and that a measure of quality has to be asserted to it to reflect its usability. This property is known as temperature [12].

Chemical reactions require a certain temperature to commence and demand or release an amount of heat during the reaction. A chemical process usually consists of several chemical reactions carried out in a reactor followed by separation steps to bring a product to specification. During these processes, heat is not only added but excess heat is also removed. This excess heat is commonly referred to as waste heat and can be used to drive other processes if its temperature is high enough. Utilizing waste heat streams is called heat integration and together with advancements in process equipment can increase the energy efficiency of a process, i.e. the amount of product produced from a certain quantity of energy [14]. Increasing energy efficiency is the main strategy to reduce heat-related CO_2 emissions together with switching to low-carbon energy carriers [9, 15-17].

Switching to low-carbon energy carriers is increasingly feasible due to the significant growth in renewable energy technologies and the emergence of power-to-heat technologies [17, 18]. Power-to-heat technologies convert electrical power into heat in various ways: directly, through electric boilers; indirectly, by first producing an intermediate energy carrier like hydrogen; or by enhancing the temperature of waste heat using electricity [19, 20]. In the latter case, mechanical heat pumps mix low-temperature, high-entropy, heat with, entropy-free, (renewable) electricity to elevate the temperature of waste heat, as depicted in Fig. 2 [21]. This method increases the energy efficiency of a process whilst enabling a switch to a low-carbon energy carrier, and is therefore a preferred solution.

In recent years, research activities on heat pumps have increased and new technologies have been brought to the market to foster the adoption of heat pumps by industry [22-24]. However, implementing this technology in practice is challenging, primarily due to the difficulty of finding an economically viable heat pump solution [23]. This challenge arises not only from the complexities of identifying appropriate process connections but also from configuring the heat pump itself to achieve both technical feasibility and economic viability [23, 25-31].

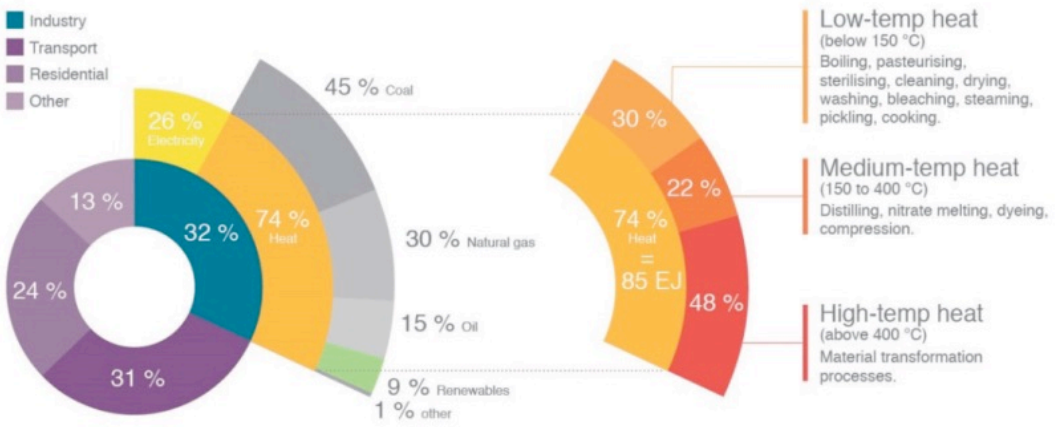

Figure 1 *Share and breakdown of industrial heat demand– Source: IEA, 2017 Renewable Energy for industry [4]*

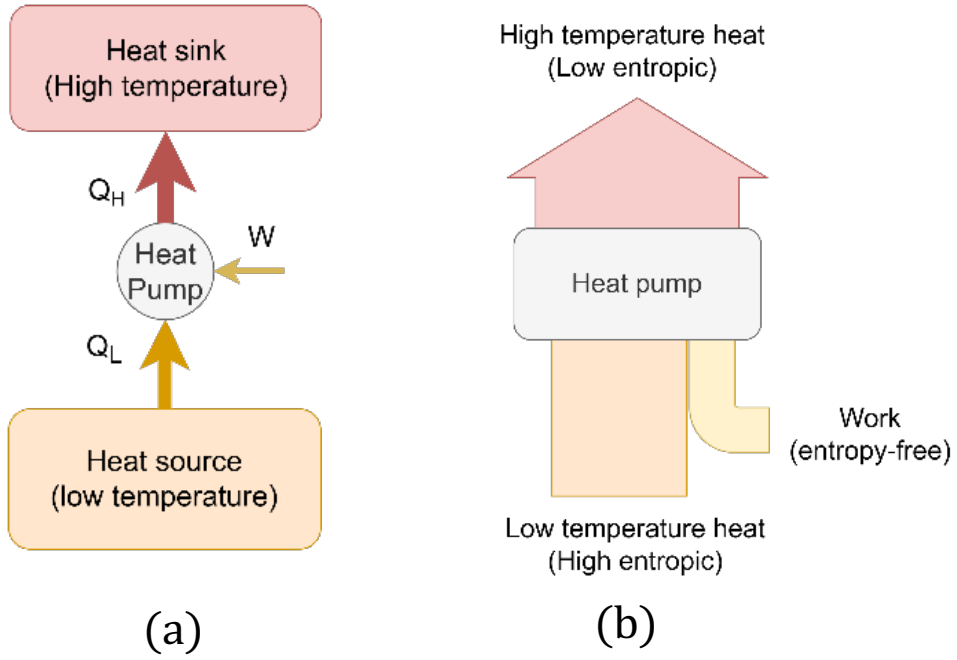

Figure 2 *Heat flows from a theoretical heat pump*
a*. a heat pump process where work (W) is used to lift heat (Q_L) from a low temperature heat source to aa high temperature heat sink by forming high temperature heat (Q_H).*
b*. a Sankey diagram of a heat pump.*

In a process, economically viable heat pump connections can be identified by using pinch analysis [14]. Pinch analysis was originally developed to optimize the heat integration of complex processes by aggregating all heating and cooling requirements in their respective composite curve, as in Fig 3.a [14]. The method helps to identify the heat integration bottleneck, i.e. the pinch point, that separates the process into a region with a net heat requirement and a region with a net heat demand, as shown in Fig. 3.b [14]. Townsend and Linnhoff [32, 33] showed that a heat pump can only reduce the heating requirements when it connects these two regions (Fig. 3.c). However, the location of the pinch point can change with the introduction of CO_2 mitigation measures and potentially reduce the effectiveness of the heat pump, as depicted in Fig. 3.d [34]. This complicates the identification of economically feasible heat pump solutions as it is unclear which technologies can effectively be placed alongside a heat pump and how their deployment sequence affects their combined CO_2 reduction. Hence, design tools are needed at a pre-feasibility stage to assess the impact a combined deployment.

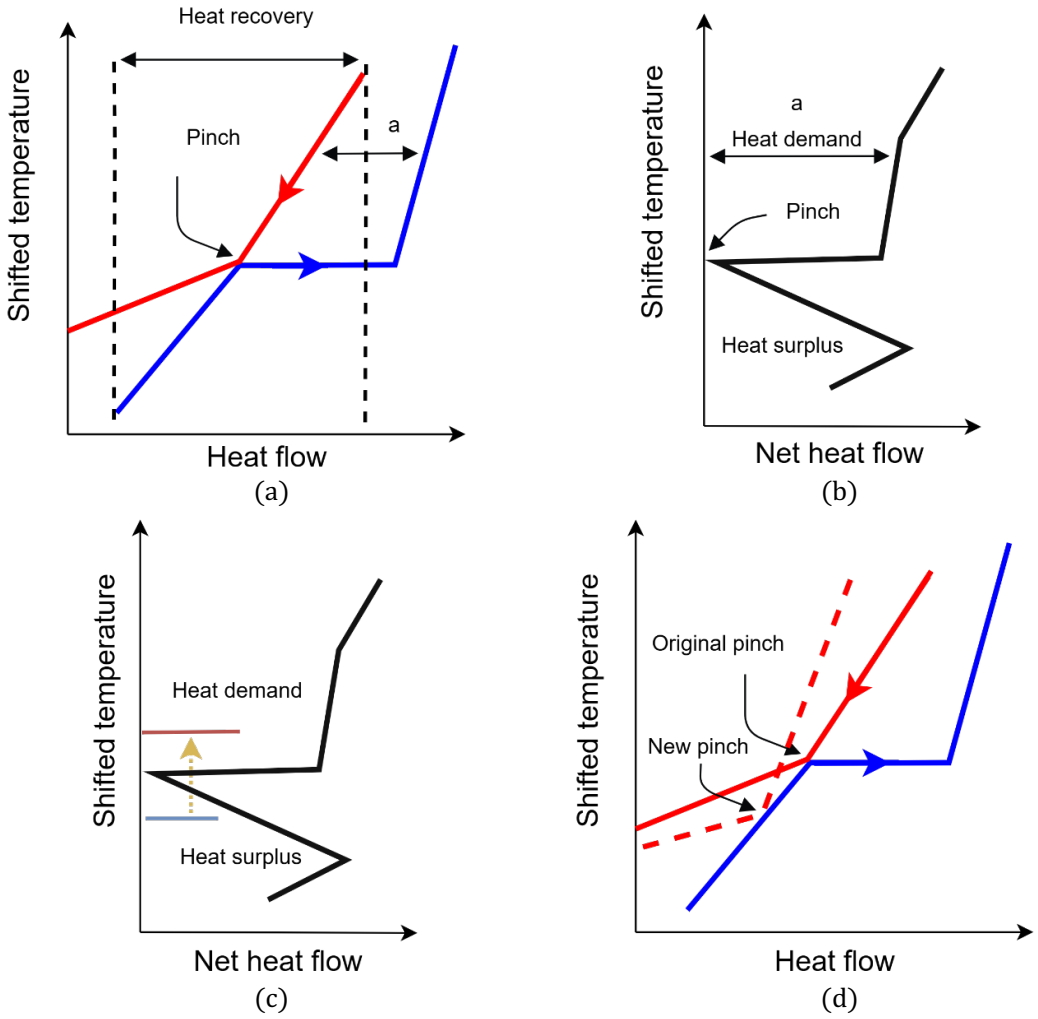

Figure 3 *Pinch analysis as a basis for heat integration;*
a. *Hot (red) and cold (blue) composite curve of a process;*
b. *Grand composite curve with net heat requirements at each temperature;*
c. *Appropriate placement of a heat pump connecting the heat surplus below the pinch to the heat demand above it, and*
d. *A shifted pinch point due to process changes.*

In addition to the selection of the heat pump connections to the process, the heat pump's configuration (i.e. its components in a specific order, as presented in Fig.4.a), is also an important factor in its economic viability. Recent literature reviews by Arpagaus et al. [23], Jiang et al. [35], and Adamson et al. [22] identify more than 70 different heat pump layouts. These layouts result from adding components to a basic heat pump layout (Fig. 4.b) and or changing the work domain of the cycle with respect to the critical point of the working media (i.e., subcritical, transcritical, or supercritical). A study by Farshi et al. [36] has shown that the loss in thermodynamic efficiency with increasing temperature lift differs between different types of heat pump cycles. This effect is also highlighted by a benchmark study by Bless et al. [37], who compared different steam-generating heat pumps with a similar Coefficient of Performance (COP), i.e. the ratio between the heat delivered by and the work added to the heat pump,

according to the literature. They observed that the COP differed by a factor of two when applied to the same case. To help select the economically preferred heat pump configuration for a specified application, additional insights are needed into why these pressure changes cause these losses and how they develop with the temperature of the heat sink and the temperature lift.

Switching to low-carbon energy carriers further complicates the identification of heat pump solutions, due to the inherent fluctuations of renewable energy sources such as wind and solar. High shares of variable renewable energy in energy systems reduce the electricity spot price when the supply of these sources is most abundant and increase it when the supply is scarce [19]. As the penetration of renewable energy sources increases, electricity price fluctuations may become more and more pronounced when there is a mismatch between availability and demand [38]. Capitalizing on this volatility by purchasing electricity at lower or even negative prices and storing it for later use can significantly improve the business case for a heat pump solution [38, 39]. However, other (direct and indirect) power-to-heat technologies with their own conversion efficiency, storage capabilities, and equipment cost also play a role. Insights are needed into the potential roles a heat pump, or other technology, can play in an integrated energy system powered by fluctuating renewable energy [23].

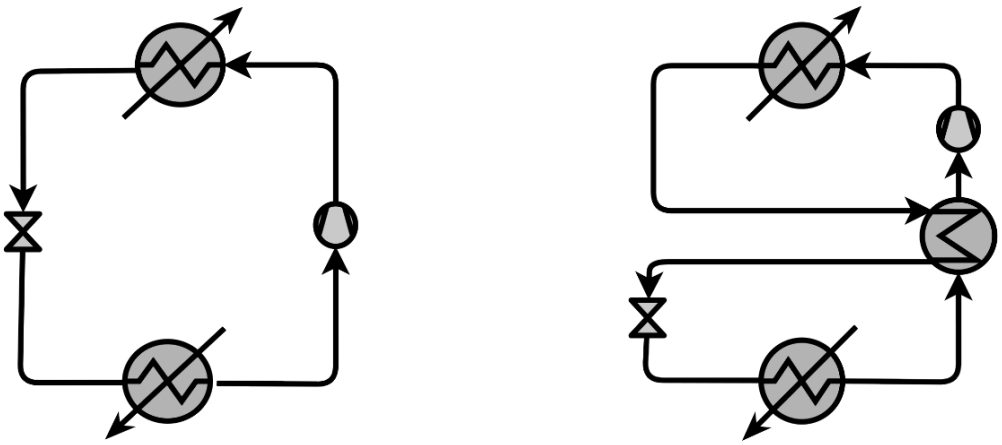

Figure 4 *Heat pump configurations;*
a. *the basic heat pump configuration for a mechanical vapour compression heat pump,*
b. *an advanced heat pump cycle with an added heat exchanger to the basic heat pump configuration*

2 Objective and research questions

The aim of this research is to develop design methods for the early stages in the design process that support the deployment of heat pump solutions in a transitioning industrial sector. This includes the impact of both technical changes to the production process and the heat pump configuration as well as changes in energy prices and equipment cost on the techno-economic viability of an industrial heat pump. Consequently, the main research question is:

How to identify optimal techno-economic heat pump solutions for industrial processes in the context of the energy transition?

To answer this question, the following research sub-questions have been formulated:

1. *How does the deployment sequence of a heat pump and other industrial CO_2 mitigation measures influence their combined CO_2 reduction potential?*
2. *How to identify CO_2 mitigation measures that improve the performance of an already installed heat pump?*
3. *How to identify the optimal techno-economic heat pump configuration in case of high temperature lifts?*
4. *How do energy prices and technology costs affect the deployment of heat pumps and other power-to-heat and storage technologies in the electrification of utility systems?*

In summary, this research introduces novel early assessment methods for integrating heat pumps in industrial processes, finding their techno-economic optimal configuration and combination with other power-to-heat and storage technologies. These methods can support industrial companies in their decisions regarding the electrification of their utility systems and their CO_2 reduction efforts, thereby contributing significantly to the EU's climate neutrality targets.

3 Research approach and outline

The research questions are clustered into three sections. In section 1, questions 1 and 2 are answered by focusses on the integration of a heat pump in a production process alongside the deployment of other technologies. Section 2 answers question 3 by delving into optimizing heat pump configurations. Section 3 discusses the electrification of industrial utility systems under fluctuating energy prices and technology cost and answers research question 4. These sections are followed by a closing section with an overview of research outcomes, limitations, overall conclusions and recommendations.

Section 1: Integrating heat pumps

Research questions 1 and 2, both related to the integration of the heat pump, are studied using two case studies: a biodiesel and a vinyl chloride monomer production process (Chapter 2). A literature review is carried out to identify which energy efficiency measures can be integrated alongside the heat pump and how these changes can be studied from a heat integration perspective. Relevant technologies are listed and ranked based on their performance. The top-ranking technologies at different process sections, or 'onion' levels (reaction, separation, heat integration, and power), are selected for deployment. Their listed performance were used to establish an energy and mass balances, which are used in a pinch analysis. The results of the pinch analysis are then used to estimate the performance of the heat pump after the deployment of the energy efficiency measures. By comparing different deployment sequences, research question 1 is answered.

The output of the literature study on energy efficiency measures is also used for studying the impact of process changes on an already installed heat pump (Chapter 3). For this study, Process Change Analysis is used to investigate how the placement of the heat pump relates to the pinch of the rest of the process. This method is combined with exergy analysis to account for the work-value of heat which makes the impact of process changes on the work target of the heat pump explicit. The resulting Split-Exergy Grand Composite Curve supports in assessing the impact of process changes on the work target of the heat pump and helps to identify process changes that do not negatively impact the performance of the already installed heat pump.

Section 2: Optimizing heat pump configurations

Research question 3 is answered by studying a steam-generating heat pump (SGHP) because of its high relevance to industry. A SGHP commonly requires a large temperature lift that renders the standard, subcritical simple cycle, uneconomical due to large irreversibilities. To solve this problem, energy efficiency measures are added to the cycle to increase its economic performance.

These energy efficiency measures are added to the section of the heat pump cycle that causes the highest operational cost. Chapter 4 compares the use of energy- and exergy-based methods for the identification of the section. Energy analysis is used as a reference because of its dominant role in literature [23, 27, 37]. Exergy-Based Cost Minimization is used to monetize the component-level exergy destruction according to the cost of additional work requirements by the compressor.

Chapter 5 explores the development and origin of thermodynamic losses in order to get insight into how to improve a cycle's performance. A set of frequently suggested steam-generating heat pump configurations in literature is investigated. Their exergo-economic cycle- and component-level performance are explored for a range of source and sink temperatures to understand how the performances change with increasing temperature lifts, sink and source temperatures. Advanced exergy analysis is used to study the origin of the thermodynamic losses. This method is based on the concept of hybrid cycles where all but one component in a configuration works reversibly to identify whether the losses are due to the performance of this component or due to the configuration of the cycle.

Section 3: Electrification of utility systems under fluctuating energy prices

The impact of fluctuating energy prices on the sizing and operation of heat pumps and other power-to-heat and storage technologies is answered by studying the electrification of the utility system of a paper mill with a variable heat demand in North-West Europe (Chapter 6). In the evaluation, direct and indirect electrification technologies, i.e. an electric boiler and hydrogen as an intermediate energy carrier, resp., as well as a heat pump are added to the existing fossil infrastructure with a connection to the electricity grid. The optimal sizing of the components of this utility system is determined by minimizing the total annual cost on a half-hourly basis, whilst keeping the installed capacities constant. This is done for different energy and technology price scenarios to investigate how it affects the technology sizing and operation. In the study, different energy price scenarios are explored where the mean electricity price, fluctuation in energy prices and the electricity-to-gas price ratio are varied. Moreover, the impact of the technology cost is also studied for these energy price scenarios by working with relatively high and low technology cost of the heat pump in respect to the other technologies.

References

[1] H. L. a. J. R. e. IPCC [Core Writing Team, "Climate Change 2023: Synthesis Report. Contribution of Working Groups I, II and III to the Sixth Assessment Report of the Intergovernmental Panel on Climate Change," IPCC, Geneva, Switzerland, 2023.

[2] ECMWF. "Global temperatures: 2023 warmest year on record, close to 1.5°C above pre-industrial level." https://climate.copernicus.eu/global-climate-highlights-2023# (accessed 11-6, 2024).

[3] D.-G. f. C. A. EU. "2030 climate targets." https://climate.ec.europa.eu/eu-action/climate-strategies-targets/2030-climate-targets_en#:~:text=In%202023%2C%20the%20EU%20adopted,climate%2Dneutral%20continent%20by%202050. (accessed 11-6, 2024).

[4] IEA, "Renewable Energy for Industry," 2017.

[5] IEA. " Emissions - Europe." https://www.iea.org/regions/europe/emissions (accessed 6-12-2024.

[6] A. Marina, S. Spoelstra, H. Zondag, and A. Wemmers, "An estimation of the European industrial heat pump market potential," *Renewable and Sustainable Energy Reviews*, vol. 139, p. 110545, 2021.

[7] P. J. Loftus, A. M. Cohen, J. C. Long, and J. D. Jenkins, "A critical review of global decarbonization scenarios: what do they tell us about feasibility?," *Wiley Interdisciplinary Reviews: Climate Change*, vol. 6, no. 1, pp. 93-112, 2015.

[8] M. Åhman and L. J. Nilsson, "Decarbonizing industry in the EU: climate, trade and industrial policy strategies," in *Decarbonization in the European Union*: Springer, 2015, pp. 92-114.

[9] J. Cresko *et al.*, "DOE Industrial Decarbonization Roadmap," USDOE Office of Energy Efficiency and Renewable Energy (EERE), 2022.

[10] *An EU Strategy on Heating and Cooling*, 2016.

[11] e. a. Niel van J., "Net-zero electrical heat: A turning point in feasibility," 2024.

[12] I. Dincer and M. A. Rosen, *Exergy: Energy, Environment and Sustainable Development*. Elsevier Science, 2020.

[13] J. M. Honig, *Thermodynamics: principles characterizing physical and chemical processes*. Academic Press, 2020.

[14] I. C. Kemp, *Pinch analysis and process integration: a user guide on process integration for the efficient use of energy*. Elsevier, 2011.

[15] M. Pisciotta *et al.*, "Current state of industrial heating and opportunities for decarbonization," *Progress in Energy and Combustion Science*, vol. 91, p. 100982, 2022.

[16] J. Rissman *et al.*, "Technologies and policies to decarbonize global industry: Review and assessment of mitigation drivers through 2070," *Applied energy*, vol. 266, p. 114848, 2020.

[17] G. P. Thiel and A. K. Stark, "To decarbonize industry, we must decarbonize heat," *Joule*, vol. 5, no. 3, pp. 531-550, 2021.

[18] IRENA, "Innovation landscape brief: Renewable power-to-heat," International Renewable Energy Agency 2019.

[19] H. Son, M. Kim, and J.-K. Kim, "Sustainable process integration of electrification technologies with industrial energy systems," *Energy*, vol. 239, p. 122060, 2022.

[20] M. Wei, C. A. McMillan, and S. de la Rue du Can, "Electrification of industry: Potential, challenges and outlook," *Current Sustainable/Renewable Energy Reports*, vol. 6, pp. 140-148, 2019.

[21] Y. A. Cengel, "Thermodynamics: an engineering approach," ed: McGraw-Hill, 2011.

[22] K.-M. Adamson *et al.*, "High-temperature and transcritical heat pump cycles and advancements: A review," *Renewable and Sustainable Energy Reviews*, vol. 167, p. 112798, 2022.

[23] C. Arpagaus, F. Bless, M. Uhlmann, J. Schiffmann, and S. S. Bertsch, "High temperature heat pumps: Market overview, state of the art, research status, refrigerants, and application potentials," *Energy*, vol. 152, pp. 985-1010, 2018.

[24] B. Zühlsdorf, "High-Temperature Heat Pumps: Task 1–Technologies. Annex 58 about High-Temperature Heat Pump," ed: Heat Pump Center c/o RISE, 2023.

[25] C. Bataille *et al.*, "A review of technology and policy deep decarbonization pathway options for making energy-intensive industry production consistent with the Paris Agreement," *Journal of Cleaner Production*, vol. 187, pp. 960-973, 2018.

[26] H. Becker, F. Marechal, and A. Vuillermoz, "Process integration and opportunities for heat pumps in industrial processes," *International Journal of Thermodynamics*, vol. 14, no. 2, pp. 59-70, 2011.

[27] C. Mateu-Royo, C. Arpagaus, A. Mota-Babiloni, J. Navarro-Esbrí, and S. S. Bertsch, "Advanced high temperature heat pump configurations using low GWP refrigerants for industrial waste heat recovery: A comprehensive study," *Energy conversion and management*, vol. 229, p. 113752, 2021.

[28] D. Olsen, Y. Abdelouadoud, P. Liem, S. Hoffmann, and B. Wellig, "Integration of Heat Pumps in Industrial Processes with Pinch Analysis," in *12th IEA Heat Pump Conference*, 2017.

[29] S. Pezzutto, G. Grilli, and S. Zambotti, "European heat pump market analysis: assessment of barriers and drivers," *International Journal of Contemporary ENERGY*, vol. 3, no. 2, 2017.

[30] B. Zuhlsdorf, "Task 1: Technologies – State of the art and ongoing developments for systems and components," in *About High Temperature Heat Pumps*, vol. 58. https://heatpumpingtechnologies.org/annex58/task1/: International Energy Agency, 20.

[31] B. Zühlsdorf, F. Bühler, M. Bantle, and B. Elmegaard, "Analysis of technologies and potentials for heat pump-based process heat supply above 150 C," *Energy Conversion and Management: X*, vol. 2, p. 100011, 2019.

[32] D. Townsend and B. Linnhoff, "Heat and power networks in process design. Part I: Criteria for placement of heat engines and heat pumps in process networks," *AIChE Journal*, vol. 29, no. 5, pp. 742-748, 1983.

[33] D. Townsend and B. Linnhoff, "Heat and power networks in process design. Part II: Design procedure for equipment selection and process matching," *AIChE Journal*, vol. 29, no. 5, pp. 748-771, 1983.

[34] P. A. Løken, "Process integration of heat pumps," *Journal of heat recovery systems*, vol. 5, no. 1, pp. 39-49, 1985.

[35] J. Jiang, B. Hu, R. Wang, N. Deng, F. Cao, and C.-C. Wang, "A review and perspective on industry high-temperature heat pumps," *Renewable and sustainable energy reviews*, vol. 161, p. 112106, 2022.

[36] L. G. Farshi, S. Khalili, and A. Mosaffa, "Thermodynamic analysis of a cascaded compression–absorption heat pump and comparison with three classes of conventional heat pumps for the waste heat recovery," *Applied Thermal Engineering*, vol. 128, pp. 282-296, 2018.

[37] F. Bless, C. Arpagaus, and S. Bertsch, "Theoretical investigation of high-temperature heat pump cycles for steam generation," in *13th IEA Heat Pump Conference, May 11-14, 2020, Jeju, Korea, postponed to 26*, 2021, pp. 1-9.

SECTION 1

INTEGRATING A HEAT PUMP IN A PRODUCTION PROCESS

CHAPTER 2

EXPLORING IMPACTS OF DEPLOYMENT SEQUENCES OF INDUSTRIAL MITIGATION MEASURES ON THEIR COMBINED CO_2 REDUCTION POTENTIAL

This chapter was originally published as B. W. de Raad, M. van Lieshout, L. Stougie, C. A. Ramirez, "Exploring impacts of deployment sequences of industrial mitigation measures on their combined CO2 reduction potential", Energy, Volume 262, Part B, 2023, 125406, DOI: https://doi.org/10.1016/j.energy.2022.125406.

Abstract

Rapid deployment of a portfolio of heat-related CO_2 mitigation measures in the industrial sector is needed to mitigate human-induced climate change. This paper explores the effect of sequencing these measures on their combined CO_2 reduction potential. In a case study, CO_2 mitigation measures are deployed throughout a biodiesel production process. The deployment of a membrane reactor, divided wall column, heat pump, and an e-boiler in several sequences showed that the combined CO_2 reduction potential is indeed dependent on the deployment sequence. Moreso, the results of the case study show that the deployment of a heat pump after the deployment of a divided wall column was technically impossible, but that the combined deployment of a membrane reactor and a divided wall column provided new heat pump possibilities which resulted in the largest combined CO_2 reduction. Though a different heat pump design was required than when starting decarbonization with a heat pump in the reference case. The results of the case study indicate that using conservative estimates gives a good enough representation of the combined reduction potential unless a heat integration measure is considered. Therefore, sequencing approaches (e.g., MACC) are not fit for the assessment of heat integration technologies.

1 Introduction

The industrial sector has to halve its CO_2 emissions by 2030 to mitigate human-induced climate change [1, 2]. Decarbonizing heat sources and implementing energy efficiency measures have the potential to reduce the sector's overall CO_2 emissions by 80% [2]. Several studies have explored the reduction potential of individual measures. For instance, Yáñez et al. [3] calculated the expected CO_2 reduction potential of 20 energy efficiency measures in the Colombian oil industry. Similarly, Hasanbeigi et al. [4] identified 23 energy efficiency improvements for the Chinese cement industry. In these studies, the combined CO_2 reduction potential is the sum of the potential of the individual measures. The impact of plausible interactions between these measures is assumed to be covered by taking conservative estimates and working with ballpark estimates [3, 5]. However, these coarse methods may be insufficient, as interactions between measures could have a severe impact [6].

A portfolio of mitigation measures is commonly not deployed simultaneously due to, among others, limited resources [7]. The sequencing of these measures is often based on a Marginal abatement cost curve (MACC), which is a well-known approach for evaluating and identifying cost-effective options [8-11]. However, this approach has some limitations. For instance, it does not consider the effects of temporal dynamics and interactions between measures [12]. As a result, incremental CO_2 reductions by a new measure might be (partially) negated. Berghout et al. [13] worked around these limitations by adding a bottom-up analysis and studied interactions between short and medium-term mitigation measures. The authors report no significant interactions between energy efficiency measures and other CO_2 reduction measures. Wiertzema et al. [14], however, found strong CO_2 emission reduction trade-offs when explicitly studying the performance of heat integration measures based on the changes in the heat integration potential.

One heat integration measure that is increasingly gaining interest in the industrial sector is a heat pump [15, 16]. This emerging high-potential waste heat technology is often among the most cost-competitive CO_2 reduction technologies and is therefore likely to be among the first to be deployed [17]. However, the performance of a heat pump is defined by the processes it is connected to [18]. These conditions may change with the deployment of other CO_2 reduction measures. Therefore, a stand-alone assessment of heat pumps is likely to give an unjust representation of its contribution to the combined CO_2 reduction potential.

This article examines how the deployment sequence of mitigation measures affects their combined CO_2 reduction potential. The emphasis is on the interaction between heat integration measures, energy efficiency measures, and measures that decarbonize heat sources. A better understanding of the impact of the deployment sequence is needed to make more realistic estimates of the combined CO_2 reduction potential in the industrial sector, identify effective deployment sequences of CO_2 mitigation measures, and avoid lock-ins that prevent further decarbonization.

2 Method

The impact of process changes on the performance of heat integration measures, such as heat pumps, was assessed by exploring future plant layouts. The approach consists of three steps: 1. exploration of future plant layouts, 2. assessment of heat pump opportunities, and 3. deployment sequence analysis.

2.1 Exploration of future plant layouts

Interactions between different types of mitigation measures were explored by dividing the plant into a reaction section, a separation section, a waste heat recovery section, and a power section (Figure 1 Onion diagram by Douglas [22] adapted to divide production plants into connected sections) [19]. CO_2 mitigation measures with a Technology Readiness Level of at least 8, in light of the approaching 2030 reduction target, were identified for each section based on a literature review.

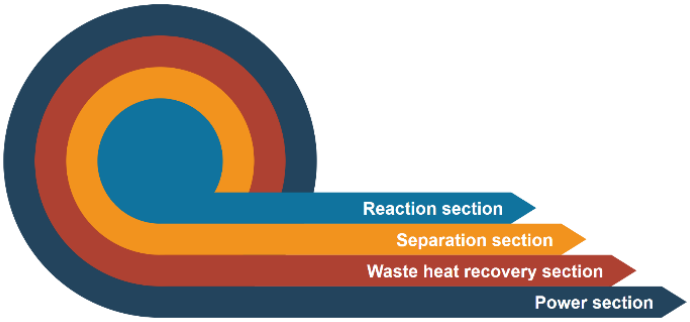

Figure 1 *Onion diagram by Douglas [22] adapted to divide production plants into connected sections*

The resulting list of CO_2 mitigation technologies was qualitatively ranked per process section. The ranking was based on the expected energy savings. A minus symbol (-) indicates an expected increase in heating requirements, a zero (0) was assigned when no significant changes are expected, while a plus symbol (+) reflects a decrease in heating requirements. The number of symbols represents the relative impact of the expected changes. The technologies with the highest individual positive impact per section were selected for the assessment. The resulting layouts enabled the assessment of the sole deployment of each technology, the combination of process improvements, the combination of each technology with a heat pump, and a combination of process improvements with a heat pump.

2.2 Assessment of heat pump opportunities

The heat pump is placed across the pinch point to effectively reduce net heating requirements [20, 21]. The pinch point was identified with the help of pinch analysis [22, 23]. In this assessment, the heat pump was coupled to the hot (in surplus of heat), and cold (in demand of heat) streams closest to the pinch, with a thermal duty of at least 10% of the total heating requirements. These streams were identified by using the PinchAnalysis software [24]. Here, the thermal requirements of the main streams (top 90%) of the process were used as input. The specific heat of the media in these streams was assumed to be constant, as the operational data showed no deviation larger than 10%. Heat integration was limited with a minimal temperature difference of 10 °C [23]. The minimal temperature driving force for the heat pump was neglected. Grand composite curves (GCC) were used to size the heat pump, as in Figure 2 Integration of a single source heat pump in a grand composite curve [20, 22, 25]. Here, heat from a cold reservoir (Q_L) is pumped to the temperature level of the high-temperature sink, where at this high-temperature heat (Q_H) is transferred to the hot sink. Here, Q_H is the sum of Q_L and the work (W) added by the heat pump.

The performance of the heat pump was expressed in the Coefficient of Performance (COP), which is calculated with COP = Q_h/W. For an ideal (Carnot) heat pump, this simplifies to $T_H/(T_H - T_L)$, where T_H is the temperature of the heat sink and $(T_H - T_L)$ the required temperature lift by the heat pump. An efficiency factor (μ) is required to calculate the non-ideal COP. A factor of 0.55 is used in this assessment, which is common for a mechanical heat pump [26, 27]

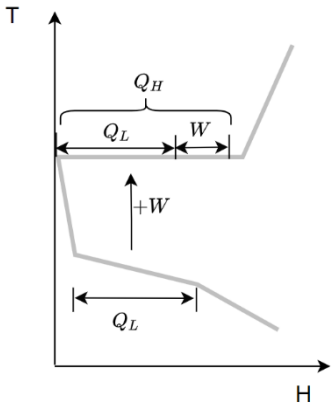

Figure 2 *Integration of a single source heat pump in a grand composite curve*

2.3 Deployment sequence analysis

All sequence variations of process changes that affect the heat integration potential are explored based on the results of the two previous steps and the conversion of heat and electricity consumption to CO_2 emissions. Process changes that did not affect the heat integration potential were exempted from this analysis for clarity of results. Emissions from heat consumption were based on a well-to-wheel emission factor of natural gas of 56,4 kg/GJ and a gas-fired boiler efficiency of 95% [28, 29]. The emissions related to electricity generation were calculated based on the expected well-to-wheel CO_2 emissions of the Dutch electricity grid, which averages at 0,569 kg/kWh between 2020 and 2029 [30]. Yearly operating hours were taken at 8760.

3 Plausible future layouts of a biodiesel production plant

The effect of the deployment sequence on the combined CO_2 reduction potential of heat integration and other CO_2 reduction measures is studied in a case study of a biodiesel production plant. This plant was selected as it represents a typical production plant in the industrial sector with moderate operational temperatures, CO_2 emissions strongly linked to heating requirements, and a relatively simple plant layout.

3.1 Process description

The most common route to produce low-carbon biodiesel is by converting oil triglycerides into fatty acid methyl esters (FAME) [31]. This conversion is commonly enabled by transesterification with methanol (molar ratio 5.5:1) and a homogeneous base catalyst (~1wt% NaOH) [32]. For this process, a plant design is available from Air Liquide, as presented in Figure 3 Plant layout of the reference case (L0) based on the Air Liquide design [32]. The top-left area is defined as the reactor section and the bottom right area is the separation section. [32, 33]. This plant layout was used as the reference case. The process starts with removing gums, phosphatides, and soaps from the crude oil in a reactor at 45 °C. Hereafter, the degummed oil is deacidified in a distillation column operating at about 240 °C. The neutralized oil is added to two cascaded continuously stirred reactors with two sedimentation tanks operating at temperatures between 50 °C and 60 °C (separators 1 and 2 in Figure 3 Plant layout of the reference case (L0) based on the Air Liquide design [32]. The top-left area is defined as the reactor section and the bottom right area is the separation section.). Here, FAME and glycerol, are separated. After a second sedimentation tank, by-products are neutralized and the FAME (<5 wt% water) is washed off. After washing, the FAME is dried to the required product quality. The excess methanol together with the washing water and contaminants are added to the glycerol-methanol mixture from the bottom of the sedimentation tanks. Methanol is recovered from this combined tank in a distillation column with a reboiler temperature of 110 °C. From the top stream, nearly pure methanol is extracted at a temperature of about 60 °C. This stream is combined with fresh methanol and catalyst before re-entering the reactor. The bottom stream, mainly glycerol and water, is dried in a series of drying columns until reaching the required product quality. The evaporated water is reused in the washing tower [31, 32, 34]. The composite curve of the process is presented in Fig. 4.

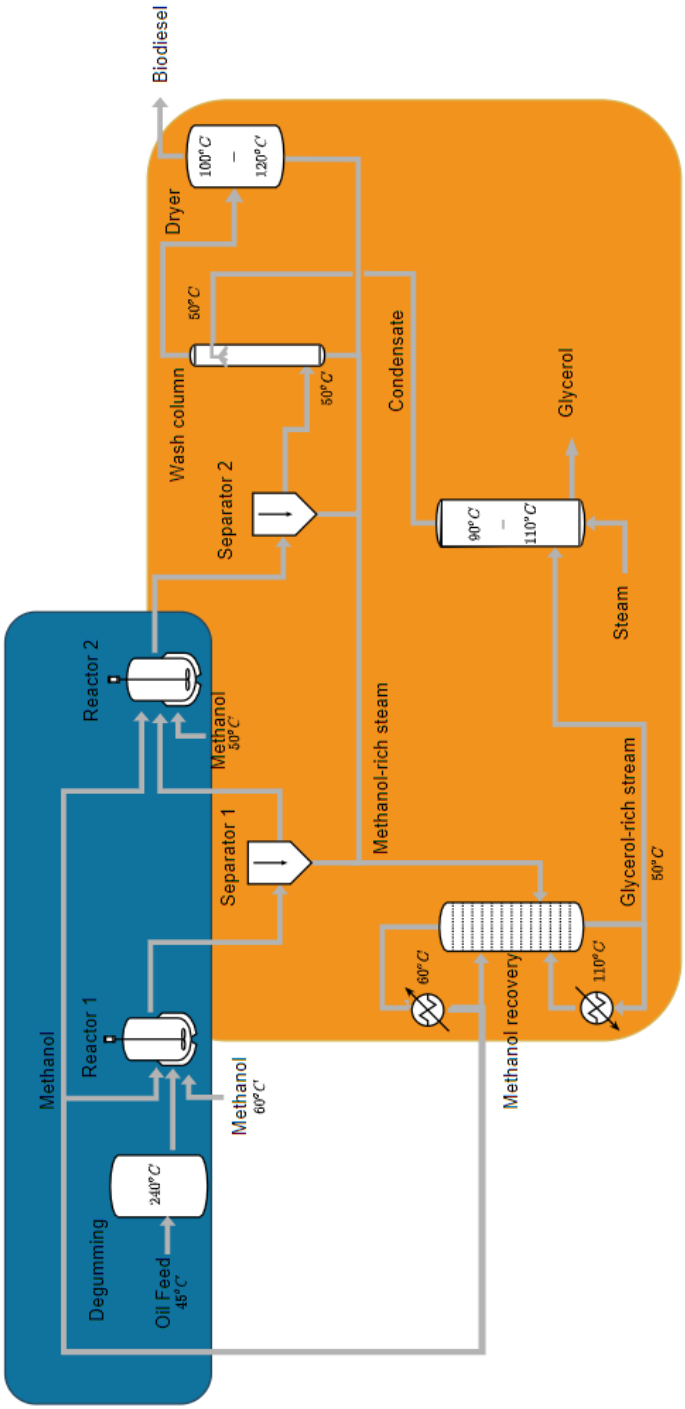

Figure 3 Plant layout of the reference case (L0) based on the Air Liquide design [32]. The top-left area is defined as the reactor section and the bottom right area is the separation section.

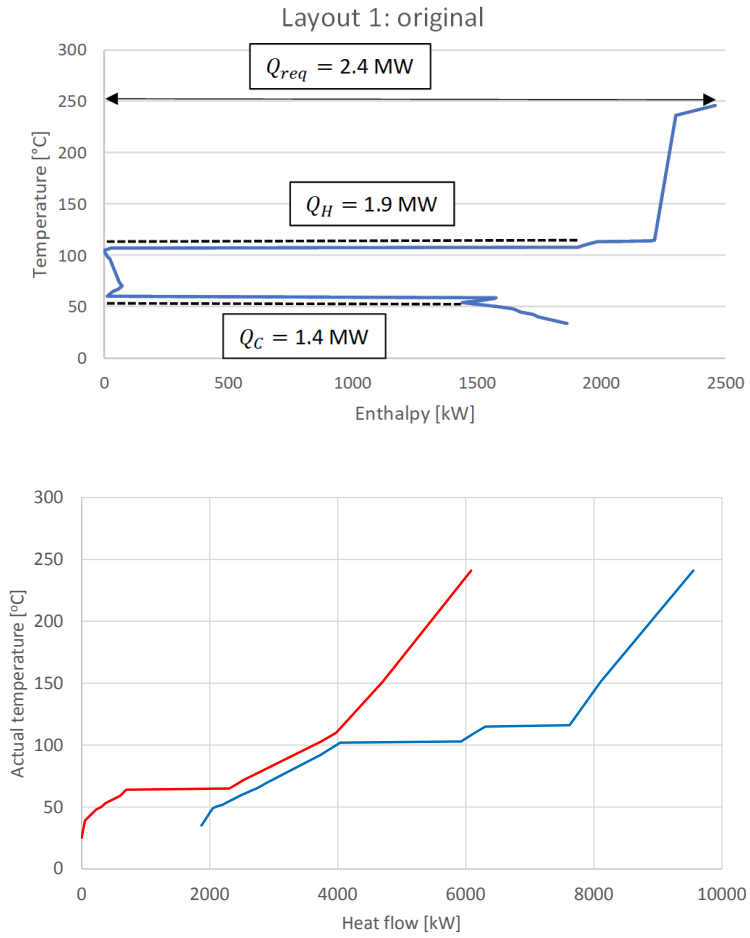

Figure 4 *Composite curve of the biodiesel process*

3.2. Future plant layouts

Possible CO_2 mitigation technologies for the biodiesel production plant are summarized in table A.1 (appendix). The following technologies were selected based on the reduction in expected heating requirement (fourth column of Table A.1):

1. a membrane reactor with methanol-recycling as an alternative technology for the reactor section,
2. a divided wall column for the glycerol stream for the separation section,
3. an e-boiler for the power section.

The basis for the overall assessment was an energy and mass balance of the main streams of the biodiesel production plant (layout 1). The presence of unreacted products and other contaminants, like free fatty oils, were omitted. The resulting model was calibrated using confidential industrial process data. This layout is called layout 2 after deployment of the heat pump.

3.2.1. Plant layout 3 and 4: modifications in the power section

The natural gas-fired boiler was replaced by an e-boiler in layout 3. The process flow diagram of this layout is the same as the reference case (Figure 3 Plant layout of the reference case (L0) based on the Air Liquide design [32]. The top-left area is defined as the reactor section and the bottom right area is the separation section) since no heat from the flue gas section is directly transferred to the production process. Hence, the energy and mass balances of the first layout remained unchanged from the reference case, just as the heat integration potential. The addition of a heat pump makes for layout 4.

3.2.2. Plant layout 5 and 6: modifications in the separation section

The methanol-recovery column and the glycerol-drying column of the reference case were replaced by a divided wall column in layout 5, which separates the column feed into three nearly pure streams, namely: methanol at the top, water in the middle, and crude glycerol at the bottom (Fig. 5). This column was based on a design by Kiss et al., [35-37] and operates at a pressure of 0.5 bar, with a reflux ratio of 0.83 and a feed stream temperature of 60 °C. The concentrations of the feed were taken from the process data. The thermal duty of the condenser was estimated based on the reflux rate (RR), the heat of evaporation (Δh_{evap}), and the methanol distillate rate ($\Phi_{m,d}$) using equation 1.

$$Q_{cond} = (1 + RR) \cdot \Delta h_{evap} \cdot \phi_{m,d} \quad (1)$$

The requirements for evaporating the water fraction (equation 1 with a reflux rate of zero) and heating the glycerol and water fraction were considered for the duty of the reboiler. The latter was calculated with equation 2, where the required duty to heat the species ($\dot{Q}$) is the product of the mass flow ($\dot{m}$), the specific heat of the species (c_p) and the temperature difference (ΔT). The average operating temperature was based on the model by Kiss and Ignar at 105 °C [36]. After the condenser, methanol is at the appropriate temperature to be sent back into the reactor. The water stream was condensed and cooled back to 50 °C before entering the washing column. The glycerol was cooled down to a temperature of 30 °C. The available heat in these coolers and condensers was calculated using equations 1 & 2. Note that as the glycerol and water leave the column in separate steams, the glycerol drying step needed in layout 1 could be omitted. The addition of a heat pump makes for layout 6.

$$\dot{Q} = \dot{m} \cdot c_p \cdot \Delta T \quad (2)$$

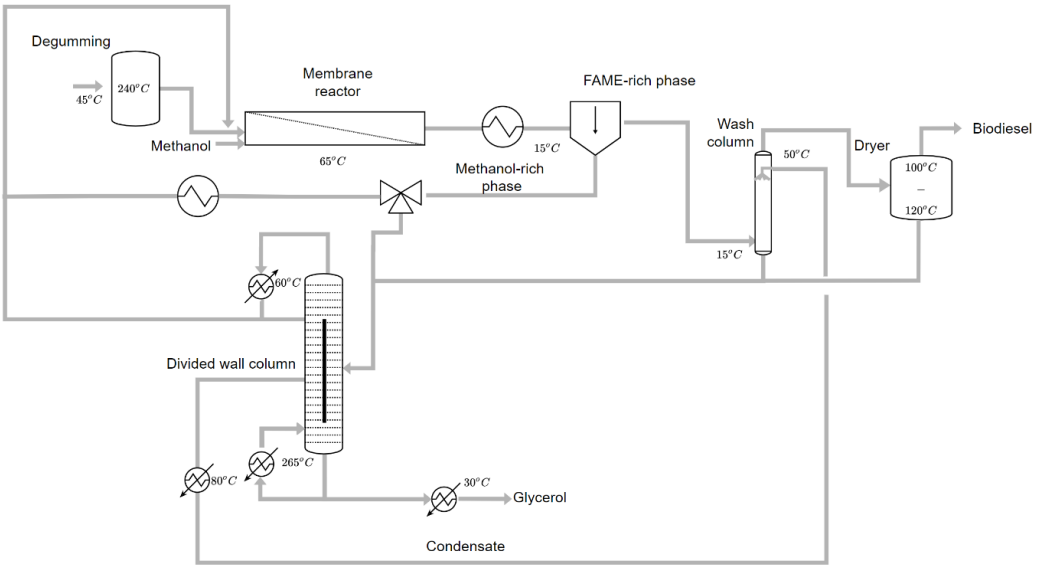

Figure 5 *Plant layout of the plant with a divided wall column (L2)*

3.2.3. Plant layout 7 and 8: modifications to the reactor section

A membrane reactor with methanol-recirculation is used for the transesterification process in layout 7, Fig. 6. The reactor design is based on the work by Cao et al. [37] and operates at 65 °C. The reactors, post reactor coolers, and their separation tanks were omitted. The resulting process flow diagram is presented in Fig. 6. The increase in conversion efficiency of about 2% is expected to have a negligible effect on the energy and mass balances [38, 39]. After the reactor, the product is cooled down to 15 °C and separated in a sedimentation tank. The available heat in the cooler was calculated with eq. 2, assuming a specific heat capacity of the mixture of 2.13 kJ/kg K. The upper, FAME-rich stream, consists only of FAME and methanol (molar ratio of 10:1), which is comparable with the current flow composition [37]. The FAME-rich phase is brought to market specifications by washing and drying. The design of the wash column was left unchanged, as the concentration of methanol in the stream is comparable with the reference case. The methanol and water used in this process are fed in the methanol-recovery column. Only 75 wt% of the total methanol-rich (>70 wt% methanol) phase was recycled into the reactor to limit the accumulation of glycerol [37]. Before entering the reactor, this stream was brought back to the reaction temperature. This heating requirement was calculated using eq. 2. The remaining 25% of the methanol-rich stream is mixed with the waste products of the FAME purification process and led to the methanol-recovery column. The recycling of methanol results in a lower flux of methanol compared to the reference case. Therefore, the reboiler and condenser of this layout were redesigned based on eq. 1 but using the same reflux rate as in the reference case, i.e., 1.2. The reboiler duty was estimated as the sum of the condenser duty and the required heat for preheating (eq. 2). The addition of a heat pump makes for layout 8.

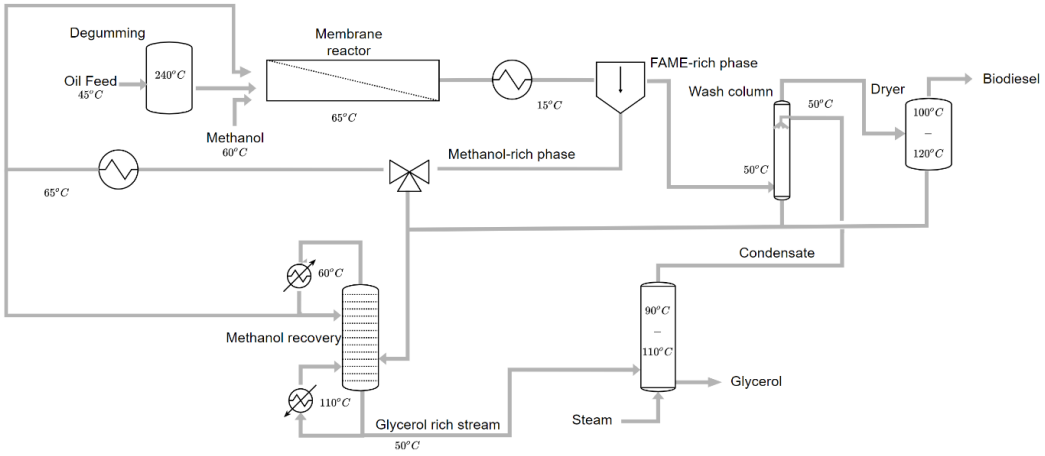

Figure 6 *Plant layout of the plant with a membrane reactor (L3)*

3.2.4 Plant layout 9 and 10: modifications to the separation and reactor section

In this layout, a membrane reactor was introduced together with a divided wall column. The resulting process flow diagram is depicted in Figure 7 Plant layout of the plant with a divided wall column and a membrane reactor (L4)7. Here, the process units were modelled in the same way as in the plant layouts 5 and 7. The addition of a heat pump makes for layout 10.

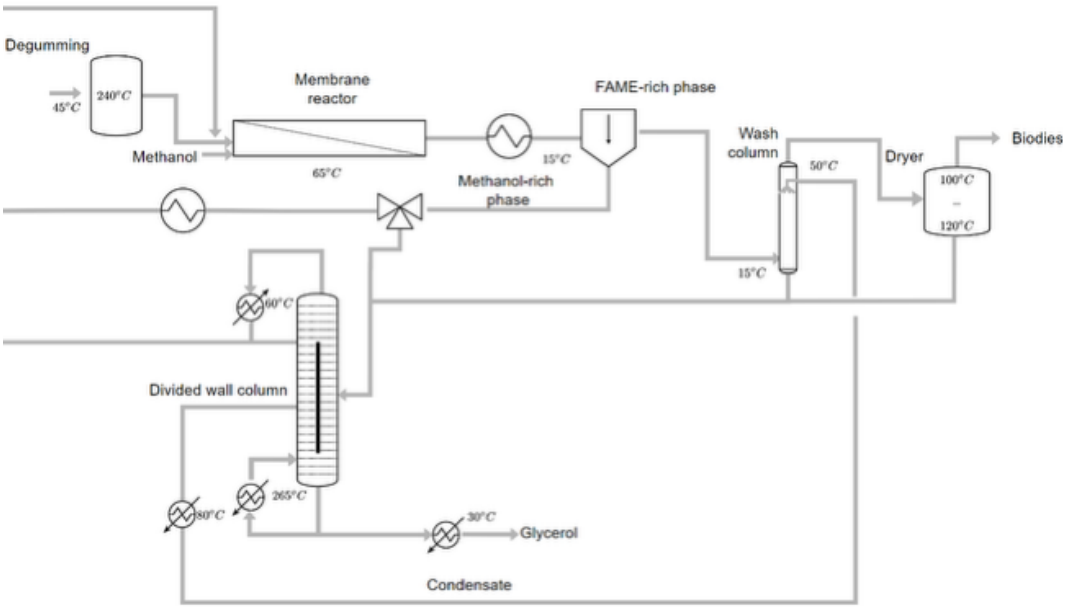

Figure 7 *Plant layout of the plant with a divided wall column and a membrane reactor (L4)*

4 Results

Interactions between the process changes are elucidated by first covering the impacts individual and combined measures had on the heat integration potential of the biodiesel production site. These results were thereafter used to build deployment sequences that help understand the impact of the deployment sequence on the combined CO_2 reduction potential.

4.1 Heat requirements of the plausible plant layouts

The grand composite curves (GCCs) of all the layouts are depicted in Figure A-H. These graphs show the changes in thermal requirements resulting from deploying the CO_2 mitigation measures. From Figure a, it can be derived that 2.4 MW of heat was required to operate the current plant layout (L1). The highest temperatures were required by the deacidification process of the crude oil before it entered the reactor at about 250 °C. Nevertheless, most heat (1.9 MW) was required around 110 °C to evaporate the methanol in the reboiler of the methanol-recovery column. The pinch was formed at about 100 °C by the FAME drying process. This pinch extends to a near pinch at about 60 °C, where the condensation heat of the methanol (1.4 MW) from the same recovery column became available. The reboiler and condenser of this column were taken as the sink and source for a heat pump. Their location in the T-H diagram is indicated by the dotted line. The effect of connecting these streams with this heat pump is depicted in Figure b. Connecting these streams required 0.4 MW. The GCC of Layout 2 (L2) shows that another heat pump could save an additional 0.25 MW. The GCC also holds for layouts 3 and 4, where the e-boiler replaced a natural gas-fired boiler.

The deployment of the divided wall column reduced heating requirements to 1.8 MW in layout 5 (Figure c). This reduction aligns with the expected savings reported by Kiss et al. of 20-30 % [40]. Most heat (1.6 MW) was required at a temperature of about 260 °C in the reboiler of the column set by the evaporation temperature of glycerol at 0.5 bara. The GGC shows a near pinch at 240 °C, where heat was required for the deacidification process. This near pinch extends via a pocket until the actual pinch temperature of about 100 °C is formed by the FAME drying process. The water condenser, 0.2 MW at about 75 °C, and the methanol condenser 1.3 MW at about 50 °C of the divided wall column were the most noticeable cooling loads below the pinch. The total cooling requirements, in this layout, were larger than those in the reference layout as exit streams were modelled to be cooled to environmental conditions. Due to the relative size and the location near the pinch, both the reboiler and the condenser of the divided wall column were potential sinks and sources for the heat pump. Nonetheless, as the temperature of the reboiler exceeded the operational range of current heat pump technologies (condenser temperatures of over 250 °C and a temperature lift of about 200 °C [41-43]), this case had no feasible heat pump solution. Neither were there other significant heat sinks to which a heat pump could be connected. Hence, layout 6 was declared infeasible (Figure d).

The deployment of the membrane reactor reduced the heating requirement to 1.9 MW in layout 7 (Figure e). This reduction is due to the reduced mass flow through the methanol-recovery column, whose reboiler duty was reduced to 1.5 MW. The effect is however limited, as most of the methanol stream originated from the wash column and the FAME dryer. These streams were contaminated with water, so they could not be recycled and had to be directly fed to the recovery column. The pinch temperature was again formed by the FAME dryers at about 100 °C and most cooling requirements were from the column's condenser (1.1 MW). The heat pump of layout 8 required 0.4 MW and used the heat to feed the reboiler (Figure f).

The introduction of both the membrane reactor and the divided wall column in layout 9 reduced heating requirements to 1.7 MW (Fig. 9g). Most of the heat was required in the reboiler of the divided wall column to 260 °C. This duty was reduced to 1.3 MW by recycling the methanol-rich stream. The largest cooling requirements stemmed from the divided wall columns methanol and water condensers, at 1.1 MW and 0.2 MW, respectively. The heat integration pocket that was formed in Layout 5 is negated by the introduction of the membrane reactor. As a result, a small heat pump could be installed to future reduce heating requirements to 1.5 MW in layout 10 (Fig. 8h). About 0.1 MW is needed to operate the heat pump. The pinch temperature is again around 100 °C, showing pinch-stability for all layouts, though the adjacent heat sinks and sources change in temperature.

4.2 Deployment sequence and CO_2 reduction potentials

The energy consumption and the yearly CO_2 emissions of the ten layouts are presented in 1. It shows that the deepest cuts in total emissions, from 4.6 to 2.5 kt/a, are achieved when the deployment starts the membrane reactor, followed by the divided wall column and thereafter the heat pump. The deployment of an e-boiler should be avoided with the assumed carbon intensity as it increases heating emissions by a factor of 2.7. The deployment sequence should also preferably start with a membrane reactor when only emissions from natural gas combustion are accounted for. The sequence should continue with the deployment of a heat pump and end with an e-boiler to fully avoid emissions from natural gas combustion. Inverting the deployment sequence would likely result in the same reduction with a slightly over-dimensioned heat pump. A sole e-boiler would be able to achieve the same results at the cost of high CO_2 emissions from electricity generation.

The membrane reactor (MR), the divided wall column (DWC), and the heat pump (HP) are used to build the six deployment sequences presented in Fig. 9, as they are the ones that affect the heat integration potential of the production plant. Fig. 9a. shows how emissions from natural gas are cut by 3.5 kt/a compared to the reference case when a heat pump is deployed. However, a large part of this reduction is at the expense of emissions from electricity generation. Moreover, the graph shows that a large part of the reduction accomplished by the heat pump is undone, when a divided wall column is introduced, as this combination is infeasible. The sequential deployment of a membrane reactor reduces the CO_2 emissions to a final 3.1 kt/a. Following the deployment of a heat pump directly with a membrane reactor results in a combined reduction of 3.7 kt/a in emissions from natural gas, whilst emissions from electricity generation are reduced by 0.5 kt/a to 1.7 kt/a (Fig. 9b). The sequential deployment of a divided wall column will again result in an infeasible solution after which the heat pump has to be discarded. An interaction that is also apparent in the second and last step of the deployment sequence of Fig. 9c and Fig. 9f, respectively. The deployment sequences of Fig. 9d-e. do not show negating of previously achieved reductions and achieve the deepest cuts in total emissions by reducing total energy related CO_2 emissions by 2.1 kt/a, which is 58% of the expected combined CO_2 emissions reductions based on the stand-alone performance of the membrane reactor (1 kt/a), the divided wall column (1.3 kt/a) and the heat pump (1.3 kt/a).

Table 1 *Comparison of layouts on their energy (heat and electricity) and related CO_2 emissions. Here, the technology that is introduced in the layout is presented in the first column. The first content-related row presents the CO_2 emissions of the reference plant. Scope 1 savings can be calculated by comparing emissions in the fourth column. Scope 2 savings can be derived from the sixth column.*

Technology	Heating requirements ([MW]	Electricity requirements [MW]	CO_2 emissions from natural gas combustion [kt/a]	CO_2 emissions from electricity generation [kt/a]	Total energy related CO_2 emissions [kt/a]
none (L1)	2.4	0	4.6	0	4.6
heat pump (L2)	0.6	0.4	1.1	2.2	3.3
e-boiler (L3)	2.4	2.4	0	12.2	12.2
e-boiler + heat pump (L4)	0.6	0.4	0	5.1	5.1
divided wall column (L5)	1.8	0	3.3	0	3.3
divided wall column + heat pump (L6)	Infeasible solution				
membrane reactor (L7)	1.9	0	3.6	0	3.6
membrane reactor + heat pump (L8)	0.5	0.4	0.9	1.7	2.6
membrane reactor + divided wall column (L9)	1.7	0	3.1	0	3.1
membrane reactor + divided wall column + heat pump (L10)	1.5	0.0	2.4	0.1	2.5

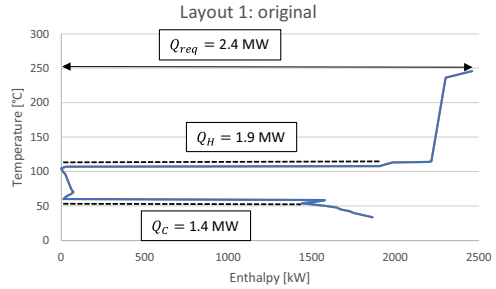

(A)

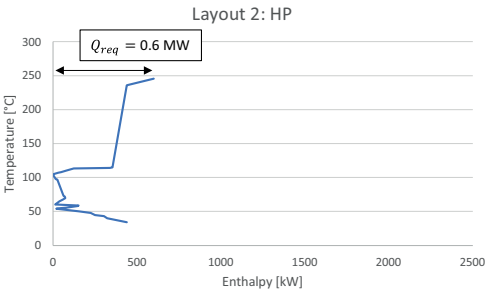

(B)

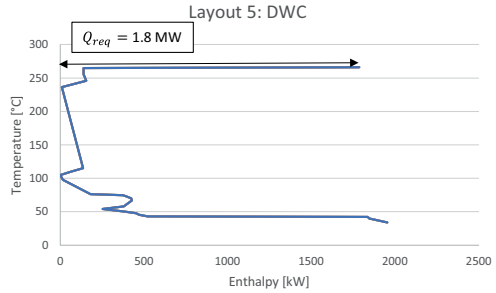

(C)

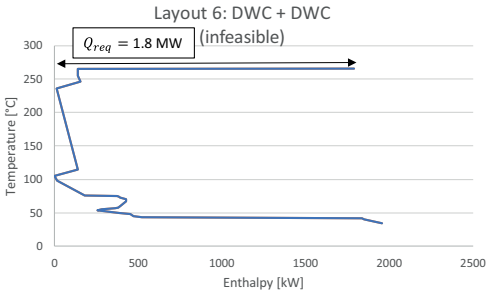

(D)

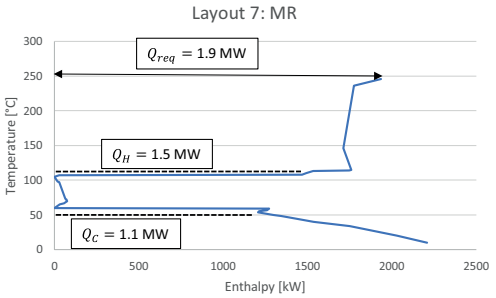

(E)

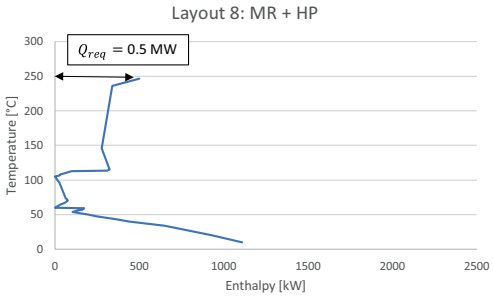

(F)

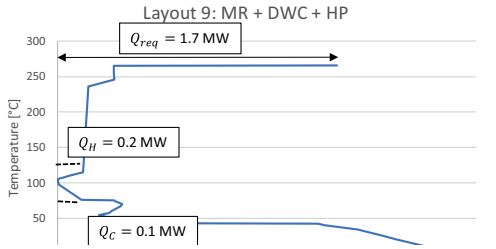

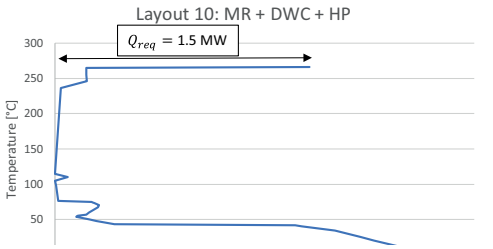

Figure 8 *Grand composite curves of the ten plausible plant layouts after the deployment of the mentioned process changes, a heat pump (HP), a divided wall column (DWC) and a membrane reactor (MR), in the order of mentions in the title of the graphs.*

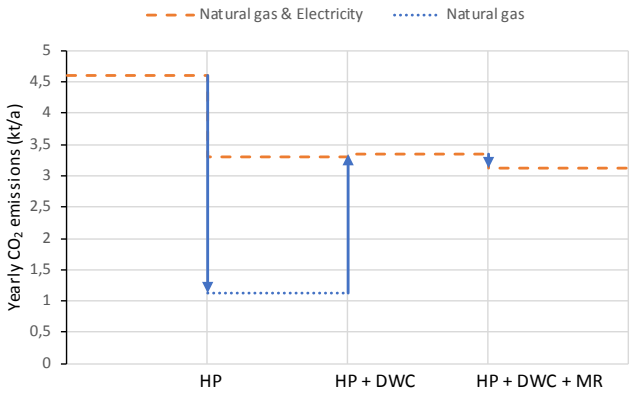
Natural gas & Electricity
Natural gas
Yearly CO_2 emissions (kt/a)
5
4,5
4
3,5
3
2,5
2
1,5
1
0,5
0
HP
HP + DWC
HP + DWC + MR

(A)

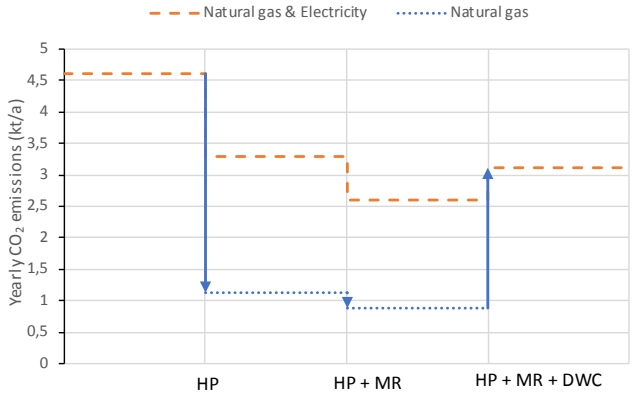
Natural gas & Electricity
Natural gas
Yearly CO_2 emissions (kt/a)
5
4,5
4
3,5
3
2,5
2
1,5
1
0,5
0
HP
HP + MR
HP + MR + DWC

(B)

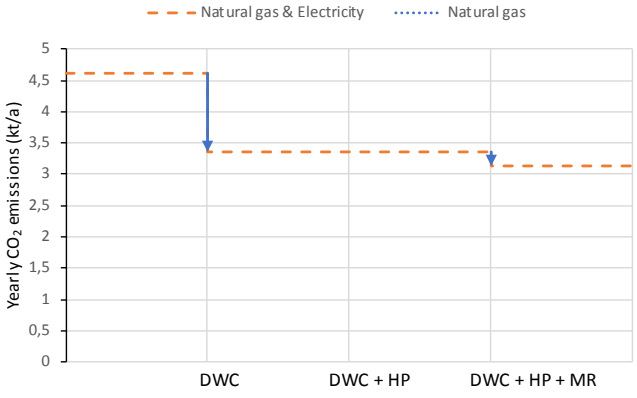
Natural gas & Electricity
Natural gas
Yearly CO_2 emissions (kt/a)
5
4,5
4
3,5
3
2,5
2
1,5
1
0,5
0
DWC
DWC + HP
DWC + HP + MR

(C)

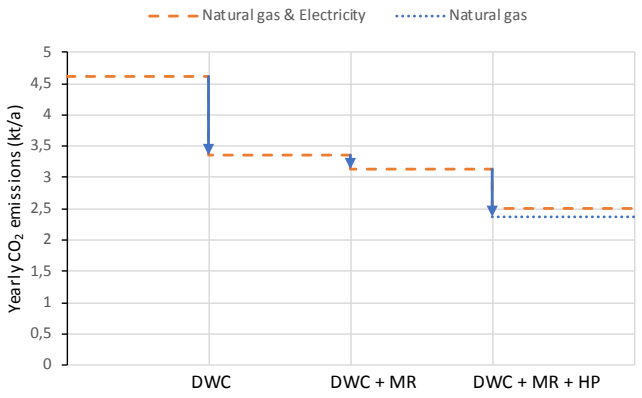

(D)

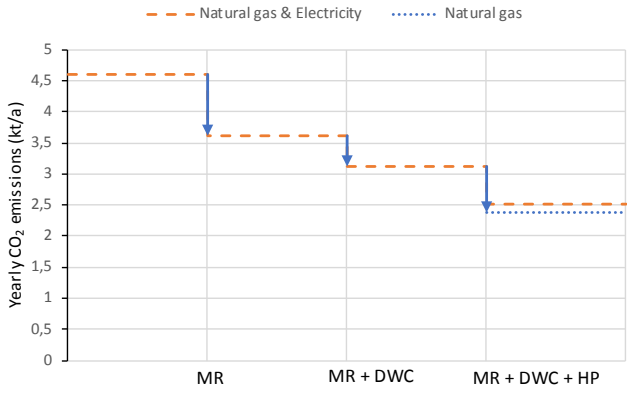

(E)

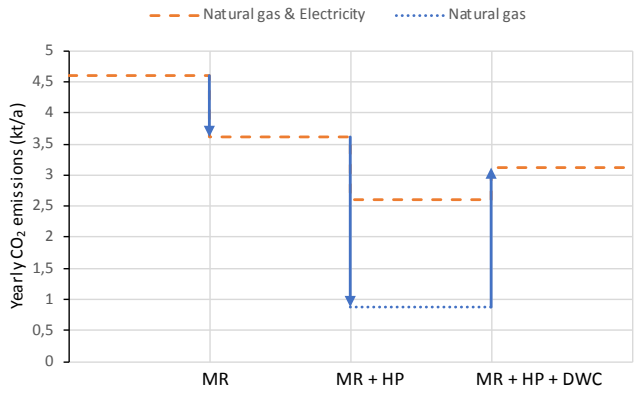

(F)

Figure 9 *Decomposition graphs of the six different deployment sequences. Changes in the amount of CO_2 emissions from natural gas combustion and electricity generation are presented in the curve. At each step, the process change (i.e., a heat pump (HP), a divided wall column (DWC), and a membrane reactor (MR)) on the x-axis is deployed. – figure width: 2 columns*

5 Discussion

The CO_2 reduction potentials of the ten layouts show that the deployment sequence significantly affects the contribution of the heat pump. The results also show that for other measures the deployment sequence is of lesser importance.

The heat pump's CO_2 reduction is least impacted (-15%) by the deployment of the membrane reactor, as the reactor only indirectly affects the heat pump connections. The deployment sequence of these measures does not affect this outcome, which indicates that the deployment sequence is of lesser importance when the process change is not to the heat pump connections. The deployment sequence has a more significant impact when the process connections of the heat pump are altered by the divided wall column. The increase in the required temperature lift by the heat pump makes this heat pump solution infeasible. The impact of the deployment sequence on the combined CO_2 reduction potential was less significant for the combination of the membrane reactor and the divided wall column, though just 65% of their performance is realized. The introduction of an e-boiler did not impact the operational conditions of the other process changes, but as it increased the carbon intensity of heat (i.e., kt of CO_2/MWh), it increased their reduction potential.

The different levels of interactions have implications for the useability of sequencing tools, like a MACC. The interactions between processes at the core and separation section of the process are of the order where conservative estimates and ballpark estimates can provide a basis for steps to be taken. The same holds for decarbonizing heat sources in this case as it does not affect the operation of other processes. However, the detrimental effects previously deployed mitigation measures can have on heat integration measures are outside of order in which conservative estimates and ballpark estimations would suffice. Henceforth, a MACC can only directly be applied under very stringent conditions and exceptions. Herein the most notable advice is to exclude heat integration measures entirely from the assessment and base their performance on heat integration potential after the considered process changes. Herein, it could be considered to only perform this extraction when changes to the heat pump connections are considered.

The assumption that the expected carbon intensity of the Dutch electricity grid will average at 0,569 kg/kWh between 2020 and 2029 has a significant impact on the performance of an e-boiler and a heat pump and favours non-electrification measures. The performance of the heat pump and the e-boiler drastically increases with the expected halving of the well-to-wheel CO_2 emissions in 2030. The total energy related CO_2 emissions from a sole heat pump would then reduce to 2.2 kt/a, 0.3 kt/a less than the current best option at 2.2 kt/a. The combination of the heat pump with the membrane reactor would be the best option in this future scenario with net yearly emissions of 1.8 kt.

The selection and modelling of technologies is a key factor in this assessment, as a different selection of measures are likely to have an impact on the presented results, just as better system integration (e.g., further lowering the operating pressure in the divided wall column to lower its operational temperatures), allowing multiple heat pump sinks and sources and technological progress (e.g., the availability of heat pumps with a higher condenser temperature) could also lead to different results. Future heat pump technologies can be combined with the divided wall column. Though, the COP of this heat pump is likely close to one, and therefore the performance of a more cost-effective e-boiler. It is however important to highlight that the focus of this study was not on finding the optimal solution for the case study, but rather on exploring whether sequencing would impact the results. In this context, the selected technologies proved to be a good selection as they covered the entire range from marginal to disruptive effects and changed the heat pump connections both directly and indirectly.

6 Conclusion

This study aimed to show how the deployment sequence of CO_2 mitigation measures affects their combined CO_2 reduction potential. Four key conclusions can be drawn:

First, the results of the case study show that the combined CO_2 reduction potential of the heat integration measures was highly sensitive to the deployment of heat related process changes.

Second, our results show that the deployment of CO_2 mitigation measures could result in a technology lock-in that hinders further decarbonization. In our case study, this was exemplified by the mutual exclusivity of a heat integration measure (i.e., a heat pump), and one of the process improvements (i.e., the divided wall column) plus the lack of another heat sink of sufficient size after its deployment which resulting on only one of the two measures being used, unless a third measure was introduced that created a new heat pump potential.

Third, the deployment of a process changes in the reaction or separation section of the production plant (i.e., a membrane reactor and a divided wall column) resulted in limited changes to one's other CO_2 reduction potential of the other measures. In that case, a conservative estimation of the reduction potential is likely to give a good enough representation of the additional savings.

Fourth, the sensitivity of heat pumps, and likely other heat integration measures, to process changes indicates a clear shortcoming in common sequencing approaches, such as a MACC, that are used to choose a deployment sequence based on stand-alone (economic) performance. In the case study, only 58% of the expected combined CO_2 reductions based on stand-alone performance was realized in the best deployment sequence. This error mainly lies with heat pumps and their connections, which should therefore be excluded from such an integrated assessment to achieve more accurate estimates.

References

[1] F. Xia, X. Zhang, T. Cai, S. Wu, and D. Zhao, "Identification of key industries of industrial sector with energy-related CO2 emissions and analysis of their potential for energy conservation and emission reduction in Xinjiang, China," Science of the total environment, vol. 708, p. 134587, 2020.

[2] M. Åhman and L. J. Nilsson, "Decarbonizing industry in the EU: climate, trade and industrial policy strategies," in Decarbonization in the European Union: Springer, 2015, pp. 92-114.

[3] E. Yáñez, A. Ramírez, A. Uribe, E. Castillo, and A. Faaij, "Unravelling the potential of energy efficiency in the Colombian oil industry," Journal of Cleaner Production, vol. 176, pp. 604-628, 2018/03/01/ 2018, doi: https://doi.org/10.1016/j.jclepro.2017.12.085.

[4] A. Hasanbeigi, W. Morrow, E. Masanet, J. Sathaye, and T. Xu, "Energy efficiency improvement and CO2 emission reduction opportunities in the cement industry in China," Energy Policy, vol. 57, pp. 287-297, 2013.

[5] C. M. Nwachukwu, C. Wang, and E. Wetterlund, "Exploring the role of forest biomass in abating fossil CO2 emissions in the iron and steel industry–The case of Sweden," Applied Energy, vol. 288, p. 116558, 2021.

[6] D. Johansson, J. Rootzén, T. Berntsson, and F. Johnsson, "Assessment of strategies for CO2 abatement in the European petroleum refining industry," Energy, vol. 42, no. 1, pp. 375-386, 2012.

[7] J. Lambauer, U. Fahl, M. Ohl, and M. Blesl, "Large-capacity industrial heat pumps. Potential, obstacles, examples; Gross-Waermepumpen in der Industrie. Potenziale, Hemmnisse und Musterbeispiele," Die Kaelte-und Klimatechnik, vol. 61, 2008.

[8] F. Bühler, A. Guminski, A. Gruber, T.-V. Nguyen, S. von Roon, and B. Elmegaard, "Evaluation of energy saving potentials, costs and uncertainties in the chemical industry in Germany," Applied Energy, vol. 228, pp. 2037-2049, 2018/10/15/ 2018, doi: https://doi.org/10.1016/j.apenergy.2018.07.045.

[9] E. Yáñez, A. Ramírez, V. Núñez-López, E. Castillo, and A. Faaij, "Exploring the potential of carbon capture and storage-enhanced oil recovery as a mitigation strategy in the Colombian oil industry," International Journal of Greenhouse Gas Control, vol. 94, p. 102938, 2020.

[10] McKinsey, "Pathways to a low-carbon economy: Version 2 of the global greenhouse gas abatement cost curve," 2010. [Online]. Available: https://www.mckinsey.com/business-functions/sustainability/our-insights/pathways-to-a-low-carbon-economy.

[11] A. Vogt-Schilb and S. Hallegatte, "Marginal abatement cost curves and the optimal timing of mitigation measures," Energy Policy, vol. 66, pp. 645-653, 2014.

[12] P. Ekins, F. Kesicki, and A. Z. Smith, "Marginal abatement cost curves: A call for caution," University College London, 2011.

[13] N. Berghout, H. Meerman, M. van den Broek, and A. Faaij, "Assessing deployment pathways for greenhouse gas emissions reductions in an industrial plant–A case study for a complex oil refinery," Applied Energy, vol. 236, pp. 354-378, 2019.

[14] H. Wiertzema, E. Svensson, and S. Harvey, "Bottom–Up Assessment Framework for Electrification Options in Energy-Intensive Process Industries," Frontiers in Energy Research, vol. 8, p. 192, 2020.

[15] IEA, "Energy Efficiency 2019," IEA, 2019. [Online]. Available: https://www.iea.org/reports/energy-efficiency-2019.

[16] A. Marina, S. Spoelstra, H. Zondag, and A. Wemmers, "An estimation of the European industrial heat pump market potential," Renewable and Sustainable Energy Reviews, vol. 139, p. 110545, 2021.

[17] S. Brückner, S. Liu, L. Miró, M. Radspieler, L. F. Cabeza, and E. Lävemann, "Industrial waste heat recovery technologies: An economic analysis of heat transformation technologies," Applied Energy, vol. 151, pp. 157-167, 2015.

[18] P. A. Løken, "Process integration of heat pumps," Journal of heat recovery systems, vol. 5, no. 1, pp. 39-49, 1985.

[19] M. J. Douglas, Conceptual design of chemical processes. McGrawHill, 1988.

[20] D. Townsend and B. Linnhoff, "Heat and power networks in process design. Part I: Criteria for placement of heat engines and heat pumps in process networks," AIChE Journal, vol. 29, no. 5, pp. 742-748, 1983.

[21] D. Townsend and B. Linnhoff, "Heat and power networks in process design. Part II: Design procedure for equipment selection and process matching," AIChE Journal, vol. 29, no. 5, pp. 748-771, 1983.

[22] I. C. Kemp, Pinch analysis and process integration: a user guide on process integration for the efficient use of energy. Elsevier, 2011.

[23] L. March, "Introduction to pinch technology," Targeting House, Gadbrook Park, Northwich, Cheshire, CW9 7UZ, England, 1998.

[24] L. Gallego, "PinchAnalysis-Console," 2019. [Online]. Available: https://github.com/LuisEduardoCorreaGallego/PinchAnalysis-Console.

[25] D. Olsen, Y. Abdelouadoud, P. Liem, S. Hoffmann, and B. Wellig, "Integration of Heat Pumps in Industrial Processes with Pinch Analysis," in 12th IEA Heat Pump Conference, 2017.

[26] G. Oluleye, M. Jobson, R. Smith, and S. J. Perry, "Evaluating the potential of process sites for waste heat recovery," Applied Energy, vol. 161, pp. 627-646, 2016.

[27] D. Van de Bor and C. I. Ferreira, "Quick selection of industrial heat pump types including the impact of thermodynamic losses," Energy, vol. 53, pp. 312-322, 2013.

[28] P. Zijlema, "Berekening van de standaard CO2-emissiefactor aardgas t.b.v. nationale monitoring 2020 en emissiehandel 2020," RVO, 2019. [Online]. Available: https://www.rvo.nl/sites/default/files/2020/05/vaststelling-standaard-co2-ef-aardgas-jaar-nationale-monitoring-2020-en-ets-2020-def_0.pdf. 2019.

[29] E. K. Vakkilainen, Steam generation from biomass: construction and design of large boilers. Butterworth-Heinemann, 2016.

[30] M. Abels-van Overveld et al., "Klimaat-en Energieverkenning 2019," 2019.

[31] J. Van Gerpen, "Biodiesel processing and production," Fuel processing technology, vol. 86, no. 10, pp. 1097-1107, 2005.

[32] D. Luna et al., "Technological challenges for the production of biodiesel in arid lands," Journal of arid environments, vol. 102, pp. 127-138, 2014.

[33] A. L.-E. Construction, "Lurgi MegaMethanol(tm)," 2021. [Online]. Available: https://www.engineering-airliquide.com/lurgi-megamethanol.

[34] F. Ma and M. A. Hanna, "Biodiesel production: a review," Bioresource technology, vol. 70, no. 1, pp. 1-15, 1999.

[35] A. A. Kiss and C. S. Bildea, "A review of biodiesel production by integrated reactive separation technologies," Journal of Chemical Technology & Biotechnology, vol. 87, no. 7, pp. 861-879, 2012.

[36] A. A. Kiss and R. M. Ignat, "Enhanced methanol recovery and glycerol separation in biodiesel production–DWC makes it happen," Applied Energy, vol. 99, pp. 146-153, 2012.

[37] P. Cao, M. A. Dubé, and A. Y. Tremblay, "Methanol recycling in the production of biodiesel in a membrane reactor," Fuel, vol. 87, no. 6, pp. 825-833, 2008.

[38] I. Atadashi, M. Aroua, and A. A. Aziz, "Biodiesel separation and purification: a review," Renewable Energy, vol. 36, no. 2, pp. 437-443, 2011.

[39] M. Dubé, A. Tremblay, and J. Liu, "Biodiesel production using a membrane reactor," Bioresource technology, vol. 98, no. 3, pp. 639-647, 2007.

[40] A. Kiss, J. Segovia-Hernández, C. Bildea, E. Miranda-Galindo, and S. Hernández, "Innovative biodiesel production in a reactive dividing-wall column," in Computer Aided Chemical Engineering, vol. 30: Elsevier, 2012, pp. 522-526.

[41] C. Arpagaus, F. Bless, M. Uhlmann, J. Schiffmann, and S. S. Bertsch, "High temperature heat pumps: Market overview, state of the art, research status, refrigerants, and application potentials," Energy, vol. 152, pp. 985-1010, 2018.

[42] C. Mateu-Royo, C. Arpagaus, A. Mota-Babiloni, J. Navarro-Esbrí, and S. S. Bertsch, "Advanced high temperature heat pump configurations using low GWP refrigerants for industrial waste heat recovery: A comprehensive study," Energy conversion and management, vol. 229, p. 113752, 2021.

[43] F. Schlosser, M. Jesper, J. Vogelsang, T. Walmsley, C. Arpagaus, and J. Hesselbach, "Large-scale heat pumps: Applications, performance, economic feasibility and industrial integration," Renewable and Sustainable Energy Reviews, vol. 133, p. 110219, 2020.

CHAPTER 3

IMPROVING PLANT-LEVEL HEAT PUMP PERFORMANCE THROUGH PROCESS MODIFICATIONS

Chapter This was originally published as B. W. de Raad, M. van Lieshout, L. Stougie, C. A. Ramirez, "Improving plant-level heat pump performance through process modifications", Applied Energy, Volume 358, 2024, 122667, DOI: https://doi.org/10.1016/j.apenergy.2024.122667.

Abstract

Heat pumps are a promising option to decarbonize the industrial sector. However, their performance at a plant-level can be affected by other process changes. In this work, process changes that improve the heat pump's performance have been identified using Process Change Analysis (PCA), where the background pinch point is used as a reference point for appropriate placement. The effects of the process changes on the heat pump's work requirements are studied by introducing exergy to PCA to form the split exergy grand composite curve. This graph shows the work potential of the streams connected to the heat pump and therefore its work targets. The framework is demonstrated in two case studies. In a biodiesel production plant it allowed to identify technologies that enhance heat pump performance while reducing overall heating requirements. Here, a heat pump transfers 1.9 MW with a COP of 4.2 but incurs a 40 kW penalty for transferring heat above the background process's pinch temperature. Replacing the wet water washer with a membrane separation unit avoided this penalty, while drastically reducing energy requirements from 0.9 MW to 0.3 MW. in a vinyl chloride monomer-purification process, PCA showed how the extraction of heat by the heat pump impacted the formation of the background pinch, from which an implementation strategy was derived that increased the heat pump's plant-level performance by 6.5% with respect to standard implementation.

1 Introduction

Numerous technologies have been developed to increase performance and reduce CO_2 emissions in the industrial sector. While many options are still in the early stages of development, high-temperature heat pumps are ready to be implemented at an industrial scale [1]. Their estimated energy reduction potential in the European chemical, paper, food, and refinery industries is estimated at about 1100 PJ/a [2]. Heat pumps are therefore likely to play a significant role in future energy systems. However, their adoption has been held up by the complexity of identifying economically feasible heat pump options and selecting the "right" heat pump technology [3]. The identification process of the heat pump is made more complex by its sensitivity to the deployment of new technologies needed to meet CO_2 reduction targets [4].

A heat pump reduces net heating and cooling requirements by transferring heat from a region with a surplus of heat to a region with a net heat demand [5, 6]. These regions can be identified with the help of pinch analysis [7]. More specifically, pinch analysis identifies the location in the process, I.e., the pinch point, where further heat transfer from hot to cold streams is limited by a minimal temperature driving force [8]. The region above this point requires a net amount of heat, whereas the region below has a surplus of heat. Transferring heat from below to above the pinch point requires work. Work that needs to be added by the heat pump. The net shaft work required by a heat pump is proportional to the difference in work potential, i.e. the exergy difference between the streams connected to the heat pump [9]. This work potential is a function of the amount of heat transferred and its temperature. Hence, heat pump connections should be taken as close to the pinch point as possible to minimize

the temperature difference between the streams and, thereby, work requirements [10]. The heat pump's (Coefficient Of) performance (COP), i.e., the ratio between the amount of heat delivered and the required work, is therefore largely determined by the temperature difference between the selected process connections on either side of the pinch point [10]. Process changes near or to the processes that form the pinch point, or even the implementation of the heat pump itself may change the pinch temperature and the shape of the pinch [11]. These changes can affect the heat pump's COP on a plant-level, as part of the transferred heat may not be across the pinch point anymore. Hence, considering how such changes impact the heat pump's performance is essential in the design process

The strive for increasing efficiencies has, in most processes, led to a wide variety of plausible newly developed technologies. When looking at a typical chemical process plant, like a biodiesel production plant, many technologies, or process changes, have been suggested. In the case of a biodiesel production plant, most of these changtes have been proposed for either the reaction or the separation section, where changes to catalysts are commonly explored. A review by Bohlouli and Mahdavian [12] listed ten categories, like enzyme base catalyst and heterogeneous alkali metal oxides. Moreso, an overview by Kiss et al. [13], listed seven subcategories of process intensification measures in the reaction section, like membrane reactors and reactive distillation. Both types of process changes are likely to affect the operation of technologies in the waste heat recovery and power sections, like heat pumps [4]. The time required to assess the sheer number of possibilities and possible interactions often overstretches the time available to process engineers.

The impact of process changes on the plant's heat integration, the basis for the deployment of a heat pump, is commonly studied with the help of Process Change Analysis (PCA) [7]. Vredeveld and Linnhoff [8] developed this framework as a combination the split grand composite curve (Split-GCC), and the plus-minus principle, which can be used to explore how a unit relates to the rest of the plant. PCA shows the effect a unit has on the formation of the pinch point by splitting (extracting) processes from the rest of the plant in a grand composite curve. The processes that are not extracted are collectively called the background process. The relation of the extracted processes to the pinch point of the background process, the background pinch point, becomes apparent by separating the extracted and background process. It thereby makes explicit whether a technology is appropriately placed and how it contributes to heat integration characteristics, like self-integrating heat pockets. The appropriate placement for a heat pump would, for example, require it to transfer heat from below the background pinch to above it. Dhole and Linnhoff [14] used this framework to explore how current pump-arounds in an existing distillation column could be used to increase heat integration with the background process. Glavic et al., [15, 16] showed how PCA could be combined with the appropriate placement rules for energy conversion technologies on the appropriate integration of endothermic and exothermic reactors with PCA, where an exothermal reactor was modelled as a chemical heat pump and an endothermal reactor as a chemical heat engine. Wiertzema et al. [17] showed how PCA could be used to explore the impact of deploying a new processing unit with a fundamentally different heat profile. In their study, PCA uncovered that the loss of waste heat by electrifying processes in an oxo-synthesis plant increased overall energy requirements off-setting the envisioned CO_2 savings. These examples have all used PCA to assess the impact of already selected technologies, whereas the selection of technologies itself is one of the main challenges in decarbonizing the industry. However, PCA can be a valuable tool in this technology selection process as it is able to highlight required changes that improve overall heat integration in respect to, for example, a heat pump.

In this study, the concept of exergy will be added to the framework of PCA to assess the effects of (sequentially) adding decarbonization technologies on the performance of the heat pump in the pre-feasibility phase of design. The overall aim of this article is to show how PCA can help identifying process changes that reduce overall heating requirements whilst increasing the performance of a heat pump and how the placement of the heat pump itself may impact the heat pump's performance. This knowledge will help to identify promising technology combinations that can increase the combined CO_2 reduction of the mitigation measures and discard unfruitful options in the early stages of the technology selection process.

2 Method

The overall method consists of three phases: (1) extraction of heat pump connections, (2) selection of process changes, and (3) assessment of the impact of process changes on the heat pump's COP.

2.1 Extraction of heat pump connections

The basis of the analysis was a consistent process model based on operational process data and chemical equilibria and covering over 90% of a real production plants' energy consumption. Impurities were not considered in the model. The specific heat of the considered streams was linearized to allow for a max error of 10% and the temperatures represent the yearly averages. The resulting energy and mass balance were used as input for a pinch analysis, and the results were visualized in a grand composite curve. For the pinch analysis, a minimal temperature difference of 10 °C was adopted. Heat pump connections were defined as the streams closest to the pinch point with a size of at least 10% of the total heating requirements. If multiple streams met this criterion, the ones with the largest heat capacity flowrates were selected. For both, the heat source and the sink, a single process connection is considered to limit the integration cost of the heat pump. This limits the thermal duty of the heat pump's heat sink (Q_{sink}). The required amount of energy needed from the heat source (Q_{source}) was based on Eq. (1):

$$\mathrm{Q_{source}} = Q_{sink} - W_{comp}, \tag{1}$$

where, W_{comp} was defined as the work added by the heat pump's compressor, which was approximated based on the exergy values of the heat source (X_{source}) and sink (X_{sink}) and an exergetic efficiency (η_{ex}), as indicated in Eq. (2):

$$\mathrm{W_{comp}} = \frac{1}{\eta_{ex}}(\mathrm{X_{sink}} - \mathrm{X}_{source}), \tag{2}$$

where the exergy values were defined as in Eq. (3):

$$\mathrm{X_i} = \eta_c Q_i, \tag{3}$$

Where, $_i$ was either the source or the sink and was the Carnot factor (1-T_0/T) with the environmental temperature (T_0) set at 15 °C [18]. An exergetic efficiency ($''^{ex}$) of 0.59 was assumed to compensate for irreversibilities [19, 20].

Three heat extraction options were considered when there was a significant excess of heat available (>10% heat source). The first option involved utilizing the heat from the top-end of the stream to minimize the temperature lift and compressor work. The remaining thermal duty of the stream was added to the background processes, as depicted in Fig. 1.a-b. The second option utilized the bottom-end of the stream to establish a pinch point and ensure appropriate integration, while the top-end was considered a background process. The third option involved a split integration, extracting heat from the entire temperature range of the source but only from a smaller (split) stream, while the rest of the stream was added to the background process.

The process-heat pump connections were used in a pinch analysis, just as the remaining background processes. Both were visualized in a Split-GCC and split exergy grand composite curve (Split-EGCC). The latter curve was formed with the introduction of the Carnot factor on the ordinate of the Split-GCC.

2.2 Selection of process changes

The process changes, i.e., deployment of decarbonization technologies in the reactor and separation sections, were selected for their ability to reduce overall heating requirements while improving the heat pump's performance by minimizing penalties from inappropriate placement regarding the background process pinch point, i.e., not solely transferring heat across the pinch point of the background process. Only process changes to the background process were explored in this paper, as the heat pump and its connections were assumed to be implemented first. The selection of process changes started at the pinch point, where heat integration iss most constrained. Guided by the Split-GCC, process units that influence the pinch point were listed in a table. Possible alternative processes or synthesis routes were explored based on results found in literature. Technologies should have had a minimal technology readiness level (TRL) of 6 to be able to realize them during the technical lifetime of the heat pump.

The pinch temperature of the background process was altered by replacing processes that directly or indirectly form the pinch. The temperature should be increased when a heat pump (partially) extracted heat from above the pinch point of the background process. The opposite should occur when the heat pump (partially) delivered heat below the pinch point of the background process. An increase in the pinch temperature was realized by deploying process changes that increased the net heat available above the pinch point. This was either realized by increasing heat apparent in waste heat streams or by decreasing heat demand. Decreasing the pinch temperature was realized in the opposite manner.

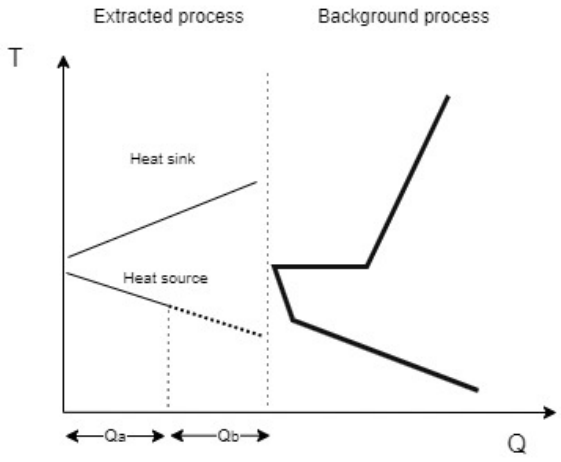

(a)

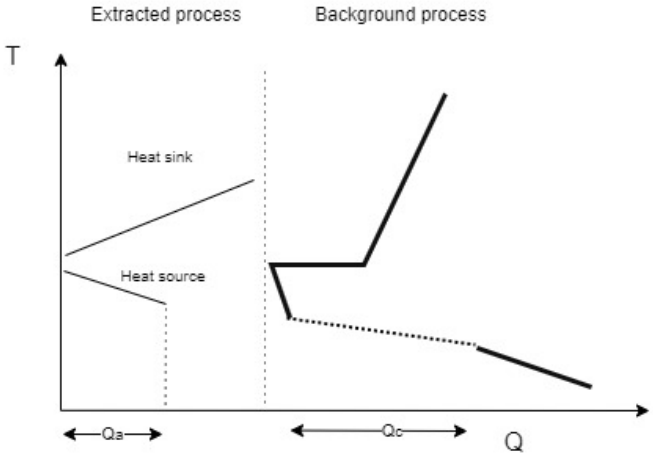

(b)

Figure 1 *Split grand composite curve. a) a split grand composite curve of a process where heat pump connections are extracted from the background process. The heat source of the heat pump is split into two sections; Q_a and Q_b, representing the top and bottom end of the stream. b) is a split grand composite curve of the same process where a heat pump is extracted, but where the bottom-end of the heat available in the heat source is transferred back into the background process, forming Qc in the process.*

2.3 Assessment of the impact of process changes on the heat pump's COP

Process changes do not necessarily reduce the COP of the heat pump itself but may likely affect its performance on a plant-level, due to penalties from inappropriate placement. The COP on a plant-level, also called the effective COP (of the heat pump, was defined based on the amount of heat transferred across the pinch of the background process (Q_{net}) and the work required to operate the heat pump, as in Eq. (4):

$$\mathrm{COP}_{eff} = \frac{\mathrm{Q_{net}}}{\mathrm{W_{comp}}} \quad (4)$$

The penalty (Q_p) resulting from the inappropriate placement was defined as the difference between the amount of heat delivered (Q_{sink}) by the heat pump and the amount of heat transferred across the pinch point of the background process (Q_{net}), as in Eq. (5):

$$\mathrm{Q_p} = Q_{net} - Q_{sink} \quad (5)$$

3 Process descriptions of the case studies

Most heat-related emissions stem from operating separation processes [1, 21, 22]. For this assessment, a biodiesel production plant in the North-West Europe was selected as an example of a process where heat integration is limited by a distillation column, characterized by an isothermal heat source and sink. This case study is used to show how exergy-extended PCA can be used to identify beneficiary process changes next to a heat pump. Additionally, a case study on the purification process of vinyl chloride monomer (VCM) in Scandinavia is included to provide insights into design choices when dealing with non-isothermal heat sources and sinks. This case illustrates how the deployment of the heat pump itself can affect the formation of the pinch point and its plant-level COP.

3.1 Case 1: Biodiesel production unit in North-West Europe

The transesterification process of vegetable oils for biodiesel production has been extensively documented in literature, see e.g., Van Gerpen [23] and Luna [24]. Fig. 2 illustrates the heating and cooling requirements of the various process stages assuming that the oil is fed at a rate of 25 t/h. Initially, the feed is heated from the environment conditions to 70 °C for the degumming process. Subsequently, the oil is further heated to 240 °C for deacidification. After neutralization, the oil feed is cooled and mixed with methanol in a reactor (Reactor 1) operating at approximately 65 °C to produce FAME (fatty acid methyl esters) and glycerol. A sedimentation tank (separator 1) is used to separate the glycerol from the FAME and unprocessed reactants. The FAME-rich stream containing unreacted reactants undergoes transesterification in a second reactor (Reactor 2) at 55 °C. The products from this reactor are once again separated in sedimentation tanks (Separator 2). By-products, contaminants, and excess methanol are neutralized and removed in a wet water washing column. The wet FAME stream is then dried to meet the desired product quality. Excess methanol, glycerol, and other compounds are directed to a methanol-recovery column. In this column, methanol is separated from the other products, with a reboiler temperature of 102 °C. The condensed top stream of 65 °C is recycled to the reactors along with fresh methanol. The bottom product, consisting primarily of glycerol and water, is dried in a multi-effect evaporator, where the first stage operates at 102 °C and subsequent stages utilize flash condensate. The evaporated water is reused in the wash column.

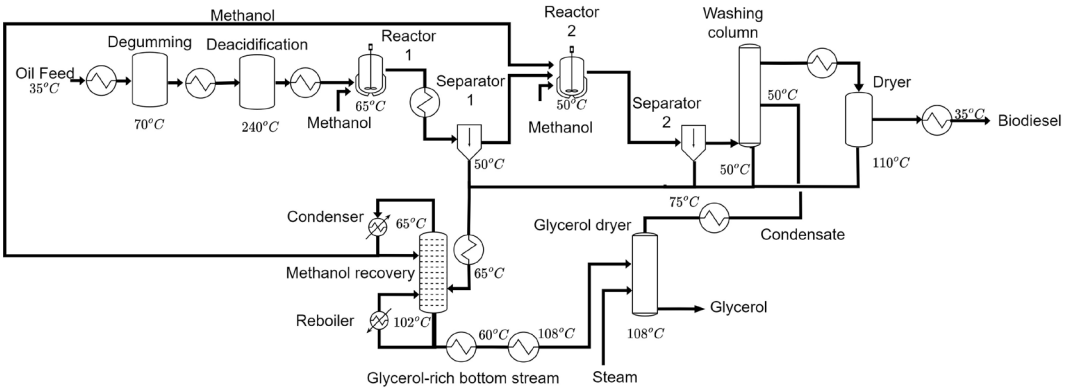

Figure 2 *Process flow diagram of the modelled biodiesel production process.*

The heating requirements are summarized in Table 1, indicating the supply temperature (T_s), target temperature (T_t), heat capacity flow rate (CP), and heat load (Q).

Table 1 *Heating requirements of the biodiesel production process in North-West Europe.*

Sub-process	Type	T_{supply} °C	T_{target} °C	CP kW/K	Q kW
Degumming	Cold	35	70	12.9	450
Deacidification	Cold	70	240	16.2	2,750
Reactor 1 feed	Hot	240	65	15.4	2,700
Separator 1 feed	Hot	65	50	10.0	150
FAME dryer preheat	Cold	50	110	15.0	900
FAME dryer	Cold	110	110	-	50
FAME cooler	Hot	110	35	15.0	1,125
Column preheat	Cold	50	65	11.0	165
Reboiler	Cold	102	102	-	1,850
Condenser	Hot	65	65	-	1,550
(Reboiler) bottom cooler	Hot	102	60	5.5	230
Glycerol dryer preheat	Cold	60	108	5.5	265
Glycerol dryer	Cold	108	108	-	200
Glycerol condensate cooler	Hot	75	50	0.4	10
Glycerol cooler	Hot	75	35	1.8	70

3.2 Case 2: Vinyl Chloride Monomer purification process in Scandinavia

The separation process of Vinyl Chloride Monomer (VCM) from ethylene dichloride (EDC) in a PVC production site in Sweden has been well documented by Lindqvist (25). Fig. 3 illustrates the heating and cooling requirements of the various separation stages. Initially, the EDC is preheated from 27 ˚C to 207 ˚C and evaporated it at that temperature before the cracking process. Preheating between 125 ˚C and 193 ˚C was integrated with the cracker and therefore exempted from this study as the cracker is integrated with another production process. Thermal duties were based on a volume flow 45 m^3/h at 23 bar exiting the EDC plant. The first separation step after cracking removed tars from the mixture of VCM, EDC, hydrogen chloride (HCl), water and tars in a cooling column. Valuable products absorbed in the tar were separated in a distillation column, where the reboiler heats the tar from 90 ˚C to 141 ˚C. The top stream of the tar column was recycled back into the cooling column. The distillate of this column was condensed in three stages from 132 ˚C to 40 ˚C caused by a partial condensation of the stream's content. A mix of EDC, VCM and HCl was fed into the HCl column, where the reboiler operates at 87 ˚C and HCl was condensed at the top at -32 ˚C and sequentially evaporated until a temperature of 21 ˚C to comply with the process conditions set by connecting processes. The bottom stream consisting of VCM and EDC was heated and partially evaporated at 158 ˚C after which the VCM was condensed at 40 ˚C and brought back to environmental conditions. All heating requirements were summarized in Table 1, indicating the supply temperature (T_s), target temperature (T_t), heat capacity flow rate (CP), and heat load (Q).

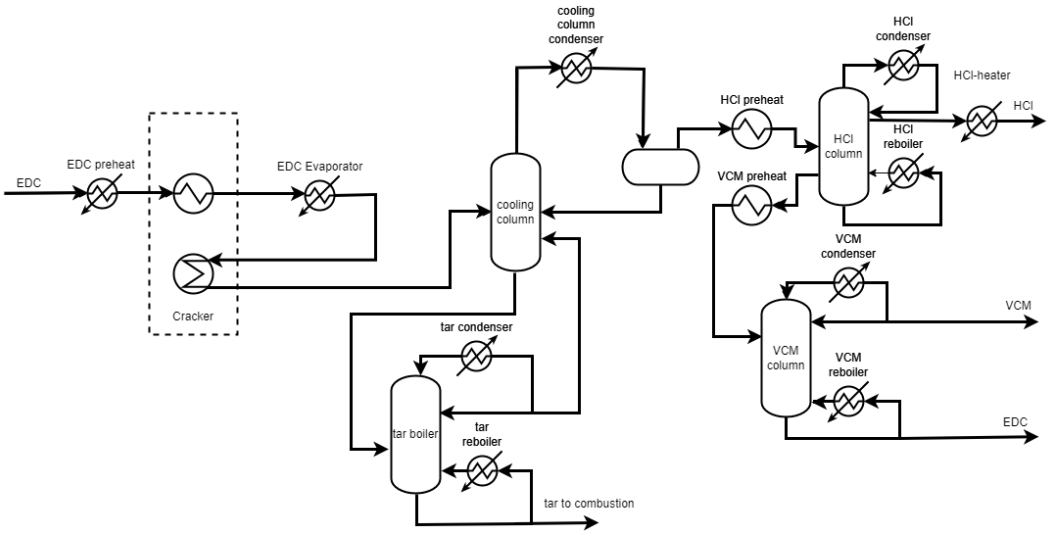

Figure 3 *Process flow diagram of the reference VCM separation process adapted from (25).*

Table 2 Process data table of the reference VCM separation process adapted from (25).

Sub-process	Type	T_s °C	T_t °C	CP kW/K	Q kW
EDC-preheat I	cold	27	125	20.2	1980
EDC- preheat II	cold	193	207	27.5	385
EDC-evaporator	cold	207	207	-	3,045
Cooling column condenser A1	hot	132	112	-145.3	2,905
Cooling column condenser A2	hot	112	66	-89.2	4,105
Cooling column condenser B	hot	66	40	-80.8	2,100
HCl-preheat	hot	40	13	-4.1	110
HCl-condenser	hot	-32	-32	-	1,640
HCl-heater	cold	-32	21	2.1	110
HCl-reboiler	cold	87	87	-	1,560
VCM-preheat	cold	82	85	153.3	460
VCM-condenser	hot	40	40	-	2,500
VCM- subcooler	hot	39	17	-16.6	365
VCM-reboiler	cold	158	158	-	2,210
Tar-reboiler	cold	90	141	3.5	180
Tar-condenser A	hot	92	85	-8.6	60
Tar-condenser B	hot	85	52	-1.7	55

4 Results

The result section consists of two parts, where the results of the study on the biodiesel case are presented in section 4.1, and those of the VCM case in section 4.2. In the biodiesel case study of section 4.1, the emphasis is on the impact of process changes on the heat pump's plant-level performance. The impact of deploying a heat pump on its plant-level performance itself is of lesser interest due to the heat pump's latent heat source and sink in the distillation column. This is not the case for the VCM-purification process, where the pinch is formed by sensible streams, which is the central theme of section 4.2.

4.1 Case 1: biodiesel production

The results of the biodiesel case are structured in accordance with the steps presented in the method section.

4.1.1 Extraction of heat pump connections

The grand composite curve of the original process is presented in Fig. 4.a. The difference between net hot and cooling requirements resulted from the inability to recover heat from the FAME dryer and from not including minor streams like the waste streams of the deacidification process. From Fig. 4.a. it can be derived that the pinch is formed at a shifted temperature of 60 °C. Heating requirements are limited to 107 °C. At this temperature, the first stream with a significant heating requirement (1.85 MW) is the reboiler of the methanol recovery column. The condenser of the column is situated at the pinch and has a cooling requirement of 1.6 MW. These streams are selected to be the connections to the heat pump, as they are the closest to the pinch point that meet the set criteria of representing at least

10% of the total heating requirements. Other heat requirements are at a comparable temperature, hence, overproduction of heat by the heat pump could, without significant losses in efficiency, be utilized in other processes. In total 2.6 MW (Q_h) is needed to operate the production plant, of which about 1.9 MW (Q_c) could be recovered from the major waste heat streams. Heat pump connections are extracted from the background process in the Split-GCC of Fig. 4.b, where the reboiler and condenser are depicted on the left side of the graph and the background process is depicted on the right. The graph shows that the extracted process operates above the pinch of the background process and that heating and cooling requirements are reduced to 0.9 and 0.4 MW, respectively, when a heat pump provides the utility requirements of the extracted process.

4.1.2 Selection of process changes

4.1.2.1 Selection criteria for process changes

A comparison between the extracted and background process in Fig. 4.b. shows that the shape of the grand composite curve is dominated by the methanol-recovery column, which is represented by the isothermal lines at a shifted temperature of 60 °C and 108 °C. Of the original 2.6 MW, only 0.9 MW of heat is required to operate the entire background process. The remaining 1.9 MW is needed to operate the reboiler of the methanol-recovery column. More importantly, the figure shows that the heat pump transfers heat above the pinch temperature of the background process at 55 °C. Hence, a heat pump that connects the streams in the extracted processes does not solely transfer heat across the pinch point of the background process. This inappropriate placement will lead to a penalty of 40 kW when all the condenser's heat is utilized by a heat pump [5, 6], as depicted in the zoom in of Fig. 4.b. Its effective COP will therefore be lower than the COP of the heat pump itself. Process changes should therefore increase the temperature of the background pinch to at least 60 °C to avoid this loss. The temperature of the background pinch can be lifted by either reducing the cooling requirements and their temperature or by increasing heating requirements and their temperature just above the pinch.

4.1.2.2 Plausible process changes

The processes that release heat just above the pinch are listed in table 3. Though the process of the bottom cooler provides heat untill the shifted pinch temperature, it does not add to the amount of net heat available as the same amount of heat is required in the glycerol preheat at the same shifted temperatures. The same holds for the FAME cooler, which is integrated with the FAME preheat. This leaves the separator 1 feed cooler as the most dominant of other streams due to its larger heat capacity flow rate. The purpose of the separation feed cooler is to enable the separation process in the sedimentation tank [24]. Alternative separation methods could occur at higher temperatures and omit the need for this cooling step [26, 27]. However, a similar heat exchanger would be necessary after the separation unit, as separation efficiencies of alternative technologies are comparable and the temperature requirements of the second reactor remain based on a chemical equilibrium with by-products [23]. Thus, the same amount of heat would become available after such a modification. Changes to the glycerol cooler could, however, reduce the net heat available just above the pinch as this process is not directly integrated with a preheater. The glycerol cooler and the rest of the drying step are required as the water added in the FAME purification process needs to be removed to bring the glycerol up to market conditions. Hence, exploring process changes to the FAME purification step, the wet water washing process, would therefore be a preferred route.

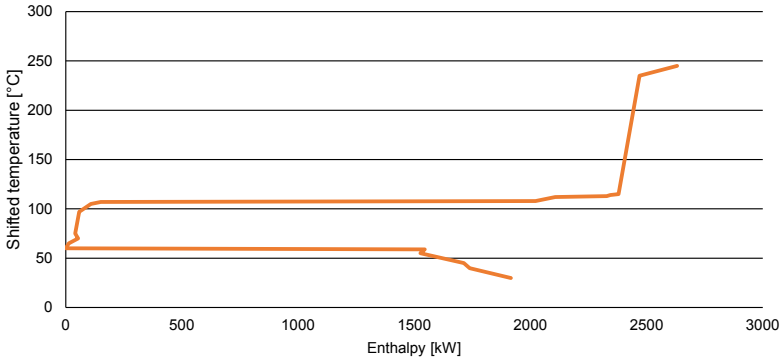

(a)

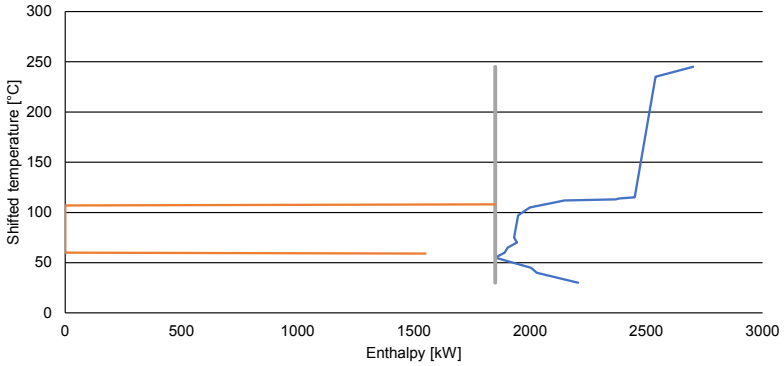

(b)

Figure 4 *Heat integration of the reference biodiesel production process:*
a) *grand composite curve,*
b) *split-grand composite curve with the heat pump connections extracted on the left side and the background process on the right. The operation of the heat pump above the background pinch point and the resulting deployment penalty is highlighted in the zoom at the top left of the graph.*

Table 3 *Data of processes releasing heat just above the background pinch point.*

Process	Type	Ts °C	Tt °C	CP kW/K	Q kW
Separator 1 feed	Hot	65	50	10.0	150
FAME cooler	Hot	110	35	15.0	1,125
Bottom cooler	Hot	102	60	5.5	230
Glycerol condensate cooler	Hot	75	50	0.4	10
Glycerol cooler	Hot	75	35	1.8	70

4.1.2.3 Process changes to the FAME purification step

A comparative study by Atadashi et al. [28] explored three technologies for purifying crude biodiesel: wet washing, dry washing, and membrane refining. In their comparison, they showed that using a membrane process would be the preferred option, as other technologies do not meet the required ASTM D6751 and EN14214 standards, which set requirements for biodiesel to be used as a fuel. Suthar et al,. [29] confirmed these findings whilst in search of less energy-intensive separation technologies for biodiesel production. The process integration of a membrane process is depicted in Fig 5. In this design, it is assumed that no additional heat is required to operate the membrane as the temperature of the stream after the second sedimentation tank is of the same order as the temperatures used in the biodiesel separation experiments by for example Cao [26] and Dube [30]. The resulting process data table is presented in table 4.

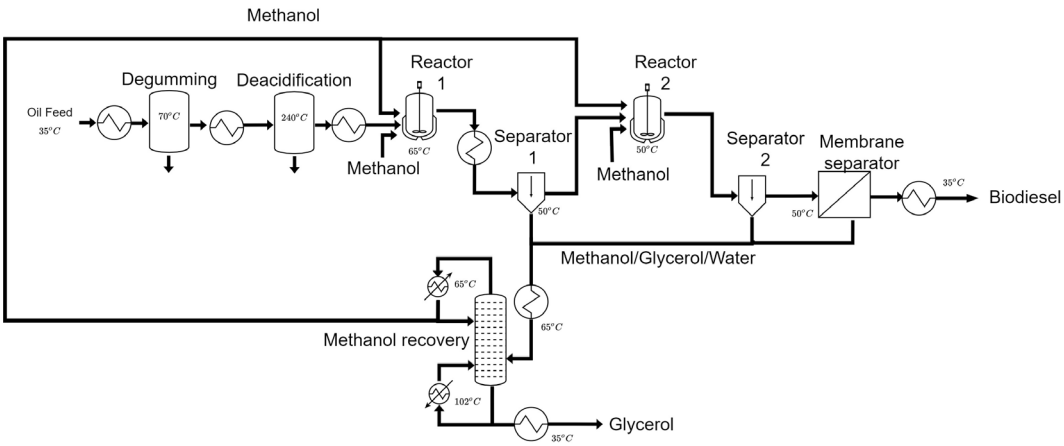

Figure 5 *Process flow diagram of the biodiesel production process after deployment of the membrane separation unit.*

4.1.2.4 Impact of process changes on the heat integration

The impact of replacing the wet water washer with a membrane separation unit on the grand composite curve of the background process is presented in Fig. 6. It shows that the pinch temperature of the background process increased to 97 ˚C and overall heat requirements in the background process were reduced to about 0.3 MW. Thereby, it shows that this modification not only helps in reducing heat-related CO_2 emissions but also increases the performance of the heat pump as it now operates across the pinch of the background process. Also note that the net excess of heat produced by the heat pump will increase if the duty in the heat pump's source is not lowered, as the required duty by the reboiler will fall by about 150 kW to 1.7 MW. Moreover, deploying the heat pump will, therefore, no longer come with an inappropriate placement penalty, as the heat pump solely transfers heat across the pinch point of the background process.

Table 4 Process data table of the biodiesel production process after deployment of the membrane separation unit based on the experiments of Cao (26) and Dube (30).

Sub-process	Type	T_s °C	T_t °C	CP kW/K	Q kW
Degumming	Cold	35	70	12.9	450
Deacidification	Cold	70	240	16.2	2,750
Reactor 1 feed	Hot	240	65	15.4	2,700
Separator 1 feed	Hot	65	50	13.3	200
Column preheat	Cold	50	65	3.3	50
Reboiler	Cold	102	102	-	1,700
Condenser	Hot	65	65	-	1,550
Bottom cooler	Hot	102	35	1.9	130

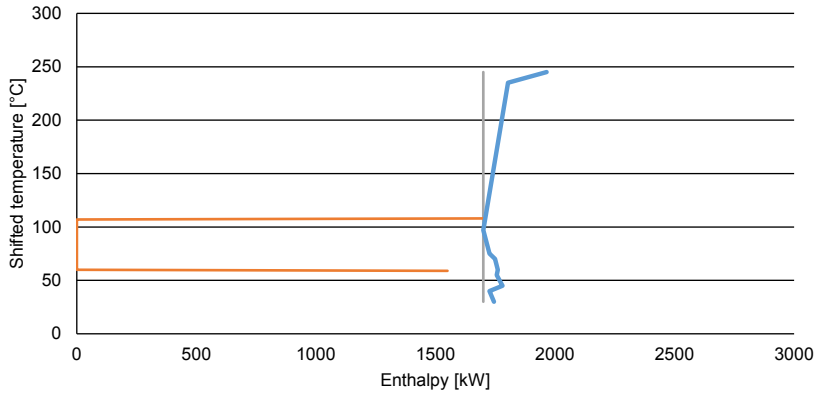

Figure 6 *The split grand composite curve of the biodiesel production process after deployment of the membrane separation unit, where the heat pump connections are extracted (left) from the background process (right).*

4.1.3 Assessment of the impact of process changes on the heat pump's COP

The Split-EGCC of the original production plant layout and the layout after the deployment of the membrane process are depicted in Fig. 7.a. and Fig. 7.b., respectively. Based on these figures, the shaft work required to transfer the heat between the column's condenser and the reboiler is estimated at 0.5 MW in the original layout, and 0.4 MW after process changes due to the reduced water content in the feed stream of the column. The heat pump was able to transfer 1.9 MW of heat in the original layout with a penalty of 40 kW, which brings it near 1.8 MW, resulting in an effective COP of 4.0. After deploying the membrane separation process, 1.7 MW of heat could be effectively transferred with a COP of 4.1, as the thermal duty of the reboiler was reduced. In this case, 0.3 MW remains unutilized at the heat source.

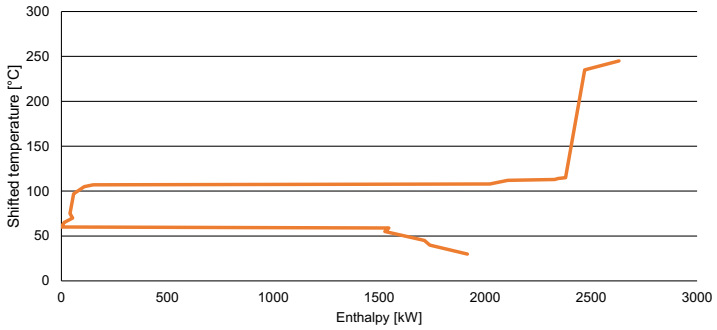

(a)

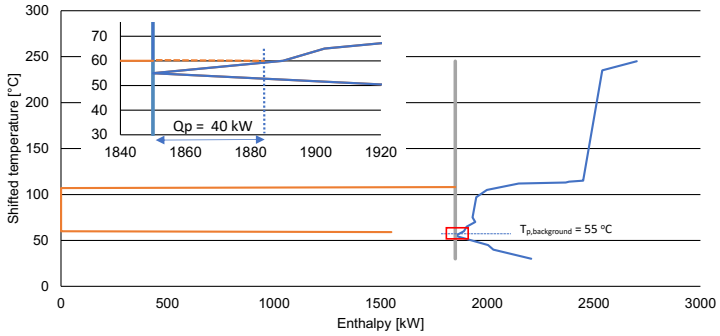

(b)

Figure 7 *Split exergy grand composite curves of:*
a) *the original biodiesel production process,*
b) *the biodiesel production process after deployment of the membrane separation unit.*

4.2 Case 2: Vinyl Chloride Monomer purification process

For the VCM case, only the impact of the deployment of the heat pump itself on the heat integration of the background process is explored. The impact of deploying other decarbonization technologies is not included to emphasize the role of heat extraction, and thereby the role of heat pump placement.

4.2.1 Extraction of heat pump connections

The grand composite curve of the reference model is presented in Fig. 8.a. The process requires 5.8 MW of heat and 7.6 MW of cooling to operate. The additional 0.8 MW of cooling is a result of the sub-ambient requirements of HCl. The pinch of the process forms at 127 °C as heat from the cooling column cannot be used to meet the demand of the tar-reboiler and the EDC-preheat. However, heat from the cooling column's condenser defines the shape of the curve just below the pinch, as it is the stream with the largest heat capacity flow rate from a shifted temperature of 127 °C to 105 °C. Hence, it is selected to be the heat source for the heat pump. The VCM-reboiler is selected to be the sink of the heat pump, as it is the first stream that has at least 10% of the total heating requirements above the pinch at a shifted temperature of 163 °C. However, the condenser surpasses the thermal duty of the VCM-reboiler, 2.9 MW vs. 2.2 MW, respectively. This imbalance is also visualized in the Split-GCC (Fig. 8.b). As a result, not all energy from the condenser could be utilized in the reboiler. Hence, either the top, the bottom, or a split of the hot stream should be utilized.

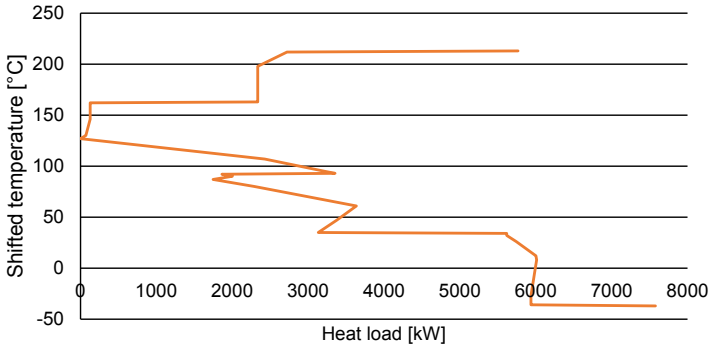

(a)

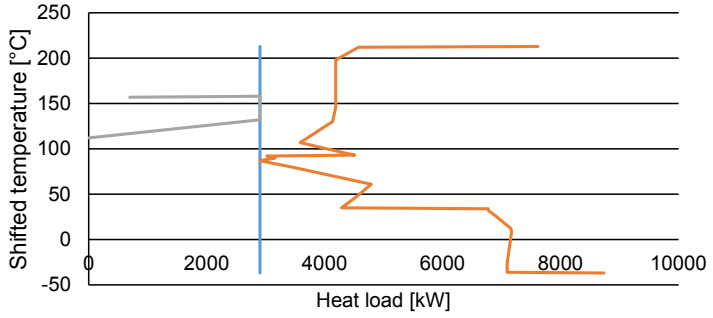

(b)

Figure 8 *Heat integration of the reference Vinyl Chloride Monomer purification process:*
a) *grand composite curve,*
b) *split-grand composite curve with the heat pump connections extracted on the left side and the background process on the right.*

4.2.2 Selection of process changes

4.2.2.1 Top-end heat pump integration

The heat pump must deliver 2.2 MW of heat at a shifted temperature of 163 °C from a sensible 132 °C heat source with a capacity flow rate of 145 kW/°C. Solving the energy balance and estimating the heat pump's COP with Eq. (1-3) indicates that the source should be cooled by 1.6 MW to 121 °C and that the compressor needs 0.57 MW, as presented in Table 5 and Fig 9.b. Fig. 9.a. shows the impact on the background process of reverting the excess energy of the heat source back into the background process. As a result, the pinch point of the background process is formed at a shifted temperature of 116 °C. This is below the pinch that is formed by the heat pump between a shifted temperature of 158 °C and 127 °C. This inappropriate placement comes with a penalty of 0.26 MW.

4.2.2.2 Bottom-end heat pump integration

As with the top-end integration, the heat pump must deliver 2.2 MW at a shifted temperature of 163 °C from a sensible heat source with a capacity flow rate of 145 kW/°C. However, in this scenario 1.5 MW is extracted between 123 °C and 112 °C and 0.65 MW is required by the heatz pump, as presented in Table 5 and Fig 9.d. Fig. 9.c. shows that the heat pump transfers heat entirely across the pinch point of the background process at a shifted temperature of 127 °C. As a result, the heat pump faces no inappropriate placement penalty.

4.2.2.3 Split heat pump integration

The heat capacity flow rate of the heat pump's heat source must be reduced to deliver the requested 2.2 MW at the heat sink. The split stream set-up utilizes the entire temperature range from the heat source, 132 °C to 112 °C. The heat pump requires 0.61 MW to achieve this temperature lift with an uptake of 1.6 MW by the heat pump, as presented in table 5 and Fig 9.f. This is realized by creating a stream with a capacity flow rate of 80 kW/°C. The impact of reverting the excess energy of the heat source back into the background process is shown in Fig. 9.e. Due to this change, the heat pump is appropriately placed across the pinch point of the background process at a shifted temperature of 127 °C and faces no penalty.

4.2.3 Assessment of the impact of integration strategy on the heat pump's COP

The top-end heat pump integration reduces the process heat requirements by from 5.77 MW in the reference case by 1.9 MW to 3.82 MW, as can be seen in Table 5. This 0.3 MW less than the 2.2 MW that is delivered at the heat pump's sink. This difference is due to the inappropriate placement penalty as the heat pump partially operates above the pinch point of the background process, as shown in Fig. 9.a. The other two options transfer heat entirely across the pinch (see Fig. 9.c. and 9.e). However, due to the lower exergy value of the heat sources, these two options require more work from the compressor, which results in a penalty in the form of additional exergy destruction. As a result of this trade-off between a heat and work penalty, the net COP of the Top-end and Bottom-end heat pump integration are quite comparable, with a COP of 3.45 and 3.41, respectively. The split heat pump integration, however, can transfer heat without facing a penalty and maximize the work potential of the heat source and come to a net COP of 3.63. Resulting in an overall increase of 6.5% compared to the top-end approach.

Table 5 Comparison of heat extraction strategies for heat pump implementation

	Process heat [MW]	Energy source [MW]	Exergy source [MW]	Work target [MW]	Work required [MW]	Exergy destruction [MW]	Net energy consumption [MW]	COP_{ne}
Reference	5.77						5.77	
Top-end	3.82	1.65	0.46	0.33	0.57	0.23	4.38	3.45
bottom-end	3.56	1.56	0.41	0.38	0.65	0.27	4.21	3.41
split	3.56	1.60	0.43	0.36	0.61	0.25	4.17	3.63

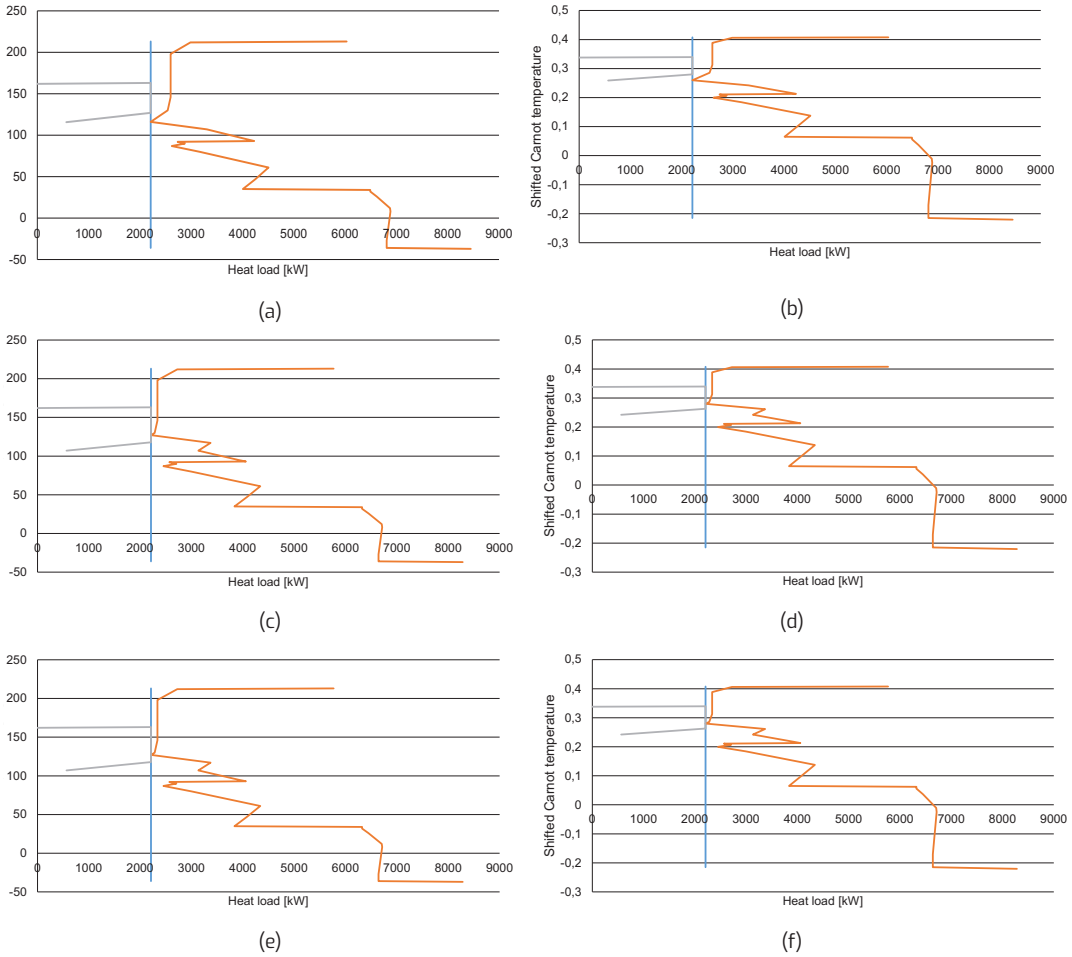

Figure. 9. *Heat integration profiles: a) grand composite curve in case of top-end heat extraction, b) exergy grand composite curve in case of top-end heat extraction, c) grand composite curve in case of bottom-end heat extraction, d) exergy grand composite curve in case of bottom-end heat extraction, e) grand composite curve in case of split heat extraction, f) exergy grand composite curve in case of split heat extraction.*

5 Discussion

Both cases were selected because of their limited complexity to clearly demonstrate how process change analysis (PCA) can be used to identify how process changes will impact a heat pump's performance. However, the layout of the biodiesel production unit, consisting of a set of reactors and sequential separation processes, is typical for a large part of the industrial sector. Just as the heat integration is being dominated by a single separation step, as is also the case in for example a paper mill [31]. However, the vinyl chloride monomer (VCM) purification case also showed how to apply the method in case multiple processes form the pinch point. Challenges may arise when considering highly complex plant layouts, as upstream changes may have unforeseen impacts on the energy and mass balance, and thus the heat integration, further down the line.

Another dimension of complexity is the use of multiple heat sinks or sources, though a single sink-source system is commonly the most cost-effective strategy [10]. A possible exception to this is the case where low-pressure steam is being produced for the heat sink with the lowest temperature and excess steam is being (re)compressed to supply heat to higher temperature sinks. This added complexity requires heat extraction/delivery strategies akin to that of the VCM-case but include the extraction of additional streams. The use of multiple heat sinks is a likely improvement for the biodiesel case, where other relatively large heat sinks are apparent close to the reboiler and the condenser still has 0.1 or 0.3 MW of heat left respective of the reference or the altered case. This energy should be transferred back to the background process, as is demonstrated in the VCM-case, when this energy is not utilized. This heat will help to avoid the 40 kW penalty incurred in the case of the reference process. This cancellation will always occur when the amount of excess heat in the heat source exceeds that of the heating requirements at the same shifted temperature in the background process.

Another potential challenge is the formation of a new pinch point by a "near pinch" resulting from a large heat integration pocket. This scenario was not included in the cases, but there are no fundamental barriers that would not allow for the use of PCA with the split (exergy) grand composite curve (Split-(E) GCC) when this is the case. The formation of the new background process pinch point would be clearly visible in a Split-EGCC, which would allow for appropriate integration of the heat pump and help to identify process changes that modify the background pinch point in a similar way as for the original pinch point. Additional, "pocket-heat pumps" could also be used to overcome this challenge [32]. The same argument holds for processes where a larger inappropriate placement penalty is encountered.

However, it should be noted that in its current form the approach is limited to continuous steady-state processes. It is not suited for discontinuous processes, e.g., batch processes, and should be expanded with methods like the time-slice model of floating pinch analysis to cope with this added complexity [7].

A practical drawback to the approach is its abstract representation of a process, as is inherent to pinch analyses. This may make it difficult to communicate results to non-experts, like financial decision makers. It is therefore advised to use this approach as an exploratory tool and communicate results via conceptual designs based on the results.

6 Conclusions

Process Change Analysis (PCA) extended with the split- exergy grand composite curve (split -EGCC) proved to be a valuable tool in assessing the impact of process changes on the performance of a heat pump. In the biodiesel production process, it showed that when a heat pump transfers heat between the condenser and the reboiler of the methanol recovery column it faces an inappropriate placement penalty of 40 kW. PCA helped to identify which processes caused this penalty and how it could be avoided whilst reducing the process's overall heat requirements. This was achieved by replacing the wet water washing column with a membrane separation unit. The deployment of this unit resulted in a reduction of heating requirements from 0.9 MW to 0.3 MW, whilst increasing the plant-level COP from 4.0 to 4.1.

Furthermore, PCA effectively identified the optimal utilization of a sensible heat source in the vinyl chloride monomer (VCM) process. Extracting heat from the top-end minimized work requirements by leveraging the steam's high exergy value but led to an inappropriate heat pump placement penalty. Utilizing bottom-end heat avoided this penalty but resulted in higher work requirements due to the streams lower exergy content. Splitting the heat source achieved the highest plant-level COP. Overall, this strategy yielded a deviation of over 6.5% in COP values. These findings underscore the importance of strategic heat extraction to optimize heat pump performance.

Further research needs to establish how PCA can include the temporal aspects of heat sources and sinks to accommodate process fluctuation and those demanded by the energy system.

Overall, the results underline the importance of the combined assessment of process changes, stream selection and heat integration technologies by highlighting the effect of process changes have on the performance of a heat pump. PCA will therefore be a valuable tool in a period of continuous retrofitting that will include technologies, like heat pumps.

Nomenclature

Letter symbols	
CC	Composite curve
COP	Coefficient of Performance
CP	Heat capacity flow rate, kW/K
Split-EGCC	Split exergy grand composite curve
GCC	Grand composite curve
Q	Stream heat load/ heat, kW
T	Temperature, ˚C
Split-GCC	Split grand composite curve
X	Exergy, kW
Greek symbols	
η	efficiency

Subscripts and superscripts	
0	environment
c	Carnot
net	net
p	penalty
pl	plant-level
source	heat source
sink	heat sink
s	source
t	target

References

[1] F. Schlosser, M. Jesper, J. Vogelsang, T. Walmsley, C. Arpagaus, and J. Hesselbach, "Large-scale heat pumps: Applications, performance, economic feasibility and industrial integration," Renewable and Sustainable Energy Reviews, vol. 133, p. 110219, 2020.

[2] A. Marina, S. Spoelstra, H. Zondag, and A. Wemmers, "An estimation of the European industrial heat pump market potential," Renewable and Sustainable Energy Reviews, vol. 139, p. 110545, 2021.

[3] J. Lambauer, U. Fahl, M. Ohl, and M. Blesl, "Large-capacity industrial heat pumps. Potential, obstacles, examples; Gross-Waermepumpen in der Industrie. Potenziale, Hemmnisse und Musterbeispiele," Die Kaelte-und Klimatechnik, vol. 61, 2008.

[4] M. v. L. B. de Raad, L. Stougie, C.A. Ramirez, "Exploring impacts of deployment sequences of industrial mitigation measures on their combined CO2 reduction potential," Energy, vol. Volume 262, Part B, 2023.

[5] D. Townsend and B. Linnhoff, "Heat and power networks in process design. Part I: Criteria for placement of heat engines and heat pumps in process networks," AIChE Journal, vol. 29, no. 5, pp. 742-748, 1983.

[6] D. Townsend and B. Linnhoff, "Heat and power networks in process design. Part II: Design procedure for equipment selection and process matching," AIChE Journal, vol. 29, no. 5, pp. 748-771, 1983.

[7] I. C. Kemp, Pinch analysis and process integration: a user guide on process integration for the efficient use of energy. Elsevier, 2011.

[8] B. Linnhoff, "Pinch technology has come of age," Chem. Eng. Progr., vol. 80, no. 7, pp. 33-40, 1984.

[9] B. Linnhoff and V. R. Dhole, "Shaftwork targets for low-temperature process design," Chemical engineering science, vol. 47, no. 8, pp. 2081-2091, 1992.

[10] E. Wallin and T. Berntsson, "Integration of heat pumps in industrial processes," Heat Recovery Systems and CHP, vol. 14, no. 3, pp. 287-296, 1994.

[11] P. A. Løken, "Process integration of heat pumps," Journal of heat recovery systems, vol. 5, no. 1, pp. 39-49, 1985.

[12] A. Bohlouli and L. Mahdavian, "Catalysts used in biodiesel production: a review," Biofuels, vol. 12, no. 8, pp. 885-898, 2021.

[13] A. A. Kiss, Process intensification technologies for biodiesel production: reactive separation processes. Springer Science & Business Media, 2014.

[14] V. Dhole and B. Linnhoff, "Distillation column targets," Computers & chemical engineering, vol. 17, no. 5-6, pp. 549-560, 1993.

[15] P. Glavič, Z. Kravanja, and M. Homšak, "Heat integration of reactors—I. Criteria for the placement of reactors into process flowsheet," Chemical engineering science, vol. 43, no. 3, pp. 593-608, 1988.

[16] Z. Kravanja and P. Glavič, "Heat integration of reactors—II. Total flowsheet integration," Chemical engineering science, vol. 44, no. 11, pp. 2667-2682, 1989.

[17] H. Wiertzema, E. Svensson, and S. Harvey, "Bottom–Up Assessment Framework for Electrification Options in Energy-Intensive Process Industries," Frontiers in Energy Research, vol. 8, p. 192, 2020.

[18] M. N. Hamsani, T. G. Walmsley, P. Y. Liew, and S. R. W. Alwi, "Combined Pinch and exergy numerical analysis for low temperature heat exchanger network," Energy, vol. 153, pp. 100-112, 2018.

[19] L. Yiqing, F. Shengke, S. Changjiang, and Y. Xigang, "A two-step design method for shaft work targeting on low-temperature process," Chinese Journal of Chemical Engineering, vol. 22, no. 6, pp. 664-668, 2014.

[20] G. Oluleye, M. Jobson, R. Smith, and S. J. Perry, "Evaluating the potential of process sites for waste heat recovery," Applied Energy, vol. 161, pp. 627-646, 2016.

[21] D. Olsen, Y. Abdelouadoud, P. Liem, S. Hoffmann, and B. Wellig, "Integration of Heat Pumps in Industrial Processes with Pinch Analysis," in 12th IEA Heat Pump Conference, 2017.

[22] F. Bühler, A. Guminski, A. Gruber, T.-V. Nguyen, S. von Roon, and B. Elmegaard, "Evaluation of energy saving potentials, costs and uncertainties in the chemical industry in Germany," Applied Energy, vol. 228, pp. 2037-2049, 2018/10/15/ 2018, doi: https://doi.org/10.1016/j.apenergy.2018.07.045.

[23] J. Van Gerpen, "Biodiesel processing and production," Fuel processing technology, vol. 86, no. 10, pp. 1097-1107, 2005.

[24] D. Luna et al., "Technological challenges for the production of biodiesel in arid lands," Journal of arid environments, vol. 102, pp. 127-138, 2014.

[25] Å. Lindqvist, "Process integration study for increased energy efficiency of a PVC plant," 2011.

[26] P. Cao, M. A. Dubé, and A. Y. Tremblay, "Methanol recycling in the production of biodiesel in a membrane reactor," Fuel, vol. 87, no. 6, pp. 825-833, 2008.

[27] I. Atadashi, M. Aroua, A. A. Aziz, and N. Sulaiman, "The effects of catalysts in biodiesel production: A review," Journal of industrial and engineering chemistry, vol. 19, no. 1, pp. 14-26, 2013.

[28] I. Atadashi, M. Aroua, and A. A. Aziz, "Biodiesel separation and purification: a review," Renewable Energy, vol. 36, no. 2, pp. 437-443, 2011.

[29] K. Suthar, A. Dwivedi, and M. Joshipura, "A review on separation and purification techniques for biodiesel production with special emphasis on Jatropha oil as a feedstock," Asia-Pacific Journal of Chemical Engineering, vol. 14, no. 5, p. e2361, 2019.

[30] M. Dubé, A. Tremblay, and J. Liu, "Biodiesel production using a membrane reactor," Bioresource technology, vol. 98, no. 3, pp. 639-647, 2007.

[31] K. Onarheim, S. Santos, V. Hankalin, P. Kangas, and A. Arasto, "Techno-economic evaluation of retrofitting CCS in an integrated pulp and board mill-Case studies," 2016.

[32] M. J. Bagajewicz and A. F. Barbaro, "On the use of heat pumps in total site heat integration," Computers & Chemical Engineering, vol. 27, no. 11, pp. 1707-1719, 2003.

SECTION 2

OPTIMIZING HEAT PUMP CONFIGURATIONS

CHAPTER 4

IDENTIFYING TECHNO-ECONOMIC IMPROVEMENTS FOR A STEAM-GENERATING HEAT PUMP WITH EXERGY-BASED COST MINIMIZATION

This chapter was originally published as B. W. de Raad, M. van Lieshout, L. Stougie, C. A. Ramirez, "Identifying techno-economic improvements for a steam-generating heat pump with exergy-based cost minimization", Applied Thermal Engineering, Volume 267, 2025, 125632, DOI: https://doi.org/10.1016/j.applthermaleng.2025.125632.

Abstract

Steam generating heat pumps show great potential for reducing carbon emissions in the industrial sector. However, predicting their performance is challenging as the exergy destruction of e.g., compressors and expansion valves increases with the temperature lift and condenser temperature. With over seventy design improvements mentioned in the literature, selecting the most effective design improvements is cumbersome. In this study, energy and exergy-based methods were compared in their ability to identify favourable design changes to a single stage subcritical heat pump to produce steam from hot condensate. The energy-based method suggested the addition of a sequential compressor with an intermediate cooler; however, this design did not improve the heat pump's techno-economic performance. The suggestion of adding either an internal heat exchanger or a flash vessel by exergy-based methods did lead in both cases to improved techno-economic performance. The internal heat exchanger performed best and increased the coefficient of performance from 2.3 to 2.8 and reduced operational costs by 0.8 M€ after 5 years of operation. Additionally, the initial investment decreased by 135 k€, and the total costs of operation decreased from 10.3 M€ to 8.7 M€. These findings show that exergy-based methods are the way forward in identifying effective design improvements for steam generating heat pumps.

1 Introduction

Heat pumps are increasingly recognized as a crucial technology for the energy transition [1]. Marina et al. [2] estimated that heat pumps can reduce industrial CO_2 emissions by 30% when using renewable electricity to upgrade waste streams. However, their deployment is hindered by unfavourable economics compared to other (fossil) heating alternatives [3]. Yet, Marina et al. [4] also identified that most industrial heat is supplied in the form of steam. Utilizing existing steam infrastructure could significantly reduce integration cost, thereby improving the economic feasibility of heat pumps in industry [5].

1.1 Steam-generating heat pumps

Various steam-generating heat pumps (SGHPs) are being developed, or have already come to market, leveraging this economic advantage [6, 7]. For instance, Marina et al. [8] have developed an experimental SGHP that produces steam at 150 °C. Their design consists of a cascade cycle with an intermediate temperature evaporator and internal heat exchangers to superheat suction gas before the compressor of each stage. Similarly, the Kobelco company [9] offers a SGHP that supplies steam at 120 °C. This heat pump uses a two-stage compressor with intermediate cooling and an internal heat exchanger to produce hot water. This hot water is thereafter flashed to produce saturated steam. Higher steam temperatures are achieved by successive steam (re)compression [9]. Both the design by Marina et al. [8] and Kobelco [9] are a more advanced version of the common subcritical single-stage (SS) heat pump cycle aimed at improving the techno-economic performance.

1.2 Economics and exergy analysis of steam-generating heat pumps

The SS cycle becomes uneconomical at higher temperature lifts because of increased operational costs from various irreversibilities. Advanced heat pump configurations aim to minimize these irreversibilities which results in less work being required by the compressor and therefore a higher coefficient of performance (COP). The proposed process alterations in advanced cycles involve adding components such as expanders, compressors, flash vessels, mixers, ejectors, heat exchangers, or entire top or bottom cycles [10]. Additionally, changing the working fluid could also be used to improve performance [11].

Exergy analysis is a technique that helps to identify where irreversibilities occur within a process. Exergy is defined as the theoretical maximum useful work obtained when a system is brought into thermodynamic equilibrium with the environment by means of processes in which the system interacts only with its environment [12]. Exergy analysis has helped to design heat pumps since its initial conception in the 1960s [12]. However, only a few studies exist for high-temperature heat pumps, while Bergamini et al. [13] showed that the distribution of exergy destruction over the components of the high temperature heat pump cycle differs from low temperature heat pumps. Cao et al. [14] studied six single- and two-stage compression heat pump cycles that are frequently discussed in the literature. These heat pump systems can produce hot water at temperatures up to 95 °C from wastewater with a mean temperature of 45 °C. The results demonstrated that a two-stage heat pump with a flash vessel and a two-stage heat pump with a flash vessel as well as an intercooler had significantly less exergy destruction than an SS cycle. Both cycles showed a 10% increase in overall exergy efficiency compared to the SS cycle. Similarly, Arpagaus et al. [15] compared the performance of several multi-temperature heat pump cycles based on designs mentioned in literature and concluded that multi-stage compressor cycles exhibit the best cycle performance as well. However these authors only evaluate the performance at a cycle-level and do not examine the origin of the increased efficiency on a component-level.

The performance of individual components was examined by researchers such as Bergamini et al. [13], Hu et al. [16] and Mateu-Royo et al. [17]. Bergamini et al. [13] used exergy analysis to study the exergy destruction in a high-temperature single-stage ammonia heat pump that produced heat up to 140 °C from an isothermal 30 °C source. They found that the exergy destruction in components increased at different rates. For instance, the exergy destruction in the expansion valves was the most sensitive to the temperature lift and was the highest of all components at high temperature lifts, whereas its contribution to the total exergy destruction was limited at low temperature lifts. Hence, the dominant source of exergy destruction in the heat pump varied among components as the temperature lift increased. Hu et al. [16] found similar results when assessing a multi-stage heat pump that produced pressurized water at 120 °C from a heat source ranging from 50 to 90 °C. Mateu-Royo et al. [17] used exergy analysis to identify possible further improvements to an experimental IHX-cycle setup for heat sinks up to 140 °C. They found that the expansion valve had the lowest exergy efficiency, whereas the compressor had the largest contribution to the total exergy destruction. Whether, design changes would improve the techno-economic performance of these heat pump cycles is not explored in these studies. Yet, exergy analysis provide a basis for economic assessment of a heat pump. For instance, Farshi et al. [18] used exergy-based cost analysis to compare a novel ejector-boosted hybrid heat pump with existing absorption, compression, and absorption-compression heat pumps. Their results show that the newly proposed design provides clear techno-economic advantages over the reference cycles at high temperature lifts. Wang et al. [19] applied the exergy-based economic analysis to compare the performance of mechanically and thermally driven heat pumps. They demonstrate that exergy loss per capital investment, as a function of temperature lift, differs between mechanically and thermally driven heat pumps. Based on this distinction, they formulated a guide map to aid technology selection. In a follow-up study, Wang et al. [20] used the same principles when evaluating the performance of a transcritical heat pump cycle for hot water production and increased the COP of an originally single-stage transcritical cycle by 7% based on design suggestions made in the literature.

The aforementioned studies of high-temperature and/or steam-generating heat pumps either compare previously described heat pump cycles from the literature or use these literature-based cycles to benchmark new cycle layouts. However, they do not demonstrate how exergy-based methods can be used to identify techno-economic design improvements for high-temperature applications and to aid in identifying design improvements. Tsatsaronis and Moran [21] addressed this gap for energy-conversion technologies overall by proposing the method of exergy-aided cost minimization. In their method, they rank the components of a system in descending order of combined cost of investment and exergy destruction. Subsequently, they use this ranking to evaluate how much an additional component would increase both the technical and economic performances.

This study aims to demonstrate how exergy-based cost minimization can systematically identify techno-economic improvements for a steam-generating heat pump, adding a new perspective to the limited body of literature on this topic. The method was illustrated with a case study where 10 tonnes per hour of 2 bar(a) steam are produced from 50 kg/s of wastewater with an initial temperature of 80 °C, as summarize in Table 1. This case study was chosen due to its relevance across various industries, including chemical, paper, and food production. All configurations were modelled using refrigerant R-1234ze(Z) due to its high critical point, low global-warming potential, and ozone depletion potential [22].

Table 1 *Process data of the case study*

Name	Value	Unit
Medium heat sink	Water	-
Pressure heat sink	2	bar(a)
Mass flow heat sink	10	tonnes/hour
Medium heat source	Water	-
Initial temperature heat source	80	°C
Mass flow heat source	50	kg/s
Working medium heat pump	R-1234ze(Z)	-

2 Method

This section outlines the systematic approach used to identify techno-economic improvements for steam-generating heat pumps. Section 2.1 provides a general description of the overall methodology, including the key steps involved. Section 2.2 details the thermodynamic analysis, explaining the principles and calculations used to assess the heat pump's performance. Section 2.3 focuses on the economic evaluation, describing the cost calculations and economic indicators considered.

2.1 Identification of techno-economic improvements

Advancements to a heat pump cycle were explored by using the following four-step method: 1. setting cost targets, 2. performing energy, economic and exergy analysis (3E-analysis), 3. assigning costs to exergy losses, and 4. assessment of design changes. Step 1 was used to make an initial assessment of a heat pump's economic viability compared to an electric boiler (e-boiler). When the resulting investment budget for a heat pump seemed plausible, the next step was initiated. Steps 2 to 4 were part of an iterative loop to repeatedly improve the cycle's performances. For clarity purposes, this loop was demonstrated only once for a SS cycle.

Step 1: To set cost targets, the economic performance of an ideal (i.e., Carnot) heat pump was compared with an e-boiler. This comparison is common in industry because both are a way to realise industrial electrification. The heat pump was defined to be economically viable when the total costs of ownership (TCO) after five years of full-time operation (8000 h) were lower than that of an e-boiler. The cost of electricity was taken to be 0.041 €/kWh based on the expected average electricity costs between 2022 and 2030 in the Netherlands for large consumers [23]. The required capital investment for an e-boiler of the required size was based on an installed capital cost price of 165 €/kW [23]. For the heat pump, an installation cost factor of 3 was used to convert bare unit costs to installed costs [24]. Based on the TCO of an e-boiler and the operational costs of an ideal heat pump, the maximal capital investment for a heat pump was calculated. If the calculated maximal capital costs price of the heat pump was within a realistic cost price range (100-1000 €/kW) [25], the next step was initiated.

Step 2: The energy, economic and exergy (3-E) analysis of the heat pump cycle was performed as follows. The thermodynamic states of the heat pump were fixed by the outlet conditions of both the evaporator and the condenser. For both heat exchangers the pinch point temperature difference was set to 5 K [26]. The vapour exiting the evaporator and the condenser was assumed to be saturated. When subcooling or superheating were considered, the amount of heat transferred was limited by the temperature at the outlet of the compressor to limit the degradation of compressor lubricants and seals. The performance assessment of the compressor included both an isentropic and a mechanical efficiency. The costs of the bare units, e.g., the heat exchangers, were based on their duty and cost functions. The bare unit costs were indexed to December 2022 with the Chemical Engineering Price Index (CEPI) [27] and converted into a total capital investment (TCI) using an installation factor to account for the cost of integrating the unit, contingencies and other fees. The performance of the cycle was defined based on four performance indicators: 1. the total costs of ownership, 2. the initial investment, 3. the coefficient of performance, and 4. the total exergy destruction. Of these, the first two indicated economic viability, whereas the third and fourth gave insight into the technical and environmental performance of the proposed configuration, respectively. The values used in this evaluation are presented in Table 2.

***Table 2**. Modelling parameters*

Name	Abbr.	Value	Unit	Source
Isentropic efficiency compressor	η_{is}	70	%	[28]
Maximal outlet temperature compressor		175	°C	[11]
Intermediate pressure correction		+0.35	bar	[31]
Efficiency mechanical drive	η_m	85	%	[26]
Heat transfer coefficient evaporator	U	1000	W/m²K	[26]
Heat transfer coefficient condenser	U	1250	W/m2K	[26]
Operational hours	t	40,000	h	
Cost of electricity	c_{el}	0.041	€/kW	[23]
Reference state temperature	T_0	298.15	K	
Reference state pressure	p_0	101325	Pa	

Step 3: The exergy-based cost minimization was based the exergy-aided cost minimization algorithm by Tsatsaronis and Moran [21], where the exergy flow rate and is used to calculate the cost flow rate. Since the exergy destruction in the heat pump results in additional work requirements that have to be met by the compressor's drive, the price of exergy destruction was uniformly set to that of electricity. The resulting costs per component were listed in descending order. The process causing the losses in the top ranking component was selected to be changed in step 4.

Step 4: The design change was realized by adding one or several of the standard cycle's components, i.e., a compressor, an expansion valve, an internal heat exchanger, an ejector, a flash tank, a desuperheater, a cascade condenser, and/or an expander. The selection among these components was based on the origin of the exergy destruction and the estimated costs of the design change. Moreover, the way these components were integrated into the cycle was based on the cycles presented in the aforementioned studies by Adamson et al. [10], Arpagaus et al. [3, 15], Mateu-Royo et al. [11], and Schlosser et al. [29].

After changing the cycle configuration in step 4, step 2 was repeated to evaluate the techno-economic performance of the change in the design. The change was approved when it improved the techno-economic performance of the previously evaluated heat pump configuration, which was followed by suggesting further improvements based on repeating steps 3 and 4. When the change of step 4 was disapproved in step 2, the design change was discarded and the iterative optimization was ended.

Cycle improvements were also based on an energy analysis to benchmark the results of the exergy-based cost minimization with a more common approach.

2.2 Thermodynamic analysis

2.2.1 Energy analysis

The basis of the energy balance was a consistent mass balance. The mass flow rate of the refrigerant (m_r) was defined by the heat transfer required in the condenser (Q_{cd}) and the enthalpy difference ($m_r \Delta h_{cd}$) over the condenser, as shown in Eq. (1):

$$Q_{cd} = m_r \Delta h_{cd} \quad (1)$$

The refrigerant exited the condenser as a saturated liquid. All open systems were assumed to operate in a steady state, thus without mass accumulation. This also holds in the case of a (flash) vessel, where the vapor left in a saturated state and an enthalpy balance defined the mass ratio of its outgoing streams.

Work added to the system (W_c) by the compressor was based on the isentropic enthalpy difference (Δh_{is}) over the compressor and an isentropic efficiency (η_{is}) [28, 30], as indicated in Eq. (2):

$$W_c = \frac{m_r \Delta h_{is}}{\eta_{is}} \quad (2)$$

The work required by the compressor's drive (W_D) was based on a correction for electrical, volumetric, and mechanical losses based on overall motor efficiency (η_m) [26], as shown in Eq. (3):

$$W_D = \frac{W_c}{\eta_m} \quad (3)$$

The intermediate pressure (p_i) was corrected by 0.35 bar when multiple pressure stages were considered based on the work by Mateu-Royo et al. [31], as in Eq. (4):

$$p_i = \sqrt{p_1 p_2} + 0.35 \quad (4)$$

where p_1 and p_2 are the pressures before and after the compressor, respectively. Pressure relief in expansion valves was considered isenthalpic. Other forms of pressure loss were neglected, as well as heat losses. The coefficient of performance (COP) of the heat pump was based on the heat delivered at the condenser and the work required by the compressor's drive, as shown in Eq. (5):

$$COP_{hp} = Q_{cd}/W_D \quad (5)$$

The energy balance of the heat pump was closed by defining the required thermal duty of the evaporator as the difference between the duties of the condenser and the compressor.

2.2.2 Exergy analysis

The influx of exergy ($\dot{E}x_{in}$) equals the outflux of exergy ($\dot{E}x_{out}$) plus exergy losses. The loss of exergy was the sum of internal exergy destruction (Ex_{des}) and transfer of exergy to external sources [32]. Since heat loss to the environment was neglected and all heat transferred from the heat pump to the environment was valuable, the exergy balance simplifies to Eq. (6):

$$\dot{E}x_{des} = \Sigma\dot{E}x_{in} - \Sigma\dot{E}x_{out} \quad (6)$$

Exergy destruction was zero in the case of an ideal operation. In that case, the exergy flowing into the system in the form of heat at the evaporator and work by the compressor was equivalent to the exergy of the outflow of heat at the condenser. The exergy value of the streams was defined by the enthalpy (H) and entropy (S) of the stream shown in Eq. (7) [33]:

$$Ex = H - H_0 - T_0(S - S_0) \quad (7)$$

Where subscript "0" denoted the reference state at T_0 = 298.15 K and p_0 = 101325 Pa. Substituting Eq. (7) in Eq. (6) and accounting for the exergy value of heat: at a thermodynamic mean temperature and that of work: W, results in Eq. (8):

$$\dot{E}x_{des} = \left(1 - \frac{T_0}{T}\right)\dot{Q} + \dot{W} - \dot{m}[h_2 - h_1 - T_0(s_2 - s_1)] \quad (8)$$

Exergy destruction due to mechanical losses in the drive was taken as equivalent to the loss of work during transfer.

2.3 Economic evaluation

The total cost of ownership and the total capital investment were taken as the key performance indicators for the economic evaluations. These costs were based on the indexed bare unit costs of the components, the cost of installation, and operation. The bare unit costs ($C_{0,p}$) required for the heat pump's components were based on the costs function provided by Zühlsdorf et al. [26], which is presented in Eq (9):

$$\log(C_{0,p}) = k_1 + k_2 \log x + k_3 (\log x)^2 \quad (9)$$

where "x" is the scaling parameter of a certain technology and "k_i" is a calibrated value. Table 3 shows the used values adapted from Zühlsdorf et al. [26].

Table 3 *Parameters for estimation of component capital costs according to Zühlsdorf et al. [26]*

Component	Scaling Parameter X	Range	k_1	k_2	k_3	f_{cepi} [34]	f_{if}
Compressor	Fluid power	450 - 3000 kW	2.2897	1.13604	-0.1027	2.3749	2.8
Drive	Shaft power	75 - 2600 kW	1.9560	1.7142	-0.2282	2.3749	1.5
Plain vessel	Volume	1 – 800 m^3	3.5970	0.2163	0.0934	2.0793	3.0
Shell & tube heat exch.	Area	10 – 900 m^2	3.2476	0.2264	0.0953	2.0793	3.2
Radial turbine	Fluid power	100 – 1500 kW	2.2476	1.4965	-0.1618	2.3749	3.5

The values in this table were harmonized into the equivalent costs of the components for December 2022 with fcepi based on the Chemical Engineering Price Index (CEPI) [34]. That is, the indexed bare unit cost (C0,ind) were calculated according to Eq. (10):

$$C_{0,p,ind} = C_{0,p} f_{cepi} \tag{10}$$

The indexed bare module costs were converted into capital investment (CI) using the installation costs factor (f_{IF}), as shown in Eq. (11):

$$CI_p = C_{0,p,ind} f_{IF} \tag{11}$$

The total capital investment (TCI) was calculated by taking the sum of all components in the configuration. For benchmarking purposes, this value is expressed as a factor of the condenser duty. For the centrifugal compressor and its drive, Eq. (4) was used as input for the scaling parameter by either including or excluding, respectively. The resulting costs were benchmarked to the cost data provided in the DACE booklet [35] and found to be plausible. In case multiple compressors were used, their scaling parameters were combined to account for the economics of scale. Their respective costs were based on the ratio between the scaling factor of the individual component and the scaling factor of the combined components. The volume of a vessel was based on being able to supply the outlet streams for 10 minutes without an influx of new refrigerant. The heat exchanging area (A) of the heat exchangers was calculated using Eq. (12):

$$Q_{hx} = U \cdot A \cdot \Delta T_{lm} \tag{12}$$

where "U" is the heat transfer coefficient and was the logarithmic mean temperature difference between the hot and cold streams. A heat transfer coefficient of 1000 W/m^2K was used for heat transfer between a liquid and an evaporating liquid and 1250 W/m^2K was used when both sides were changing phases [26]. The operational cost ($C_{op,hp}$) of the heat pump (hp) was defined to be equivalent to the price of electricity (c_{el}) times the exergy destruction by component (p) and time of operation (t), as shown in Eq. (13):

$$C_{op,hp} = \sum \dot{E}x_{des,p} \cdot c_{el} \cdot t \tag{13}$$

From Eq. (13), the cost of compensating irreversibilities (i) required due to exergy destruction of component "p" ($\dot{C}_{i,p}$) can be calculated as Eq. (14):

$$\dot{C}_{i,p} = \dot{E}x_{des,p} \cdot c_{el} \cdot t \quad (14)$$

Economically viable investments were those with an investment cost lower than savings according to Eq. (14) after five years of full-time operation. Moreso, by combining the TCI and the $C_{op,hp}$ the total cost of ownership (TCO) was calculated, as in Eq. (15):

$$TCO = TCI + C_{op,hp} \quad (15)$$

The TCO was calculated based on five years of near full-time operation (40,000 hours).

3 Results

This section presents the findings from the techno-economic analysis of steam-generating heat pumps. Section 3.1 compares the economic viability of an ideal heat pump with that of an electric boiler (e-boiler), establishing a baseline for comparison. Section 3.2 provides the results of the energy, economic, and exergy (3-E) analysis of the subcritical single-stage (SS) cycle, highlighting key performance metrics. Section 3.3 evaluates the performance of proposed cycle improvements, detailing the enhancements and their impacts. Finally, Section 3.4 compares the different configurations, summarizing the overall findings and identifying the most effective design modifications.

3.1 Cost targets for a steam-generating heat pump

Producing 10 t/h of 2.0 bar(a) steam with an e-boiler required 6.6 MW of electricity. Based on the assumed installed costs of 165 €/kW and an electricity price of 0.041 €/kWh, this resulted in a total cost of ownership (TCO) of 11.9 M€ after 5 years, as listed in Table 4. The total costs of ownership of the heat pump must be below that of the e-boiler to be competitive. An ideal heat pump would operate with a COP of 6.6 and reduce electricity consumption by 85%. As a result, it would require 1.0 MW to operate, or 1.6 M€ after five years. Therefore, the total installed costs of the heat pump must be below 10.3 M€, or 520 €/kW_{th}, to be economically viable.

Table 4. Costs comparison of an ideal e-boiler with an ideal heat pump based on 5 years of operation, 8000 h/year, and an electricity price of 0.041 €/kWh

Unit	Supplied power [MWth]	Required power [MWe]	Specific costs [€/kWx]	Bare unit costs [M€]	Total installed costs [M€]	Operational costs [M€]	Total costs of ownership [M€]
e-boiler	6.6	6.6	-	-	1.1	10.8	11.9
Heat pump	6.6	1.0	<520	<3,4	<10.3	<1.6	<11.9

3.2 Energy, Exergy, and Economic performance assessment of a subcritical single-stage heat pump

The SS cycle consists of an evaporator, compressor, condenser and expansion valve. The results of the 3-E analysis of this cycle are presented in Table 5. These results show that the compressor's drive is the largest energy consumer. The electric drive of the compressor required 2.9 MW and the COP was therefore 2.3. Hence, compared to the ideal heat pump's 1.0 MW electricity consumption, 1.9 MW is required to compensate for exergy destruction. No costs were assigned to the expansion valve as the required capital investment was two orders of magnitude less than that of the other components. The compressor and its electric drive cost 3.2 M€, making up for more than 70% of the total installed costs. Total costs of ownership (TCO) of 9.2 M€ were based on the electricity consumption of the drive and the total installed costs. The indexed bare unit cost of the module was 233 €/kW.

The results presented in Table 5 highlight that energy is solely required by the compressor and its drive. Consequently, enhancing the compressor's efficiency emerges as a logical solution based on the energy analysis. The table also shows that the expansion valve is responsible for most of the exergy destruction, accounting for 689 kW (or 37% of total exergy destroyed) and incurring operational losses of over 1.1 M€ after 5 years of operation. The compressor is the second largest source of exergy destruction (23% of total exergy destroyed at 545 kW) and adds 0.9 M€ to the operational losses after 5 years. The impact of the heat exchangers on the operational cost is below 5%. Consequently, utilizing the exergetic potential of the stream before the expansion valve whilst trying to improve on the performance of the compressor should be pursued based on the results of the exergy analysis.

Table 5. 3E-evaluation of a SS cycle heat pump based on 5 years of operation, 8000 h/year, and an electricity price of 0.041 €/kWh.

Component	Heat transfer [MW]	Required power [MW]	Exergy destruction [kW]	Operational losses [k€]	Scaling factor [X]	Indexed bare unit costs [k€]	TCI [k€]	TCO [M€]
Evaporator	4.1	0.0	95	156	278	161	514	
Compressor	0.0	2.4	545	894	2,448	724	2,028	
Drive	0.0	2.9	432	708	2,880	412	1,153	
Condenser	6.6	0.0	87	142	1,054	248	792	
Exp. Valve	0.0	0.0	689	1,131				
Total			1,848	3,031		1,544	4,488	9.2

3.3 Improving the subcritical single-stage heat pump configuration

The results of the energy analysis indicated that increasing the efficiency of the compressor is pursued with a two-stage compression cycle with intermediate cooling (2IC), as depicted in Fig. 1.A.

The results of the exergy analysis indicated that utilizing the exergy before the expansion valve. Utilization of exergy in another process step can either be achieved by exergy transfer through heat exchange or mixing. The use of an internal heat exchanger (IHX) (Fig. 1.B) is a cost effective way to exchange heat [36]. Mixing is realized in the two-stage compression with a flash vessel (2FV) cycle (Fig. 1.C). This cycle also increases the compressor's efficiency by reducing the inlet temperature of the high pressure compression stage [17]. For this reason, this cycle design is selected over the additionally listed two-stage compression cycle with a closed economizer by Adamson et al. [10], as that option does not have this benefit. Another benefit of the 2FV cycle is that many industrial scale compressors allow for some form of two-stage compression within the same compressor unit and hence two-stage compression does not significantly increase equipment cost when applying intermediate cooling, something that would not be possible with a cascade cycle [7].

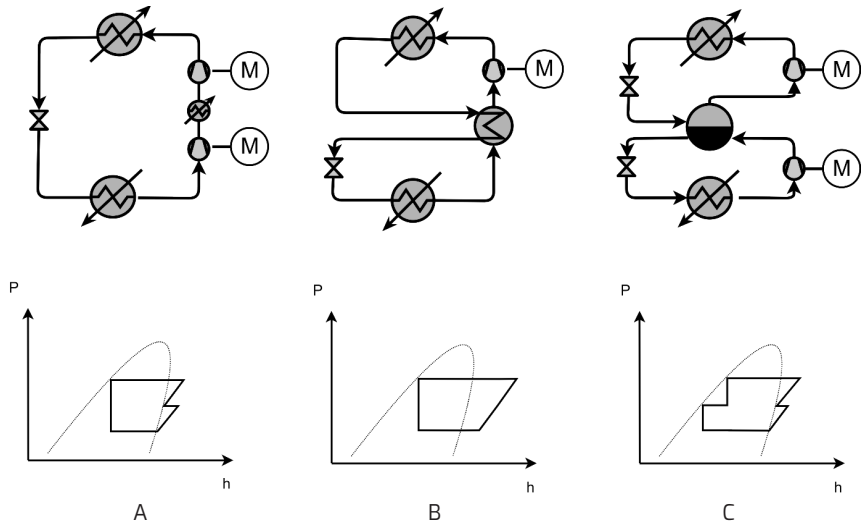

Figure 1 *Overview of advanced configurations and their log p-H diagrams. A) two-stage compression and intermediate cooler (2IC) cycle, B) Internal heat exchanger (IHX) cycle, and C) two-stage compression with a flash vessel (2FV) cycle.*

3.3.1 Subcritical two-stage compression with intermediate cooling cycle

The introduction of a second compression stage with an intermediate cooling to transform the SS cycle into the 2IC cycle, configuration A, reduces the COP from 2.3 to 2.2. Exergy losses are dominated by the expansion valve at 641 kW, or 32% (Table 6). However, combined losses in both compressors and drives account for 1,042 kW of the total 2,016 kW exergy destroyed, i.e. 53%. Though the specific work requirements by the compressor were slightly reduced by the intermediate cooling step, these gains are negated by the required increase in refrigerant mass flow to meet the energy demand in the condenser. This is partially a result of not being able to utilize the apparent heat in the intercooler due to its relatively low temperature of 89 – 92 °C and an initial sink temperature of 80 °C with an advised minimal temperature difference of at least 5 K [26]. Due to the higher work requirements and the additional investment, the total cost of ownership of this configuration is higher than that of the original SS cycle. The total installed costs of the configuration are 4.9 M€, with a TCO of 9.4 M€, or 254 €/kW as a bare module.

Table 6 *3E-evaluation of the two-stage compression and intermediate cooling cycle based on 5 years of operation, 8000 h/year, and an electricity price of 0.041 €/kWh.*

Component	Heat transfer [MW]	Required power [MW]	Exergy destruction [kW]	Operational losses [k€]	Scaling factor [X]	Indexed bare unit costs [k€]	TCI [k€]	TCO [M€]
Evaporator	4.3	0.0	174	286	282	161	516	
Compressor 1	0.0	1.4	343	563	1,392	397	1,112	
Drive 1	0.0	1.6	246	403	1,637	223	625	
intercooler	0.3	0.0	55	90	102	121	388	
Compressor 2	0.0	1.2	264	433	1,183	338	946	
Drive 2	0.0	1.4	209	342	1,392	190	530	
Condenser	6.6	0.0	84	138	1,054	248	792	
Exp. Valve	0.0	0.0	641	1,052				
Total			2,016	3,307		1,678	4,909	9.4

3.3.2 Subcritical single stage with internal heat exchanger cycle

The addition of an internal heat exchanger (IHX) to the SS cycle, to form the IHX cycle (configuration B), significantly increases the overall performance of the heat pump, leading to a reduction in the total costs of ownership (TCO) by 0.5 M€ compared to the SS cycle. Although the installation of the IHX increases the initial installed costs by 0.5 M€, the reduction in the size of the compressor and electric drive results in savings of 135 k€ in installed costs and a reduction of 0.8 M€ in operational costs after 5 years (Table 7). The total cost of ownership for the heat pump with the IHX is 8.7 M€ or 248 €/kW as a bare module.

The lower operational cost are reflected in the increase in the COP from 2.3 to 2.8. The total exergy destruction is reduced by 490 kW to 1,358 kW. The compressor is the main source of exergy destruction at 379 kW (28% of the total exergy destruction), followed by its driver at 351 kW (25%) and the condenser at 290 kW (22%). The exergy destruction becomes more evenly distributed among the components with the introduction of the IHX. The increase in exergy destruction in the evaporator is due to the higher COP, requires more energy from the sink and results in a temperature drop from 55 to 54 °C of the source. The exergy destruction in the condenser significantly increases due to its high inlet temperature, which is caused by superheating the suction gas before the compressor with the IHX. The IHX itself has an exergy destruction of 64 kW.

Table 7 3E-evaluation of the internal heat exchanger cycle based on 5 years of operation, 8000 h/year, and an electricity price of 0.041 €/kWh.

Component	Heat transfer [MW]	Required power [MW]	Exergy destruction [kW]	Operational losses [k€]	Scaling factor [X]	Indexed bare unit costs [k€]	TCI [k€]	TCO [M€]
Evaporator	4.6	0.0	195	319	288	162	520	
Compressor	0.0	2.0	379	621	1,991	682	1,909	
Drive	0.0	2.3	351	576	2,342	406	1,137	
IHX	2.3	0.0	64	105	185	143	456	
Condenser	6.6	0.0	290	476	1,054	248	792	
Exp. Valve	0.0	0.0	79	130				
Total			1,358	2,227		1,640	4,814	8.7

3.3.3 Subcritical two-stage compression with a flash vessel cycle

The two-stage compression with flash vessel (2FV) cycle, configuration C, splits work requirements over two compressors with a combined duty of 2 MW, or 2.4 MW at the electric drive (Table 8). Hence, the required 6.6 MW at the condenser can be delivered with a COP of 2.8. Exergy destruction is evenly distributed among the components. The second stage compressor was the main source of exergy destruction at 269 kW (19% of total exergy destroyed), followed by its drive at 212 kW (15%) and the expansion valve directly after the condenser at 207 kW (15%). Together with the first stage and their drives, the compressors accounted for 60% of total exergy destruction, compared to 21% of both expansion valves. The exergy destruction in the evaporator increased by 100 kW as more heat was transferred. The intermediate cooling in the vessel slightly reduced exergy destruction in the condenser compared to the SS cycle. The vessel itself has a negligible amount of exergy destruction. Exergy destruction in the expansion valves went from 689 kW in the SS cycle to 294 kW for both valves. As a result, total exergy destruction was reduced by 445 kW. The reduced size of the compressors and electric drive reduced investment costs by 43 k€. However, the installation of the vessel requires an additional 0.55 M€. The TCO is 8.8 M€, or 255 €/kW as a bare module. Hence, the initial investment increases compared to the SS cycle, but the increased efficiency mitigates the impact of operational costs and reduces the TCO by 0.4 M€ during the five years.

Table 8 3E-evaluation of the two-stage compression and a flash vessel cycle based on 5 years of operation, 8000 h/year, and an electricity price of 0.041 €/kWh.

Component	Heat transfer [MW]	Work transfer [MW]	Exergy destruction [kW]	Operational losses [k€]	Scaling factor [X]	Indexed bare unit costs [k€]	TCI [k€]	TCO [M€]
Evaporator	4.5	0	192	314	287	162	519	
Compressor 1.	0	0.8	204	335	826	279	781	
Driver 1.	0	1.0	146	239	972	165	463	
Vessel	5.4	0	1	2	690	183	548	
Compressor 2.	0	1.2	269	442	1,207	407	1,140	
Driver 2.	0	1.4	213	349	1,420	241	676	
Condenser	6.6	0	84	138	1,054	248	792	
Exp. Valve 1.	0	0	207	339				
Exp. Valve 2.	0	0	87.4	143				
Total			1,403	2,301		1,685	4,919	8.8

3.4 Comparison of configurations

The results presented in tables 5 to 8 are visualized in Fig. 2. The left figure shows that all advanced cycles have a lower total exergy destruction than the SS cycle. The figure also shows the exergy destruction of the different components within the heat pump and, for example, the strong increase in exergy destruction at the evaporators of the advanced cycles due to the increased thermal demand. The figure also shows that the two exergy-based designs significantly reduced the exergy destruction in the expansion valve compared to the SS and the 2IC cycle. The IHX performed by far the best in this aspect. However, this is largely offset by the increase in exergy destruction in the condenser due to the high outlet temperature of the compressor. Due to this offset, the total exergy destruction by the IHX and the 2FV cycle are comparable. The exergy destruction in the 2FV cycle is more distributed among its components, which provides a lower basis for the next design iteration. Thermodynamically, the IHX cycle performs similar to the 2FV cycle, as the 2FV cycle has only a slightly higher total exergy destruction of 1,403 kW compared to 1,358 kW of the IHX cycle.

The figure on the right shows the required total capital investment of the four cycles on the primary y-axis and on the secondary y-axis their total cost of ownership. The graph shows the dominance of the compressor(s) and its/their drives in the total capital investment. The figure also shows that the IHX cycle economically outperforms the 2IC cycle based on by the energy analysis. The TCI of the IHX cycle is comparable to that of the 2FV cycle, as the 2FV cycle has a slightly higher TCI of 4,919 k€ versus 4,814 k€ of the IHX cycle.

Combined, the two graphs in Fig. 2 show that the designs based on exergy-based cost minimization have a higher techno-economic performance than the designs based on energy analysis. Moreover, the design change in the 2IC cycle, based on by the energy analysis, increased exergy destruction whilst increasing the TCO to 9.4. The design changes in the exergy-based cost minimization, on the other hand, had a lower TCO than the SS cycle. Both design changes increased the SS cycle's COP from 2.3 to 2.8. The introduction of the IHX increased the total capital invested by 330 k€ whilst reducing the total cost of ownership after 5 years by 0.5 M€. The 2FV cycle was slightly more costly and required an additional 0.6 M€ investment, decreasing the reduction of the total cost of ownership to 0.4 M€ with respect to the SS cycle.

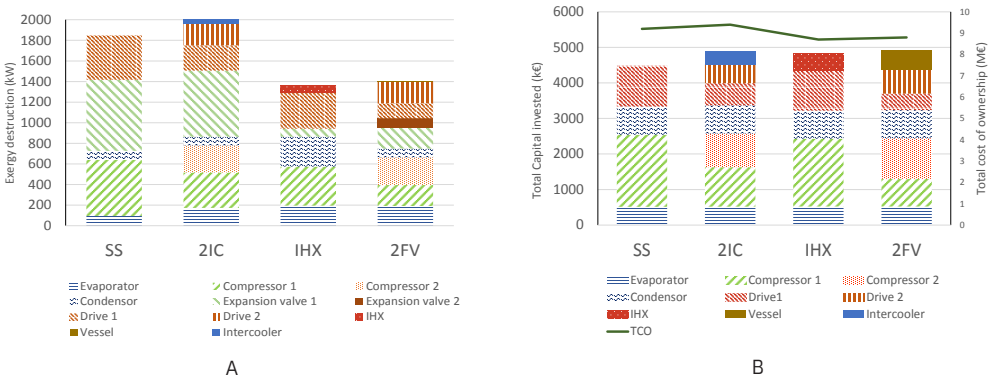

Figure 2 *Comparison of configurations. Figure A shows the exergy destruction by the subcritical single-stage (SS) cycle, compared to that of the two-stage cycle with an intermediate cooler (2IC), the cycle with an internal heat exchanger (IHX), and that of the heat pump with the two-stage compressor and flash vessel (2FV). Figure B shows the total capital invested and total cost of operation of these cycles.*
4 Discussion

4 Discussion

The findings of this study are in line with the results of Bergamini [13] and Hu [22]. Similar to their work, our results showed that the expansion valve is the largest single source of exergy destruction in the SS cycle, followed by the compressor in steam-generating applications. Moreover, the COP of 2.3 for the SS cycle is comparable to the COPs based on experiments and simulations, i.e. 1.7 to 2.3, when transferring heat of 60 - 100 °C to a heat sink of 140 °C listed by Adamson et al. [10]. Moreso, the COP of the IHX cycle is likely of the right order, as it is slightly below the 3.05 reported by Wang et al. [37] based on experiments with a SGHP with a 70 °C heat source. However, this improvement contradicts the listed performance by Adamson et al. [10] which shows that the IHX cycle does not significantly improve upon the SS's performance (Table 1), which highlights the added value of the method proposed in this paper. Moreover, the COP of the heat pump with 2FV cycle is comparable the COP of 2.9 reported by Kosmadakis et al. [36] for the same process conditions using R1234ze(Z) and a numerical model for the efficiency of the compressor.

The results also show that the exergy-based improvements of the cycles outperform energy-based improvements due to their ability to utilize waste streams. The lower thermodynamic performance and high required investment cost of the 2CI cycle make it unlikely that changes in either operational or investment cost will alter this outcome. The techno-economic performance of the IHX cycle was comparable to that of the 2FV cycle, as there is no significant difference in the amount of total exergy destruction (1,403 kW for the 2FV cycle compared to 1,358 kW for the IHX cycle) and the total capital invested (TCI) (4,919 k€ for the 2FV cycle versus 4,814 k€ for the IHX cycle). Changes in modelling assumptions, assumed cost prices or installation cost factors might bring these performances even closer together or tip the scales. Herein, a key modelling assumption is working with a constant and relatively low isentropic efficiency for the compressor. The use of temperature dependent isentropic efficiencies, as proposed by Mateu-Royo et al. [11], might be a disadvantage for the IHX cycle where suction gas is preheated. However, this disadvantage might again be compensated by using a compressor with a higher isentropic efficiency, e.g. 80% compared to the used 70% [13]. The cost functions and installation cost factors are another key factor in this evaluation as the total indexed bare unit cost only differs by 40 k€ or 2%.

Nonetheless, both solutions demonstrate that using insights from exergy-based cost minimization improve the techno-economic performance of SGHPs more than energy-based solutions. However, the method is limited because important decision aspects such as process dynamics, maintainability and environmental impact are not included. Another point to consider is that, although the method allows for the addition of top/bottom cycles, an extension of the method to identify when adding or changing the working media improves performance would be beneficial.

5 Conclusions and recommendations

An iterative method was developed to identify techno-economic improvements for a steam-generating heat pump. It was demonstrated that exergy-based cost minimization can be used as a systematic assessment tool to identify techno-economic improvements for steam-generating heat pumps (SGHPs). By applying this approach, the study adds a new perspective to the limited body of literature in exergy-based cost analysis of SGHPs. The method identified the most cost-effective design change to increase the techno-economic performance of the SS cycle. This is realized by adding an internal heat exchanger (IHX) and utilizing the exergetic potential of the stream after the condenser. This change increases the COP from 2.3 to 2.8 and lowers the total cost of ownership (TCO) from 9.2 M€ to 8.7 M€ after 5 years.

Furthermore, the results showed that exergy-based design changes resulted in a higher COP and lower TCO than energy-based ones. The results of the energy analysis indicated that improving the compressor efficiency with the help of intermediate cooling. The COP of this cycle decreased by 0.1, whilst increasing the TCO. The exergy-based design changes increased the SS cycle's COP from 2.3 to 2.8 at similar investments. Hence, the exergy-based cost minimization proved to be a better performing assessment tool than energy analysis to systematically identify improvement to SGHP cycles.

Future work should develop a more detailed thermodynamic analysis (e.g., using temperature dependent isentropic efficiencies) to improve the assessment of strengths and weaknesses of a cycle, provide a framework to link working media to exergy destruction, and expand on the considered aspects during the decision process (e.g., environmental footprint and process dynamics).

Nomenclature

2CI	two-stage compression with interm. cooling
2FV	two-stage compression with flash vessel
A	heat exchanger area (m2)
C	costs (€)
COP	Coefficient of Performance
Ex	exergy [kJ/kg]
f	factor (-)
h	enthalpy [kJ/kg]
IHX	internal heat exchanger
K	costs factor (-)
m	mass flow rate [kg/s]
q	heat transfer rate [kW]
S	entropy [kJ/kgK]
SS	subcritical single-stage
T	temperature [K]
t	time (s)
TCI	total capital investment (€)
TCO	total costs of ownership (€)
U	heat transfer coefficient [W/m2K]
W	work/power [kW]
X	scaling factor

Subscripts & superscripts

0,p	bare unit value of component “p”
c	compressor
cd	condenser
CEPI	Chemical Engineering Plant Costs Index
d	drive
des	destruction
el	electricity
evap	evaporator
hp	heat pump
hx	heat exchanger
i	intermediate
if	installation factor
in	influx
ind	index(ed)
is	isentropic
lm	logarithmic mean
m	mechanical
out	outflux
op	operational
r	refrigerant

Greek symbols

η	efficiency
Δ	difference

References

[1] F. -ISE. "Heat Pumps - A key technology for the energy transition." Fraunhofer ISE. https://www.ise.fraunhofer.de/en/key-topics/heat-pumps.html (accessed.

[2] A. Marina, S. Spoelstra, H. A. Zondag, and A. Wemmers, "An estimation of the European industrial heat pump market potential," Renewable and Sustainable Energy Reviews, vol. 139, p. 110545, 2021.

[3] C. Arpagaus, F. Bless, M. Uhlmann, J. Schiffmann, and S. S. Bertsch, "High temperature heat pumps: Market overview, state of the art, research status, refrigerants, and application potentials," Energy, vol. 152, pp. 985-1010, 2018.

[4] A. Marina, S. Spoelstra, H. Zondag, and A. Wemmers, "An estimation of the European industrial heat pump market potential," Renewable and Sustainable Energy Reviews, vol. 139, p. 110545, 2021.

[5] F. Bless, C. Arpagaus, S. S. Bertsch, and J. Schiffmann, "Theoretical analysis of steam generation methods-Energy, CO2 emission, and cost analysis," Energy, vol. 129, pp. 114-121, 2017.

[6] S. Klute, M. Budt, M. van Beek, and C. Doetsch, "Steam generating heat pumps–Overview, classification, economics, and basic modeling principles," Energy Conversion and Management, vol. 299, p. 117882, 2024.

[7] B. Zühlsdorf, "High-Temperature Heat Pumps: Task 1–Technologies. Annex 58 about High-Temperature Heat Pump," ed: Heat Pump Center c/o RISE, 2023.

[8] A. Marina, S. Smeding, A. Emmers, S. Spoelstra, and P. Kremers, "Design an d Experimental Results of a Two-Stage Steam Producing Industrial Heat Pump," i, no. 13th, 2021.

[9] T. Kaida, "Steam Grow Heat Pump / SGH120 - Kobelco Compressors Corporation," 2022. [Online]. Available: https://heatpumpingtechnologies.org/annex58/wp-content/uploads/sites/70/2022/07/technologykobelcos-gh120-1.pdf.

[10] K.-M. Adamson et al., "High-temperature and transcritical heat pump cycles and advancements: A review," Renewable and Sustainable Energy Reviews, vol. 167, p. 112798, 2022.

[11] C. Mateu-Royo, C. Arpagaus, A. Mota-Babiloni, J. Navarro-Esbrí, and S. S. Bertsch, "Advanced high temperature heat pump configurations using low GWP refrigerants for industrial waste heat recovery: A comprehensive study," Energy conversion and management, vol. 229, p. 113752, 2021.

[12] E. Sciubba and G. Wall, "A brief commented history of exergy from the beginnings to 2004," International Journal of Thermodynamics, vol. 10, no. 1, pp. 1-26, 2007.

[13] R. Bergamini, J. K. Jensen, and B. Elmegaard, "Thermodynamic competitiveness of high temperature vapor compression heat pumps for boiler substitution," Energy, vol. 182, pp. 110-121, 2019.

[14] X.-Q. Cao, W.-W. Yang, F. Zhou, and Y.-L. He, "Performance analysis of different high-temperature heat pump systems for low-grade waste heat recovery," Applied Thermal Engineering, vol. 71, no. 1, pp. 291-300, 2014.

[15] C. Arpagaus, F. Bless, J. Schiffmann, and S. S. Bertsch, "Multi-temperature heat pumps: A literature review," International Journal of Refrigeration, vol. 69, pp. 437-465, 2016.

[16] B. Hu, D. Wu, L. Wang, and R. Wang, "Exergy analysis of R1234ze (Z) as high temperature heat pump working fluid with multi-stage compression," Frontiers in Energy, vol. 11, pp. 493-502, 2017.

[17] C. Mateu-Royo, J. Navarro-Esbrí, A. Mota-Babiloni, F. Molés, and M. Amat-Albuixech, "Experimental exergy and energy analysis of a novel high-temperature heat pump with scroll compressor for waste heat recovery," Applied Energy, vol. 253, p. 113504, 2019.

[18] L. G. Farshi, S. Khalili, and A. Mosaffa, "Thermodynamic analysis of a cascaded compression–absorption heat pump and comparison with three classes of conventional heat pumps for the waste heat recovery," Applied Thermal Engineering, vol. 128, pp. 282-296, 2018.

[19] M. Wang, C. Deng, Y. Wang, and X. Feng, "Exergoeconomic performance comparison, selection and integration of industrial heat pumps for low grade waste heat recovery," Energy Conversion and Management, vol. 207, p. 112532, 2020.

[20] Y. Wang, Y. Yin, and F. Cao, "Comprehensive evaluation of the transcritical CO2 ejector-expansion heat pump water heater," International Journal of Refrigeration, vol. 145, pp. 276-289, 2023.

[21] G. Tsatsaronis and M. J. Moran, "Exergy-aided cost minimization," Energy Conversion and Management, vol. 38, no. 15-17, pp. 1535-1542, 1997.

[22] P. Hu, Q. Hu, Y. Lin, W. Yang, and L. Xing, "Energy and exergy analysis of a ground source heat pump system for a public building in Wuhan, China under different control strategies," Energy and Buildings, vol. 152, pp. 301-312, 2017.

[23] P. P. voor de Leefomgeving, "Klimaat-en Energieverkenning 2022," 2022.

[24] J. F. Richardson, Coulson and Richardson's chemical engineering V6 -Ch.6. 2002.

[25] B. Zuhlsdorf, "Task 1: Technologies – State of the art and ongoing developments for systems and components," in About High Temperature Heat Pumps, vol. 58. https://heatpumpingtechnologies.org/annex58/task1/: International Energy Agency, 20.

[26] B. Zühlsdorf, F. Bühler, M. Bantle, and B. Elmegaard, "Analysis of technologies and potentials for heat pump-based process heat supply above 150 C," Energy Conversion and Management: X, vol. 2, p. 100011, 2019.

[27] U. S. B. o. L. Statistics. "Databases, Tables & Calculators by Subject - Inflation & Prices." https://www.bls.gov/data/ (accessed 21/02/2023, 2023).

[28] A. Copco, "Steam Screw compressor SR6-2800-16 VSD," ed, 2023.

[29] F. Schlosser, M. Jesper, J. Vogelsang, T. Walmsley, C. Arpagaus, and J. Hesselbach, "Large-scale heat pumps: Applications, performance, economic feasibility and industrial integration," Renewable and Sustainable Energy Reviews, vol. 133, p. 110219, 2020.

CHAPTER 5

ADVANCED EXERGO-ECONOMIC ANALYSIS OF STEAM-GENERATING HEAT PUMP CYCLES

Abstract

SHeat pumps are key to industrial decarbonization, but their high installation costs hinder widespread adoption. Steam-generating heat pumps (SGHPs) offer a cost-effective solution by integrating with existing infrastructure. Their techno-economic performance is largely influenced by the required stream temperature and the configuration of the heat pump cycle, yet the exact causes remain unclear. This study employs advanced exergo-economic analysis to investigate these factors at a component level.

The results indicate that direct steam production via a mechanical vapor recompression (MVR) system is the most economically viable option. When direct production is infeasible, a single-stage subcritical (SS) cycle feeding steam at 80 °C into an MVR is optimal for steam temperatures above 130 °C. At intermediate temperatures between 80 °C and 130 °C, a closed cycle heat pump performs comparably or better, with the preferred configuration varying based on sink temperature and temperature lift. The study reveals that this is a result of different decline rates in efficiency and the quality of the ingoing stream. Moreover, it shows that exergy destruction becomes more endogenous to the components with higher sink temperatures and more dispersed throughout the cycle with additional components. These insights enhance the understanding of SGHP design and highlight pathways for industrial implementation.

1 Introduction

Heating processes are the primary source of industrial CO_2 emissions [1]. While upgrading waste heat with heat pumps powered by renewable electricity presents a promising decarbonization solution, the high initial investment costs of heat pumps remain a significant barrier compared to less sustainable alternatives [2]. These costs can be mitigated by integrating heat pumps with existing steam infrastructure [3]. Previous studies, such as those by Bless et al. [4] have shown that a closed cycle heat pump with sequential mechanical vapour recompression (MVR) (Fig. 1.a) is thermodynamically optimal for steam production. However, the impact of evaporation temperature and the configuration of closed cycle heat pumps on the techno-economic performance of steam-generating heat pumps (SGHPs) remains unclear.

Generating steam from waste heat requires a substantial temperature increase. The resulting thermodynamic losses render the typically used single-stage subcritical (SS) cycle heat pump (Fig. 1.b) uneconomic [5]. Adding expanders, compressors, flash vessels, mixers, ejectors, heat exchangers or entire top or bottom cycles to the SS cycle are needed to enhance its economic viability [6]. A study by Kosmadakis et al. [7] on the impact of adding an internal heat exchanger (IHX) and a flash vessel (FV) with a secondary compressor to the SS cycle (Fig. 1.c and Fig. 1.d, resp.) revealed that the thermodynamic performance depends on the sink temperature and the required temperature lift, though the reasons for this are not well understood.

Exergy analysis can identify thermodynamic inefficiencies, i.e. irreversibilities, in a system. Exergy is defined as the maximum amount of work that can be obtained from a system in relation to a specified reference environment and is, unlike energy, not a conserved quantity [8]. And exergy analysis shows how much the losses by a component add to the total work requirements and thus impact the COP of a heat pump [9]. Ally et al. [10] used exergy analysis to identify the irreversibilities in a ground source heat pump cycle for the production of domestic water at ~30 °C. They found that over 50% of the exergy destruction occurs within the compressor, 17% at the expansion valve, and 13% from desuperheating the pressure gas whilst preheating suction gas. Bergamini et al. [5] used exergy analysis to study the exergy destruction for a range of heat sources and high temperature heat sinks (e.g. heat of 140 °C from an isothermal 30 °C source) and found that the main source of exergy destruction in the heat pump shifts when the sink temperature and the temperature lift increase. Their results show that the exergy destruction of the heat pump's components increased at different rates. The exergy destruction in the expansion valve had the highest rate and became the main source of exergy destruction at high temperature lifts. Hu et al. [11] assessed the performance of a multi-stage R1234ze(Z) heat pump that produced pressurized water at 120 °C from a heat source ranging from 50 to 90 °C. They also found that the main source of exergy destruction within a heat pump changes with the temperature lift.

The rate at which the exergy destruction in a component develops partially depends on its relation to other components [12]. Such interdependencies can be studied with advanced exergy analysis. Kelly et al. [13] compared different assessment strategies for advanced exergy analysis and found that the thermodynamic cycle approach is the most convenient option with the best results for a heat pump cycle. Their assessment of a refrigeration cycle operating between -25 °C and 50 °C showed that nearly 60% of the exergy destruction in the throttling valve is caused by inefficiencies in other components. The thermodynamic cycle approach was also applied by Hu et al. [14] to a cascade high-temperature heat pump system producing hot water at 120 °C. The results of their advanced exergy analysis indicate that the exergy destruction at these conditions is mainly due to the component's performance.

The results of exergy analysis can be combined with economics to assist decision-makers in determining how additional components would affect both technical and economic performance [15]. This is known as exergo-economics. Wang et al. [16] used exergo-economics to show that exergy loss per capital investment as a function of temperature lift differs between mechanically and thermally driven heat pumps. They formulated a guide map to aid in the selection between these technologies. Moreover, in the study by Wang et al. [17] the same principles are used when evaluating the performance of a transcritical heat pump cycle for hot water production. The heat pump's cost rate decreased by 17% after adding an internal heat exchanger and an ejector (thermal vapor compressor)(Fig 1.e). However, this approach has not yet been used to study steam generating heat pumps.

In this study, exergo-economics is combined with advanced exergy analysis to study how the temperature of steam formation and the configuration of the closed cycle heat pump impact the techno-economic performance of a SGHP. New in this study is the emphasis on the development of exergy destruction within a component and the source of that exergy destruction. The understanding that follows from this study will aid in identifying techno-economically viable SGHPs and foster their adoption in industry.

2 Method

This section outlines the methodological framework used to evaluate the techno-economic performance of steam-generating heat pumps (SGHPs). Section 2.1 establishes the steady-state energy-based performance of the SGHP configurations shown in Fig. 1. Section 2.2 presents the framework to assess thermodynamic inefficiencies within each component based on advanced exergy analysis. Section 2.3 details the economic and cost equations needed for the exergo-economic evaluation.

All cycles were used to produce 10 tonnes per hour (t/h) of steam at saturated temperatures of 80 to 140 °C, in steps of 10 °C. Heat was extracted from (isothermal) heat sources with a constant temperature of 50 °C, 60 °C, 70 °C and 80 °C. These conditions were selected for their common appearance in different industries like chemicals, paper, and food production [3]. All heat pumps were modelled using refrigerant R-1234ze(Z) because of its high critical point, low global warming potential and ozone depletion potential, and proven performance [18]. The open loop cycle used refrigerant R-718 (water), in line with the scope of steam-generating heat pumps. The fluid properties were calculated with Refprop 10.0 [19] and used to build a fundamental model of the heat pump using flow sheeting software (i.e. MS Excel). For the MVR heat sources between 80 °C and 130 °C were explored with a constant feedwater temperature of 80 °C. Here, the lower limit was based on technical limitations set by the inlet pressure of screw compressors [20].

2.1 Steady-state energy balance

The mass flow rate of the refrigerant (m_r) was defined by the heat demand at the condenser and the enthalpy (h) before (in) and after (out) the heat exchanger. For all cycles, the refrigerant exited the condenser as a saturated liquid. The energy balance of the heat exchangers (k) was solved as shown in Eq. (1):

$$Q_k = m_r(h_{k,in} - h_{k,out}) \tag{1}$$

The outlet of the evaporator was assumed to be a saturated gas. When needed, a minimal level of superheating was applied to avoid wet compression. Moreover, all open systems were assumed to operate in a steady-state without mass accumulation. This also holds in the case of a (flash) vessel and ejector, where an enthalpy balance defined the quality of the vapor and thereby the mass ratio between the top and bottom cycle. The inlet of the top cycle was defined to be saturated vapor, whereas the inlet of the bottom cycle was set as a saturated liquid. The minimum temperature difference at both the condenser and evaporator was set at 5 °C [21].

For the internal heat exchanger (IHX) an effectiveness (ϵ_{IHX}) of 50% was assumed when calculating the suction temperature (T_{suc}) of the compressor based on the evaporation (and condensing temperature (T_{ev}), as shown in Eq. (2) [22]:

$$\epsilon_{IHX} = \frac{T_{suc} - T_{ev}}{T_{cd} - T_{ev}} \tag{2}$$

The amount of heat transferred by the internal heat exchanger was limited by the temperature at the outlet of the compressor, which could not by higher than 175 °C to avoid degradation of compressor lubricants and seals [23]. Work added to the system (W_c) by the compressor was based on the isentropic enthalpy difference (Δh_{is}) between the pressure stages and an isentropic efficiency (η_{is}) of 80% [5], as indicated in Eq. (3):

$$W_c = \frac{m_r \Delta h_{is}}{\eta_{is}} \tag{3}$$

Figure 1 Steam generating heat pump configurations: **a.** open loop heat pump with a multi-stage compressor with water injection (MVR) where the dotted line represents the produced steam, **b.** single-stage subcritical (SS) cycle, **c.** heat pump cycle with an internal heat exchanger (IHX), **d.** heat pump with two-stage compression and a :lash vessel (2FV), **e.** heat pump con:iguration with an ejector (EJ). Con:igurations b-e produce steam at an intermediate level and have a sequential MVR to get to the required steam conditions.

The intermediate pressures (p_{int}) were based on a quadratic compression ratio and were corrected by 0.35 bar to minimize compression work in the closed cycle [22], as shown in Eq. (4):

$$p_{int} = \sqrt{p_{in} p_{out}} + 0.35 \quad (4)$$

where p_{in} and p_{out} are the pressures before and after the compressor. The number of compression stages was equal to the number of stages drawn in Fig. 1. Pressure relief in expansion valves is considered isenthalpic. Pressure loss was neglected, as well as heat losses. The COP of the heat pump was based on the heat delivered at the condenser

$$COP_{hp} = Q_{cd}/W_c \quad (5)$$

Energy recuperated by the ejector was based on its expansion and compression efficiency. Expansion work (Δh_{exp})was defined based on isentropic expansion from the primary (a) to the secondary (b) stream and the compression work (Δh_c) from the secondary stream to the product stream [24]. From the work requirements, the required mass flow of the motive steam ($\phi_{\dot{m}}$) was calculated using Eq. (6) [24]:

$$\phi_{\dot{m}} = \frac{\dot{m}_b}{\dot{m}_a} = \sqrt{\eta_{is,tc} \cdot \eta_{is,exp} \cdot \frac{\Delta h_{exp}}{\Delta h_c}} - 1 \quad (6)$$

The isentropic efficiencies (of the thermo-compressor (tc) and expander (exp) were taken as 0.8 [24], from which the enthalpies were calculated similar to Eq. (2). The energy and mass balance were solved iteratively by equating the result of Eq. (6) with the energy balances of the condenser and evaporator.

2.2 Advanced exergy analysis

The advanced exergy analysis focussed on the interdependencies between the components in order to localize the origin of the exergy destruction [12]. The exergetic performance of the cycle and its components was mainly assessed based on its exergy efficiency (ϵ_k). This efficiency was defined as shown in Eq. (7) [25]:

$$\epsilon_k = \frac{\dot{E}x_{P,k}}{\dot{E}x_{F,k}} \quad (7)$$

Herein $\dot{E}x_{F,P}$ was the exergy that fuels component k and was its output. The exergy loss was the sum of internal exergy destruction ($\dot{E}x_D$) and transfer of exergy to external sources [26]. Since heat loss to the environment was neglected and all heat transferred from the heat pump to other systems is valuable, the exergy balance simplifies to Eq. (8) [17]:

$$\dot{E}x_D = \dot{E}x_F - \dot{E}x_P \quad (8)$$

Exergy destruction will be zero in the case of ideal operation. The exergy flowing into an ideal system in the form of heat at the evaporator and work at the compressor equals the exergy of the outflow of heat at the condenser. The exergy value of the streams (i) is defined by the enthalpy (h) and entropy (s) of the stream shown in Eq. (9) [27]:

$$\dot{E}x_i = (H_i - H_0) - T_0(S_i - S_0) \quad (9)$$

Where subscript "0" denoted the reference state at T_0 = 298,15 K and p_0 = 101325 Pa. Substituting Eq. (9) in Eq. (8) and accounting for the exergy value of heat: at the average temperature (T_{av}) of either the heat source or sink and the exergy of work: W, resulted in Eq. (10) [27]:

$$\dot{E}x_{D,k} = \left(1 - \frac{T_0}{T_{av}}\right)\dot{Q}_k - \dot{W}_k + \dot{m}[h_{in} - h_{out} - T_0(s_{in} - s_{out})]_k \quad (10)$$

The exergy destruction of a component was separated into exergy destroyed due to inefficiencies of the component itself (endogenous) and by interdependencies within the cycle (exogenous). The endogenous exergy destruction of component k was found by comparing an ideal (theoretical) cycle consisting of solely reversible operations with an ideal cycle with a real component k, i.e, a hybrid cycle [13].

Ideal heat exchangers, thus without a required minimal temperature difference and without pressure changes operated with an isentropic efficiency of 100%. In this analysis, expansion valves were replaced by ideal expanders and the ejector by an ideal turbine and compressor, both with an isentropic efficiency of 100%. Also, wet compression was allowed and no limit was set to the compressor outlet temperature. For the hybrid cycle with the internal heat exchanger (IHX), the 50% IHX effectiveness (i.e. 50% of the energy available from the source stream) was used in calculating the endogenous exergy destruction. This limit was set to mitigate the exergy destruction of the compressor and the condenser resulting from superheating. All exergy destruction at the evaporator was set to be endogenous, which is standard practice when using the theoretical cycle approach [13]. The endogenous exergy destruction of component k was set equal to the exergy destruction of component k in its respective hybrid cycle as no exergy was lost to the environment at any process step [13]. After identifying the endogenous exergy destruction ($\dot{E}x_{D,k}^{EN}$), the exogenous destruction ($\dot{E}x_{D,k}^{EX}$) was calculated with Eq (11) [25]:

$$\dot{E}x_{D,k} = \dot{E}x_{D,k}^{EN} + \dot{E}x_{D,k}^{EX} \quad (11)$$

The value of endogenous exergy destruction of a component was limited to the level of its total exergy destruction.

2.3 Exergo-economic analysis

An exergo-economic analysis added an economic perspective to the differences in exergy destruction between configurations. The total cost of ownership, the cost of exergy destruction and the total capital investment were taken as the key economic performance indicators. Morosuk and Tsatsaronis [12] also combined exergo-economics with advanced exergy analysis to study a SS refrigeration system. In their discussion, they note that the part of the advanced exergy analysis that covers the distinction between avoidable and unavoidable exergy destruction makes the routine quite complex and the results inaccurate. For this reason, the distinction between avoidable and unavoidable exergy destruction is not investigated in this research.

The capital investment costs were based on the indexed bare unit costs of the components, the cost of installation and energy consumption. The bare unit costs ($C_{0,p}$) required for all components, except the ejector.

Table 1 Parameters for estimation of component capital costs according to Zühlsdorf et al. [21] and their Chemical Engineering Price Index (CEPCI) [28]

Centrifugal compressor	Fluid power	450 - 3000 kW	2.2897	1.13604	-0.1027	2.8	394.3
Plain vessel	Volume	1 – 800 m^3	3.5970	0.2163	0.0934	3.0	444.2
Shell & tube heat exchanger	Area	10 – 900 m^2	3.2476	0.2264	0.0953	3.2	444.2
Radial turbine	Fluid power	100 – 1500 kW	2.2476	1.4965	-0.1618	3.5	394.3

and expansion valve, were based on the costs function provided by Zühlsdorf et al. [21] , which is presented in Eq (12):

$$\log(C_{0,k}) = k_1 + k_2 \log x + k_3 (\log x)^2 \quad (12)$$

where "x" was the scaling parameter (e.g. fluid power or volume) of a certain technology and "k_i" was a calibrated value. Table 1 shows the values used in this paper, which were taken from Zühlsdorf et al. [21].

The bare unit costs of Table 1 were homogenized into the equivalent costs of the components for September 2023 based on the Chemical Engineering Price Index (CEPCI) of that date: 793.3 [29]. This was done by calculating a conversion factor (f_{cepci}) which was defined as the ratio between the CEPCI value of September 2023 and the listed CEPCI value in Table 1. The cost of the expansion valve was set at € 700 in 2014 with a CEPCI-value of 576.1 [17]. The installed cost of the ejector was calculated with Eq. (13) [17].

$$C_{0,k} = 15962 m_M \left(10^4 \cdot \frac{T_M[K]}{p_M[Pa]}\right)^{0.05} (0.1 \cdot p_{out}[Pa])^{-0,75} \quad (13)$$

This cost was dated to 2019, with a CEPCI-value of 607.5. In this equation, subscript "M" stands for the ejectors primary (motive) stream conditions. For the expansion valve and the ejector an installation factor equal to that of a vessel was used. Bare unit cost were converted into (indexed) capital investment (z_k) using the installation costs factors (f_{IF}) listed in Table 1, as in Eq. (14):

$$z_k = C_{0,k} f_{cepci} f_{IF} \quad (14)$$

For the expansion valve, an installation cost factor of 3 was used [30]. When multiple compressors were used, their (fluid) power was combined to account for economies of scale. Their respective costs were based on the ratio between the scaling factor of the individual component and the scaling factor of the combined components. The volume of a vessel was based on being able to supply the outlet streams for 10 minutes without an influx. The heat exchanging area (A) of the heat exchangers was calculated using Eq. (15):

$$Q_{hx} = U \cdot A \cdot \Delta T_{lm} \quad (15)$$

where "U" was the heat transfer coefficient and is the logarithmic mean temperature difference between the hot and cold streams. A heat transfer coefficient of 1000 W/m²K was used for heat transfer between a liquid and an evaporating liquid, and 1250 W/m²K was used when both sides were changing phases [21]. The total costs of the installation were equal to the sum of all the z_k. The (total) hourly levelized cost of investment was derived with the capital recovery factor (CRF) as shown in Eq. (16) [17]:

$$CRF = \frac{i(i+1)^n}{(i+1)^n - 1} \tag{16}$$

with an interest rate (*i*) *of* 8% and a lifetime (n) of 15 years, the total (T) hourly levelized cost of investment ($\dot{z}_k^T$) was calculated with the assumption of 8000 hours of operation per year (t_{op}) as shown in Eq (17) [16]:

$$\dot{z}_k^T = \frac{CRF}{t_{op}} \dot{z}_k \tag{17}$$

The difference in cost of energy consumption was based on the cost of exergy destruction, which was assumed to equal the additional electricity cost of the compressor. The cost rate of exergy destruction ($\dot{C}_{D,k}$) was, therefore, equal to the exergy destruction in the cycle times the marginal cost of electricity consumption by the compressor (c_{el}) at 0.041 €/kWh [31], as shown in Eq. (18):

$$\dot{C}_{D,k} = \dot{E}x_{D,k} \cdot c_{el} \tag{18}$$

Similar to Eq. (11), the cost rate of exergy destruction was split into endogenous and exogenous to study the interdependencies within the cycle, see Eq. (19) [12]:

$$\dot{C}_{D,k} = \dot{C}_{D,k}^{EN} + \dot{C}_{D,k}^{EX} \tag{19}$$

The ratio between the endogenous and exogenous parts of Eq. (10) was used to split the total hourly levelized cost of investment into endogenous and exogenous [12].

3 Results

The hourly cost of the different SGHPs are compared on a cycle-level in section 3.1. Section 3.2 presents the cause of the differences in the performance of these cycles on a component-level. Section 3.3 elaborates on the origin of these differences.

3.1 Cycle-level exergo-economic comparison

The total hourly levelized cost of investment and cost of exergy destruction of the four closed SGHP cycles at different source temperatures are presented in Fig. 2. An increase in temperature lift results in a higher total hourly levelized cost of investment and cost of exergy destruction for all cases. The results also show that for temperature lifts, i.e. $T_{sink} - T_{source}$, up to 40 °C, the single-stage subcritical (SS) cycle has the lowest hourly cost as the cost of exergy destruction is comparable among all configurations, but that the total hourly levelized cost of investment is significantly lower. This can also be deduced from Table 2, where the total capital investment of the SS cycle is significantly lower than that the other cycles, i.e., 2.6 M€ compared to 2.9 M€ for the IHX cycle, which is followed by the heat

pump with the two-stage compressor and flash vessel (2FV) cycle and the ejector (EJ) cycle, which requires the largest investment based on the prices listed in section 2.3. Table 2 shows that for the 2FV and EJ cycle, the increase in investment cost mainly comes from the flash vessel, which is more expensive for the EJ cycle due to a larger mass flow.

The role of capital investment in the total hourly levelized cost of investment reduces with increasing sink temperatures and temperature lifts, as the cost of exergy destruction develops exponentially and becomes dominant. The preference for the SS cycle changes at a source temperature of 50 °C and a sink temperature of around 100 °C with (Fig. 2.a). The total cost of the different heat pump configurations is comparable at this level. The difference lies in the ratio of operational cost to investment cost. For the SS cycle, this is much higher than for the others. This share of operational cost increases with temperature lift. Similar trends can also be seen in Figs. 2.b-d. However, the temperature at which the preference shifts from the SS to the IHX increases with the source temperature. The SS cycle is preferred for temperature lifts up to 30- 50 °C, where the temperature of the heat source negatively affects the maximal temperature lift with the 30 °C belonging to an 80 °C heat source and 50 °C to that of a 50 °C heat source. The IHX cycle has the lowest hourly cost up to temperature lifts of 40-70 °C, again depending on the temperature's source. Thereafter, the 2FV cycle is the closed cycle with the lowest hourly cost.

An MVR can be used as a top cycle to the four closed cycles depicted in Fig. 1.b-e, to increase the temperature lift. Fig. 3 shows the total hourly cost of an MVR for different source and sink temperatures. This figure shows that the hourly cost is heavily dominated by the total hourly levelized cost of investment. However, a comparison between Fig. 2.d and Fig. 3, where both solutions work with a source temperature of 80 °C, shows that the hourly cost of the MVR is significantly lower than the hourly costs of the closed cycle. The results indicate that an MVR is the economically preferred option when (sub atmospheric) steam can be directly produced at the required minimal pressure with the heat available in the heat source.

If a heat source cannot directly produce steam at the minimal required pressure by the MVR, the open loop cycle has to be combined with a closed loop heat pump cycle to get the heat source to the appropriate level. The economic performance of using a closed or a combined heat pump cycle to generate steam at a temperature between 100-140 °C from a heat source between 50-70 °C is presented in tables 3 to 5.

With a source temperature of 50 °C, steam with a temperature of up to 100 °C is produced with the lowest total hourly levelized cost of investment and exergy destruction by the SS, after which the IHX cycle is preferred. Table 3 shows that the combined cycle with a SS cycle producing steam at 80 °C is the preferred option for all presented temperatures. However, Table 3 also shows that up to a sink temperature of 130 °C, the closed cycle with the lowest hourly cost, i.e. the optimal (opt.) closed cycle, can produce steam more cost-effectively than by combining a closed heat pump and an MVR. The IHX is preferred for the lower saturated steam temperature, whereas the 2FV cycle performs better at higher temperatures. Both cycles perform equally well at 110 °C.

Steam production from a 60 °C source reduces the temperature lift with respect to the 50 °C case. As a result, the levelized hourly cost of producing saturated steam temperature at 100 °C is less in the 50 °C case. The SS cycle has the lowest combined cost. The combination appears the most effective when the SS cycle delivers steam at the minimal intake pressure of the MVR (80 °C)(Table 4). The SS cycle is also the preferred option for direct steam production until 100 °C. At 110 °C, IHX and the 2FV cycle perform equally well and better than the combined cycle. At higher temperatures, the 2FV cycle performs best until a saturated steam temperature of 140 °C. The SS cycle with MVR performs best at 140 °C.

The hourly cost reduces further for a source temperature of 70 °C. The SS cycle is the preferred option for steam production until 100 °C with further reduced cost in exergy destruction. The preference shifts to the IHX cycle until the 2FV cycle is preferred at a sink temperature of 130 °C, as seen in Table 5. The closed cycles performs better for all sink temperatures with a source temperature of 70 °C.

Table 2 Component-level and total capital investment of heat pump configurations based on a low temperature lift from a 70 °C heat source to 90 °C sink (low) and a high temperature lift from a 50 °C heat source to 140 °C heat sink (high) based on the price data from Table 1.

Component	SS		IHX		2FV		EJ	
	low	high	low	high	low	high	low	high
Evaporator (k€)	694	496	695	569	695	576	696	572
Condenser (k€)	672	657	672	657	672	657	672	657
Compressor 1 (k€)	1193	1961	1184	1795	624	510	1169	1786
Compressor 2 (k€)	-	-	-	-	565	1264	-	-
Expansion valve 1 (k€)	3	3	3	3	1	1	3	3
Expansion valve 2 (k€)	-		-	-	1	1	-	-
Internal heat exchanger (k€)	-		301	294	-	-	-	-
Flash vessel (k€)	-		-		462	484	688	703
Ejector (k€)	-		-	-	-	-	307	511
Total (M€)	2.6	3.1	2.9	3.3	3.0	3.5	3.5	4.2

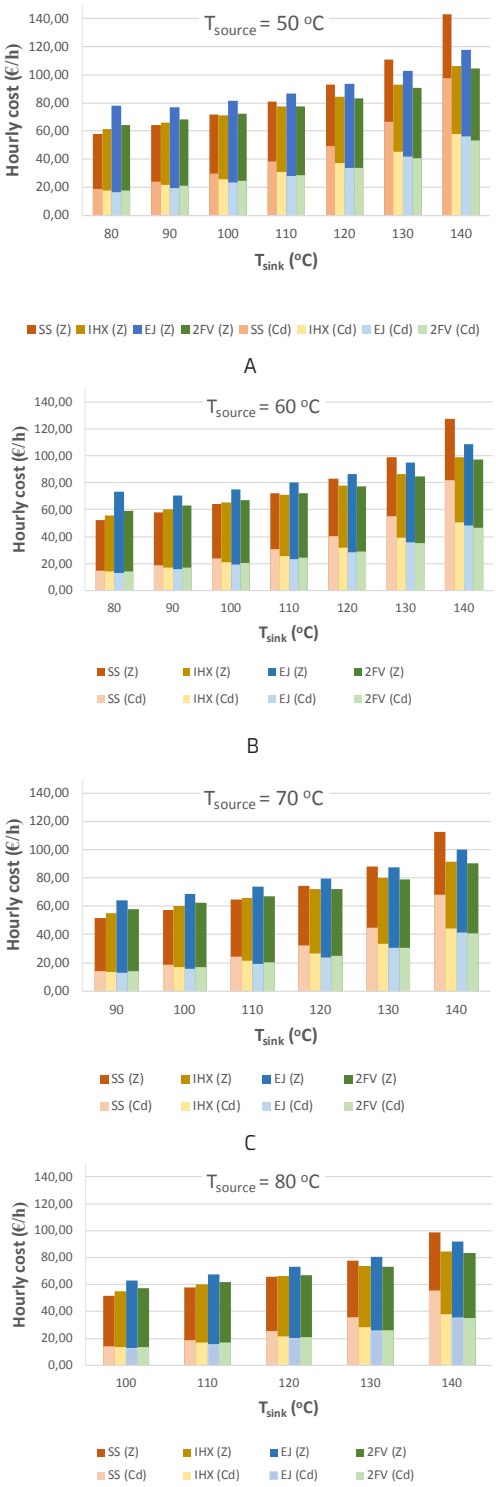

Figure 2 *Comparison of the total hourly levelized cost of investment ($\dot{z}$) and the cost of exergy destruction ($\dot{C}d$) of the closed SGHP cycles; the single stage subcritical cycle (SS), the internal heat exchanger cycle (IHX), the ejector cycle (EJ), and the cycle with a two-stage compressor and flash vessel (2FV). The subfigures depict the hourly cost with a source temperature of:*
(a) 50 °C,
(b) 60 °C,
(c) 70 °C, and
(d) 80 °C.

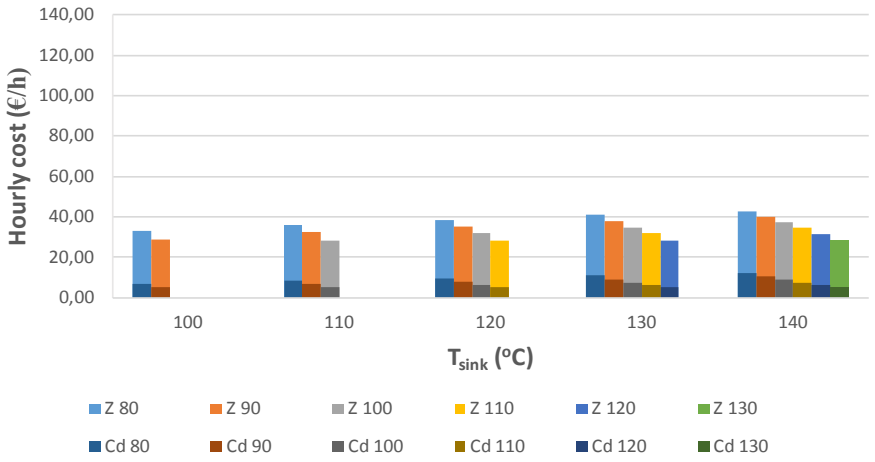

Figure 3 *Comparison of the total hourly levelized cost of investment ($\dot{z}$) and the cost of exergy destruction ($\dot{C}_d$) of an MVR for different source (noted in the legend) and sink temperatures.*

Table 3 Hourly cost (€/h) of combined heat pump cycles and the optimal closed heat pump cycle with a source temperature of 50 °C. With the single stage subcritical cycle (SS), the internal heat exchanger cycle (IHX), the mechanical vapor recompression (MVR), and the cycle with a two-stage compressor and flash vessel (2FV).

		Sink temperature [°C]			
Combination	100	110	120	130	140
SS (50-80) +MVR	91	94	97	99	101
SS (50-90) +MVR	93	97	100	102	104
IHX (50-100) +MVR	-	100	103	106	108
Opt. closed cycle	71 (IHX)	77 (IHX/2FV)	83 (2FV)	91 (2FV)	104 (2FV)

Table 4 Hourly cost (€/h) of combined heat pump cycles and the optimal closed heat pump cycle with a source temperature of 60 °C With the single stage subcritical cycle (SS), the internal heat exchanger cycle (IHX), the mechanical vapor recompression (MVR), and the cycle with a two-stage compressor and flash vessel (2FV).

	Sink temperature [°C]				
Combination	100	110	120	130	140
SS (60-80) +MVR	85	88	91	93	95
SS (60-90) +MVR	86	90	93	95	98
SS (60-100) +MVR	-	93	96	99	101
Opt. closed cycle	64 (SS)	71 (IHX/2FV)	78 (2FV)	85 (2FV)	97 (2FV)

Table 5 Hourly cost (€/h) of combined heat pump cycles and the optimal closed heat pump cycle with a source temperature of 70 °C. With the single stage subcritical cycle (SS), the internal heat exchanger cycle (IHX), the mechanical vapor recompression (MVR), and the cycle with a two-stage compressor and flash vessel (2FV).

	Sink temperature [°C]				
Combination	100	110	120	130	140
SS (70-90) +MVR	80	84	87	89	92
SS (70-100) +MVR	-	86	89	92	95
SS/ IHX (70-110) +MVR	-	-	93	96	99
Opt. closed cycle	58 (SS)	65 (SS/IHX)	72 (IHX)	79 (2FV)	90 (2FV)

3.2 Component-level exergy analysis

In this section, the differences in hourly costs between the heat pump cycles are explained with the help of a component-level exergy analysis. Here, the emphasis is on the compressor (CP) and expansion valve (EV) as they are main sources of exergy destruction at higher temperature lifts (5). Fig. 4 shows that for all cycles the exergy efficiency develops linearly for all pressure altering processes (regression coefficient is 0.998 in case of EV2 in 2FV cycle). The exponential growth in exergy destruction seen in Fig. 2 can, therefore, be explained by the exponential growth in the ingoing, fuel, exergy of a component.

Fig 4.a shows the changes in exergy efficiency for the SS cycle. The exergy efficiency at the minimal temperature lift of the expansion valve is lower than that of the compressor, or any of the other expansion processes shown in Fig. 4.b-d at the same temperature lift. The cycle performs quite well at low temperature lifts, e.g. 50 °C to 80 °C. However, the high average decline rate of exergy efficiency in the EV of 5.2 10^{-3} percent per degree Celsius (%/°C) results in a low exergy efficiency at higher temperature lifts.

The exergy efficiency of the internal heat exchanger (IHX) cycle (Fig. 4.b) is 7% higher at the minimal temperature lift. The improvement at the EV is partially offset by a reduction in exergy efficiency in the CP, due to the superheating of the suction gas. Moreover, the exergy efficiency of the internal heat exchanger (IHX) itself is always well above 90% and, therefore, does not introduce a significant source of exergy destruction. The high exergy efficiency of the EV at low-temperature lifts declines with an average rate of exergy efficiency of 4.9 10^{-3} %/°C and is reduced to 56% at the highest temperature lift.

The addition of the ejector (EJ) to the SS cycle increases the exergy efficiency of the expansion valve, as shown in Fig. 4.c. The total exergy efficiency increases even more than an IHX or 2FV for temperature lifts up to 60 °C. The expansion valve in the EJ cycle operates with an exergy efficiency of 90% at the highest temperature lift. The ejector, however, introduces a new source of exergy destruction into the system. At the lowest source temperature and temperature lift, the ejector has an exergy efficiency of 93% resulting in the most efficient cycle. The exergy efficiency declines at an average rate of 3.3 10^{-3} %/°C resulting in an exergy efficiency of 73% at the highest temperature lift.

The 2FV cycle has a high overall exergy efficiency. At high-temperature lifts, the lowest exergy efficiency is at the second expansion valve which operates with an exergy efficiency of 76 % (Fig. 4.d). The exergy destruction in this component is, however, limited due to a low fuel quality. At low-temperature lifts, all components in the cycle have an exergy efficiency above 90%. The exergy efficiency of the compressors remain relatively constant, whereas the exergy efficiency of expansion valves 1 and 2 declines at an average rate of 2.0 and 2.6 10^{-3} %/°C, respectively, at a source temperature of 50 °C. This results in the highest overall exergy efficiency of all compared closed cycles.

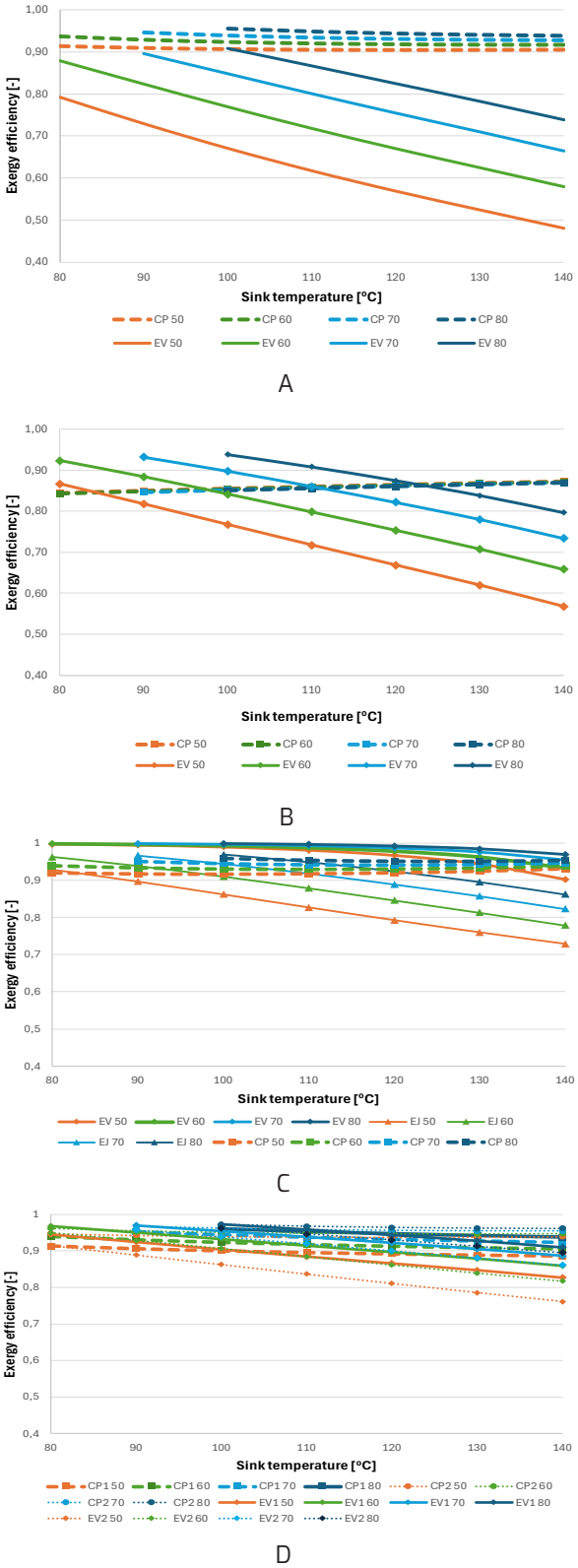

Figure 4 *The development of component-level exergy efficiency with increasing sink temperatures. The temperatures in the legend indicate the source temperature.*
a) subcritical single-stage (SS) cycle,
b) internal heat exchanger (IHX) cycle,
c) ejector (EJ) cycle, and
d) two-stage flash vessel (2FV) cycle.
Here, the abbreviations CP and EV stand for compressor and expansion valve respectively.

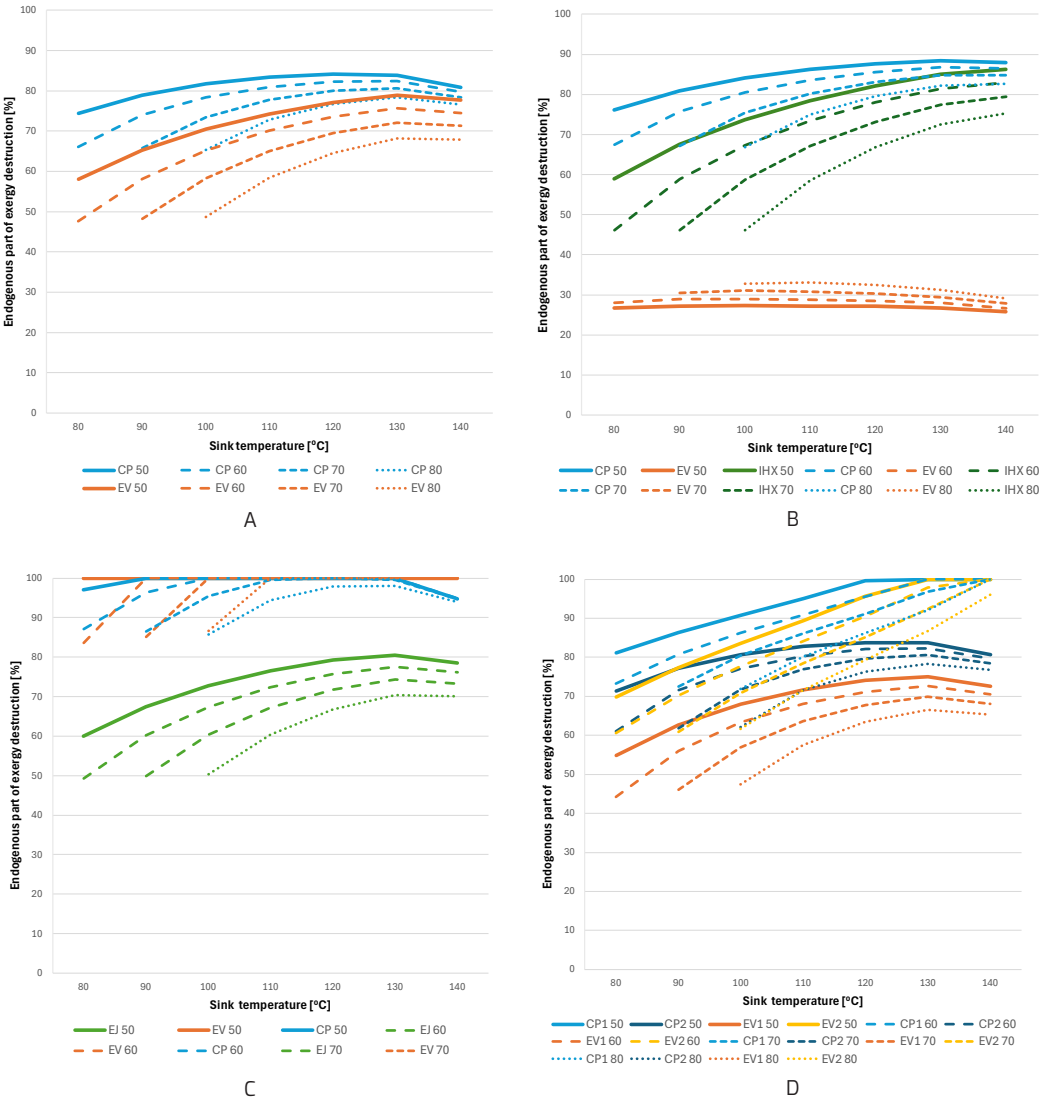

Figure 5 *Endogenous part of exergy destruction of the compressor (CP) and the expansion valve (EV) as a function of sink temperature:*
a) single-stage subcritical (SS) cycle and
b) internal heat exchanger (IHX) cycle,
c) ejector (EJ) cycle and
d) two-stage flash vessel (2FV) cycle.
Here, the abbreviations CP, IHX and EV stand for compressor, internal heat exchanger and expansion valve respectively.

3.3 The origin of exergy destruction

The exergy destruction by a component, as shown in section 3.2, cannot necessarily be allocated to that component. Interdependencies with other components may also be the cause of this exergy destruction. Insight into the origins of exergy destruction helps to identify the fundamental inefficiencies of a cycle due to interdependencies and can help explain why exergy destruction arises.

Fig. 5 shows that although the exergy destruction of the compressor and expansion valve is mostly endogenous, the ratio between endogenous and exogenous exergy destruction differs among cycles.

Fig. 5.a shows a clear trend in the exergy destruction in the SS cycle, becoming more endogenous as the temperature lift increases. The ratio of endogenous: exogenous exergy destruction is 1:1 at low-temperature lifts to nearly 4:1 at higher lifts. Overall, the compressor's exergy destruction is more endogenous than the expansion valve over the entire sink temperature range.

The addition of the internal heat exchanger (IHX) to form the IHX cycle mainly affects the origin of the exergy destruction in the expansion valve (Fig. 5.b). Whereas the exergy destruction of the expansion valve (Fig. 5.a) was mostly endogenous (48-84%), the exergy destruction of the expansion valve in combination with the IHX (Fig. 5.b) is highly exogenous (~30%). The compressor in the IHX cycle follows a similar trend as in the SS cycle. However, the compressor in the IHX cycle has a slightly higher endogenous part at each temperature lift, resulting from the higher fuel exergy due to the preheating by the IHX. The exergy destruction of the internal heat exchanger follows a trend similar to the compressor as the increasing exergy of the fuel overshadows external factors. However, this is not the case for the expansion valve in the IHX cycle, as in the model the performance of the IHX is optimized for each scenario. The introduction of the internal heat exchanger increases the exergy efficiency of the expansion valve but makes the exergy destruction more dependent on the performance of other components in the cycle.

Alternatively, the addition of the ejector greatly reduces the dependency of the compressor and expander on other components as can be seen in Fig. 5.c. The endogenous part of the ejector (EJ) itself develops similarly to the trends seen in Fig. 5.a-b of increasing endogeneity.

The 2FV cycle also shows these trends in Fig. 5.d for the high-pressure compressor (CP2) and the high-pressure expansion valve (EV1). The low-pressure compressor (CP1) and the low-pressure expansion valve (EV2) show a more linear development towards complete endogenous exergy destruction because of the highly endogenous performance and the increased mass flows in the hybrid models.

4 Discussion

The results of the exergo-economic assessment largely depend on the electricity price and the capital investment cost. An electricity price of 0.041 €/kWh was used in the assessment together with the investment cost parameters in Table 2. Fig. 2 shows the relation between the total hourly levelized cost of investment and the cost of exergy destruction. For low-temperature heat lifts (e.g., from 50 to 80 °C), the cost of the capital investment is two times the cost of the exergy destruction. However, this ratio reduces with increasing temperature lifts (e.g., from 50 to 140 °C) to 1:1 for thermodynamic efficient cycles, like the 2FV, and 2.5:1 for the less efficient SS cycle. Changes in the electricity price will impact this ratio. Lower prices will increase the role of the capital investment, whereas increased prices will reduce it. In the Netherlands, due to COVID-19 and the Ukraine war, the electricity price rose by 374 % from 0.057 €/kWh in 2020 to 0.213 €/kWh in 2023 [32]. With 2023 prices, the EJ cycle would be much more competitive as it is 9% more efficient but is currently held down by an 11% higher capital cost than the 2FV cycle when lifting heat from a 70 °C source to a 110 °C sink. Moreso, an increase in operational cost would result in more efficient cycles having lower hourly costs at lower temperature lifts. E.g., at 0.213 €/kWh, the IHX cycle would already have a lower hourly cost than the SS cycle when lifting heat from 60 °C to 90 °C , instead of from 60 °C to 110 °C at 0.041 €/kWh.

The cost factors underlying the capital investment are another major aspect. Table 2 shows that the more expensive cycles are more expensive due to the cost of added components and that this increase is partially balanced by a lower cost of the compressor due to increases in thermodynamic efficiency. However, the increase in cost is also amplified by the need for a larger and more costly evaporator. Lower cost factors for the heat exchangers, for example, could lead to a lower increase in capital investment for the more complex cycles and increase their competitiveness in respect to the SS cycle. Table 2 also shows that most added costs for the 2FV and the EJ cycle stem from the need for a flash vessel. Though significant price reductions from learning are not expected for this mature industrial technology, a smaller storage capacity could reduce the required cost. However, even halving storage time from 10 to 5 minutes reduces the investment cost of the vessel by just 20% and thereby not even close to the cost of the 2FV cycle. Moreso, learning might bring the cost of the ejector down, however, a 95% reduction is required to be competitive with multistage compressors according to the listed prices in table 2. Moreover, the costs in Table 2-5 of the compressors are based upon shaft power, whereas the volumetric flow rate is likely to impact the cost. This is especially the case for sub-atmospheric steam with its low density. Since the hourly cost difference between the optimal closed cycle and the cheapest combination of SS cycle and MVR is limited, detailing this aspect might shift the results in favour of the closed cycle heat pump.

Hence, higher electricity prices are therefore likely to favour more efficient heat pump technologies. The increase in operational cost will also lower the 40 °C economic temperature limit for the SS cycle mentioned by Bless et al. [4], Bergamini et al. [5], and Hu et al. [11]. Changes to the cost of investment of individual components in the closed cycle are not likely to change the heat pump configuration with the lowest hourly cost as the cost difference between added components is likely to remain in the same order of magnitude. Detailing the design of the MVR might shift the preference towards the closed cycle. Nonetheless, the used capital costs were comparable with the costs listed by the IEA annex 58 [33]. In our model, the SS cycle with a source temperature of 80 °C and a sink temperature of 120 °C to 140 °C, has a specific installed cost of 420 – 500 €/kW. This is in the same order as the 6 MW Heaten reciprocating custom design heat pump (250-350 €/kW) [33] and the Enertime two-stage centrifugal compressor 10 MW heat pump (300-400 €/kW) [33], though those prices exclude integration cost [20].

5 Conclusions and recommendations

The impact of the temperature of steam formation and the configuration of the closed-cycle heat pump on the techno-economic performance of a SGHP is studied by an advanced exergo-economic analysis that combines exergo-economics with advanced exergy analysis.

From the results the following key insights can be derived:

First, when a heat source can directly produce steam that meets the minimal pressure requirement of a mechanical vapor recompression (MVR) system, this is the preferred option from a exergo-economic perspective.

Second, at sink temperatures of about 130- 140 °C, a combination of a closed cycle and an MVR has a marginally better economic performance than the considered closed cycles. Here, the lowest hourly cost comes from combining an MVR with an SS cycle that produces steam at 80 °C.

Third, with an electricity price of 0.041 €/kWh, the subcritical single-stage (SS) cycle has the best exergo-economic performance for temperature lifts up to 40°C. For higher temperature lifts, the internal heat exchanger (IHX) cycle becomes the preferred option until about 70°C, depending on the heat source. Beyond this point, the two-stage flash vessel (2FV) cycle is preferred. The preference for more complex cycles increases with higher electricity costs.

Fourth, the shift in preference results from different decline rates in exergy efficiency. The average decline rate is the highest in the expansion valve of the SS cycle, which explains the cycles limited application at high temperatures. The 2FV cycle counters this decline the most without introducing new significant sources of exergy destruction like the IHX or the ejector cycle do.

Finally, the advanced exergy analysis shows that exergy destruction tends to become more endogenous with increasing temperature lifts. Moreover, it shows that overall exergy destruction in compressors is more endogenous compared to expansion valves and that adding new components to the cycle design changes the origin of exergy destruction and makes it more evenly distributed throughout the cycle.

This study shows how the exergo-economic performance of steam-generating heat pumps is affected by the temperature of steam formation and the configuration of the closed cycle. Further research is needed to address how factors like operability, compatibility with other (electrified) utilities and storage, part-load performance, and dynamic response to foster the adoption of Steam Generating Heat Pumps.

Nomenclature

2FV	two-stage compression and a flash vessel
A	heat exchanger area (m2)
C	costs (€)
COP	Coefficient of Performance
CRF	Capital Recovery Factor
Ex	exergy [kJ/kg]
EJ	ejector
f	factor (-)
h	specific enthalpy [kJ/kg]
i	interest rate
IHX	internal heat exchanger
K	costs factor (-)
m	mass flow rate [kg/s]
MVR	Mechanical Vapor Recompression
s	specific entropy [kJ/kgK]
SGHP	Steam Generating Heat Hump
SS	single-stage subcritical
T	temperature [K]
t	time (s)
TCI	total capital investment [€]
TCO	Total costs of ownership (€)
Q	heat (flow)
q	heat transfer rate [kW]
U	heat transfer coefficient [W/m^{2}K]
W	work/power [kW]
X	scaling factor
z	total hourly levelized cost of investment

Greek symbols

ɳ	efficiency
Δ	difference
	effectiveness

Subscripts

c	compressor
cd	condenser
d	destruction
el	electricity
en	endogenous
ev	evaporator
ex	exogenous
exp	expander
f	fuel
hp	heat pump
hx	heat exchanger
in	flux
int	intermediate
if	installation factor
Ihx	internal heat exchanger
is	isentropic
lm	logarithmic mean
k	component
M	motive
p	product
r	refrigerant
suc	suction
T	total
tc	thermo-compressor

References

[1] E. Krtková, R. Saarikivi, and M. Müllerová, "Approximated EU greenhouse gas inventory," 2020.

[2] M. Wei, C. A. McMillan, and S. de la Rue du Can, "Electrification of industry: Potential, challenges and outlook," Current Sustainable/Renewable Energy Reports, vol. 6, pp. 140-148, 2019.

[3] A. Marina, S. Spoelstra, H. Zondag, and A. Wemmers, "An estimation of the European industrial heat pump market potential," Renewable and Sustainable Energy Reviews, vol. 139, p. 110545, 2021.

[4] F. Bless, C. Arpagaus, S. S. Bertsch, and J. Schiffmann, "Theoretical analysis of steam generation methods-Energy, CO2 emission, and cost analysis," Energy, vol. 129, pp. 114-121, 2017.

[5] R. Bergamini, J. K. Jensen, and B. Elmegaard, "Thermodynamic competitiveness of high temperature vapor compression heat pumps for boiler substitution," Energy, vol. 182, pp. 110-121, 2019.

[6] K.-M. Adamson et al., "High-temperature and transcritical heat pump cycles and advancements: A review," Renewable and Sustainable Energy Reviews, vol. 167, p. 112798, 2022.

[7] G. Kosmadakis, C. Arpagaus, P. Neofytou, and S. Bertsch, "Techno-economic analysis of high-temperature heat pumps with low-global warming potential refrigerants for upgrading waste heat up to 150° C," Energy Conversion and Management, vol. 226, p. 113488, 2020.

[8] I. Dincer and M. A. Rosen, Exergy: energy, environment and sustainable development. Newnes, 2012.

[9] G. Tsatsaronis and M. J. Moran, "Exergy-aided cost minimization," Energy Conversion and Management, vol. 38, no. 15-17, pp. 1535-1542, 1997.

[10] M. R. Ally, J. D. Munk, V. D. Baxter, and A. C. Gehl, "Exergy and energy analysis of a ground-source heat pump for domestic water heating under simulated occupancy conditions," International journal of refrigeration, vol. 36, no. 5, pp. 1417-1430, 2013.

[11] B. Hu, D. Wu, L. Wang, and R. Wang, "Exergy analysis of R1234ze (Z) as high temperature heat pump working fluid with multi-stage compression," Frontiers in Energy, vol. 11, pp. 493-502, 2017.

[12] T. Morosuk and G. Tsatsaronis, "Advanced exergy-based methods used to understand and improve energy-conversion systems," Energy, vol. 169, pp. 238-246, 2019.

[13] S. Kelly, G. Tsatsaronis, and T. Morosuk, "Advanced exergetic analysis: Approaches for splitting the exergy destruction into endogenous and exogenous parts," Energy, vol. 34, no. 3, pp. 384-391, 2009.

[14] X. Hu, Y. Liu, S. Dong, G. Li, Z. Sun, and Y. Liu, "Comparison study of conventional and advanced exergy analysis on cascade high temperature heat pump system based on experiment," Case Studies in Thermal Engineering, vol. 40, p. 102552, 2022.

[15] M. J. Moran, "Fundamentals of exergy analysis and exergy-aided thermal systems design," Thermodynamic optimization of complex energy systems, pp. 73-92, 1999.

[16] M. Wang, C. Deng, Y. Wang, and X. Feng, "Exergoeconomic performance comparison, selection and integration of industrial heat pumps for low grade waste heat recovery," Energy Conversion and Management, vol. 207, p. 112532, 2020.

[17] Y. Wang, Y. Yin, and F. Cao, "Comprehensive evaluation of the transcritical CO2 ejector-expansion heat pump water heater," International Journal of Refrigeration, vol. 145, pp. 276-289, 2023.

[18] P. Hu, Q. Hu, Y. Lin, W. Yang, and L. Xing, "Energy and exergy analysis of a ground source heat pump system for a public building in Wuhan, China under different control strategies," Energy and Buildings, vol. 152, pp. 301-312, 2017.

[19] E. W. Lemmon, M. L. Huber, and M. O. McLinden, "NIST reference fluid thermodynamic and transport properties–REFPROP," NIST standard reference database, vol. 23, no. 2002, p. v7, 2002.

[20] B. Zühlsdorf, "High-Temperature Heat Pumps: Task 1–Technologies. Annex 58 about High-Temperature Heat Pump," ed: Heat Pump Center c/o RISE, 2023.

[21] B. Zühlsdorf, F. Bühler, M. Bantle, and B. Elmegaard, "Analysis of technologies and potentials for heat pump-based process heat supply above 150 C," Energy Conversion and Management: X, vol. 2, p. 100011, 2019.

[22] C. Mateu-Royo, J. Navarro-Esbrí, A. Mota-Babiloni, M. Amat-Albuixech, and F. Molés, "Theoretical evaluation of different high-temperature heat pump configurations for low-grade waste heat recovery," International Journal of Refrigeration, vol. 90, pp. 229-237, 2018.

[23] X.-Q. Cao, W.-W. Yang, F. Zhou, and Y.-L. He, "Performance analysis of different high-temperature heat pump systems for low-grade waste heat recovery," Applied Thermal Engineering, vol. 71, no. 1, pp. 291-300, 2014.

[24] S. Klute, M. Budt, M. van Beek, and C. Doetsch, "Steam generating heat pumps–Overview, classification, economics, and basic modeling principles," Energy Conversion and Management, vol. 299, p. 117882, 2024.

[25] Y. Tian et al., "Conventional and advanced exergy analysis of large-scale adiabatic compressed air energy storage system," Journal of Energy Storage, vol. 57, p. 106165, 2023.

[26] G. Tsatsaronis, "Recent developments in exergy analysis and exergoeconomics," International Journal of Exergy, vol. 5, no. 5-6, pp. 489-499, 2008.

[27] M. Moran and E. Sciubba, "Exergy analysis: principles and practice," 1994.

[28] C. E. Magazine. "The Chemical Engineering Plant Cost Index." https://www.chemengonline.com/pci-home (accessed 27-6, 2024).

[29] U. S. B. o. L. Statistics. "Databases, Tables & Calculators by Subject - Inflation & Prices." https://www.bls.gov/data/ (accessed 21/02/2023, 2023).

[30] J. V. Walden, B. Wellig, and P. Stathopoulos, "Heat pump integration in non-continuous industrial processes by Dynamic Pinch Analysis Targeting," Applied Energy, vol. 352, p. 121933, 2023.

[31] P. P. voor de Leefomgeving, "Klimaat-en Energieverkenning 2022," 2022.

[32] CBS. "Eindverbruikersprijzen aardgas en elektriciteit." https://www.cbs.nl/nl-nl/cijfers/detail/85666NED (accessed 4-6-2024.

[33] B. Zuhlsdorf, "Task 1: Technologies – State of the art and ongoing developments for systems and components," in About High Temperature Heat Pumps, vol. 58. https://heatpumpingtechnologies.org/annex58/task1/: International Energy Agency, 20.

SECTION 3

ELECTRIFICATION OF INDUSTRIAL UTILITY SYSTEMS UNDER VARYING ENERGY PRICES

CHAPTER 6

THE IMPACT OF ENERGY PRICES ON THE ELECTRIFICATION OF UTILITY SYSTEMS IN INDUSTRIES WITH FLUCTUATING ENERGY DEMAND

This chapter is currently in press as S.E. Bielefeld, B.W. de Raad, L. Stougy, M. Cvetkovic, M. van Lieshout, C.A. Ramirez, "The impact of Energy Prices on the Electrification of Utility Systems in Industries with Fluctuating Energy Demand", in Elsevier's Energy.

Abstract

Industrial greenhouse gas emissions, primarily carbon dioxide (CO_2), constitute about one-third of global emissions, and 75% are caused by the generation of heat from fossil fuels. Electrifying heat generation using renewable sources and power-to-heat technologies is therefore a key decarbonization strategy. This study explores the impact of the energy price on the optimal choice and sizing of power-to-heat and storage technologies in existing energy-intensive industries with a variable heat demand. A mixed integer linear program is used to find the technology portfolio which leads to the lowest total annual cost of the utility system, while ensuring that heat demand is always fulfilled. The results of a case study in the Netherlands show that adding power-to-heat and storage technologies to a fossil fuel-based combined heat and power plant is economically viable under all explored scenarios. The mean and the variance of electricity prices significantly influence the sizing of heat pumps, electric boilers, and thermal energy storage. High and stable electricity prices lead to larger heat pump capacities compared to scenarios with low and more variable electricity prices. Electric boilers are primarily sized based on the variance of electricity prices and the capacity of thermal energy storage, which plays a crucial role in managing electricity price fluctuations. The study emphasises the potential for cost-effective electrification and provides valuable insights for reducing industrial CO_2 emissions.

1 Introduction

International commitments aim to reduce greenhouse gas (GHG) emissions significantly [1]. Approximately one-third of global GHG emissions stem from the industry, consisting mainly of CO_2 emissions [2]. Roughly 75% of these emissions are related to the combustion of fossil fuels for fulfilling heating requirements [3]. Therefore, electrifying heat generation with renewable sources is considered a key pathway to reducing industrial CO_2 emissions [4].

Power-to-heat (PtH) technologies have gained attention as they can a) directly convert electrical power into heat (using, e.g., an electric boiler (ElB)), b) use electrical power to produce an intermediate energy carrier, such as hydrogen (H2), that can be stored and thereafter converted into heat, or c) use electrical power to upgrade waste heat streams (with, e.g., a heat pump (HP)) [5]. Among the three options, waste heat-upgrading technologies such as heat pumps require the least electricity to generate heat [5, 6]. Yet, the technical performance of a heat pump is highly dependent on the temperature at which heat is demanded and available [7]. Combining PtH technologies with energy storage can increase the use of renewable electricity, reduce CO_2 emissions and improve the economic performance of an industrial plant's energy conversion facility (utility system) as they enable energy use when it is abundant and cheap [8-11]. However, identifying cost-effective combinations of PtH and storage technologies is challenging due to varying and uncertain equipment costs and efficiencies, as well as the fluctuating availability and cost of renewable electricity.

This challenge has been studied from different perspectives in the literature and can be categorized into three groups. The first compares different PtH technologies with each other in scenarios with constant energy price and demand. Son et al. [12], for example, study the potential role of PtH technologies in an oil refinery with a pinch analysis and identify economically feasible HP and ElB solutions. Wiertzema et al. used the same approach to study the impact of electrifying the utility system on the heat integration

of a chemical process and found that replacing a gas boiler with an electric boiler reduces the waste heat and therefore the potential for heat integration. However, they also found that the operational cost of the selected electric boiler halved in 2040, compared to a 2030 energy market scenario [13]. Kim et al. used pinch analysis at the site level and found several electrification options, but excluded an assessment of their economic performance [14]. Walden and Stathapopoulos used a time-sliced pinch approach to study the impact of a fluctuating heat demand on the optimal integration of a heat pump and found that a heat pump can provide flexibility up to a point at which part-load behaviour leads to diminishing returns [15].

The second group considers fluctuating energy prices, but only for a single PtH (e.g. a heat pump) and storage technology. Walden et al. [15], for example, used optimisation to study the operation of a high temperature heat pump and a sensible thermal energy storage with electricity coming from the power grid and a wind turbine in a process with a constant heat demand. Trevisan et al. used mixed integer linear optimisation to study the techno-economic feasibility of molten salt-based thermal energy storage with embedded electrical heaters for a process with a variable heat demand and different electricity spot market prices [16].

The third group considers multiple PtH and storage technologies and fluctuating energy prices. Baumgaertner et al. [17], for example, studied the impact of time-dependent grid emissions on the design and operation of an electrified utility system with a mixed integer linear model for a pharmaceutical facility with a fluctuating energy demand. While they include varying electricity prices in their study, the gas price is kept constant. Reinert et al. [18] expanded this work and added the possibility of pumped thermal energy storage. However, again, gas prices were kept constant. Previous work by some of the authors of this study explored the potential for cost-optimal electrification of existing utility systems for chemical plants with fluctuating electricity and gas prices. Direct and indirect electrification with electric and hydrogen boilers was considered, but the option to upgrade waste heat with a heat pump was not included [19]. Fleschutz et al. [20] studied using the combination of an ElB, hydrogen as an energy carrier, a heat pump and forms of energy storage for electrification for industrial applications. However, the assessment was carried out for low-temperature heat requirements, for which the performance of the heat pump is significantly different from the performance in the case of high-temperature applications.

The studies presented thus far do not analyse the impact of energy price profiles on the combination of PtH and storage technologies under fluctuating energy prices and operational conditions for existing high-temperature industrial applications. Insight into the potential role of electrification technologies under these circumstances is needed to enable cost-effective electrification of current fossil industrial heating systems.

The aim of this work is thus to evaluate the impact of variable energy prices on deploying PtH and storage technologies in an energy-intensive industry with variable high-temperature heat demand and existing heating infrastructure. Herein, the trade-off between options with a higher efficiency and a higher cost, i.e., heat pumps, and options with lower efficiency and cost, i.e., electric boilers, is explored. The contribution to the existing literature on electrified utility systems for industrial plants is twofold;

1. This work presents a feasibility assessment of technology portfolios that enable cost-effective electrification of fluctuating high-temperature heat demand requiring minimal changes to the plant's existing infrastructure.

2. The impact of the mean and variance of energy prices and the electricity to gas price-ratio on the selection and sizing of technologies, specifically on heat pumps, is shown.

2 Methods

This section introduces the model used to design and simulate the utility system and the energy price and technology cost scenarios that were explored (sections 2.1 and 2.5). The model is formulated in section 2.2. Then, the industrial plant that served as a case study is presented (section 2.3.) and a reference utility system is formulated in 2.4.

2.1 Existing utility system and potential investment options

The model used to design and assess cost-optimal electrified utility systems is based on an existing utility system fueled by natural gas (NG). This system, shown in Figure 1, comprises a bidirectional connection to the local power grid, a gas-fired gas turbine (GT) and a heat recovery steam generator (HRSG) with additional natural gas co-firing in a gas boiler (GB). The co-firing allows additional heat generation without producing power and enables the system to react to fluctuations in process heat demand. The GT, HRSG, and GB are referred to as combined heat and power plant (CHP) for the remainder of this paper. Since the CHP has already been installed, it is assumed that it does not require further investments. Investments due to maintenance are also not included. To electrify the utility system, PtH technologies and storage technologies can be added to the system as shown in Figure 2. The PtH technologies considered in this study include an HP, which utilises excess heat from a heat recovery unit, an electric boiler (ElB), and a hydrogen boiler (H2B) fueled with hydrogen generated by a proton exchange membrane water electrolyser (H2E). The decision to include hydrogen is based on low-cost storage opportunities in hydrogen tanks (see Table 5). The storage units considered are a Li-Ion battery (Bat), a sensible TES and a hydrogen storage tank (H2S). Due to the different temperature levels at which the PtH technologies produce heat, in practice, they would not be connected to the same TES unit. To reduce complexity, the TES is considered one unit in the model. Furthermore, it is assumed that the HP and the TES produce heat at the temperature required by the process and that the heat from the ElB is cascaded down to the required level by using throttling valves. The cost of these valves is not included in the model as it is considered minor compared to the cost of the PtH and storage equipment.

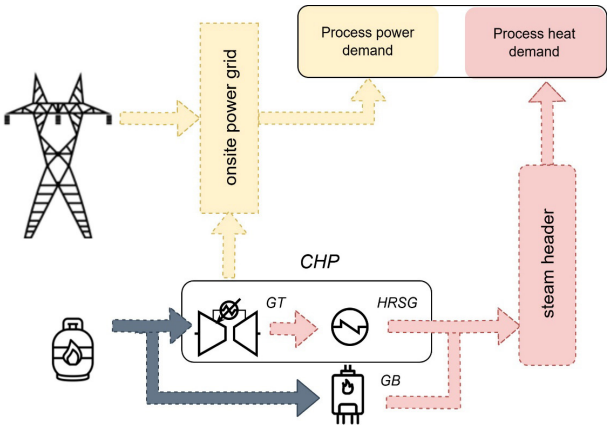

Figure 1 Fossil fuel-based utility system assumed to be the existing utility system for the plant considered in this study. Note that the onsite power grid and steam header are added to the figure for better readability, but are not included in the model. The heat demand is supplied by a CHP, which consists of a gas turbine (GT) and a heat recovery steam generator (HRSG) with additional natural gas co-firing in a gas boiler (GB). The power demand is supplied by the power produced by the GT or by electricity from the national power grid.

2.2 Model formulation

This work explores how changes in the electricity price affect the technology portfolio and economic performance of the system. Deterministic optimisation in combination with scenario analysis is used as the paper does not aim to find the best solution for all uncertain parameters but rather to understand the model's response to them. The model is implemented using the Python-based optimisation package 'Pyomo' and solved using Gurobi solvers. Its time resolution is Δt = 0.5 h, following the resolution of the demand data of the case study. The solving time depends on the scenario. Some scenarios could not be solved to full optimality on a laptop (with Intel CORE i7 vPRO processor) and had to be solved on a supercomputing cluster. The default optimality gap was set to 0.005%.

The model departs from a model presented in [18] and was extended to include an HP and a more flexible CHP. The objective of the optimisation is to minimise the total cost of the utility system for the duration of one operational year, including the investment cost (CapEx) and the operational costs (OpEx), see Eq. (1). Since the model runs in half-hourly steps and the operational time of the process is 8000 hours, assuming 760 hours of downtime per year, the model includes 16000 time steps.

$$\min \sum_{t=0}^{t=16.000} OpEx(t) + CaPex \tag{1}$$

The OpEx is calculated using Eq.(2). It consists of the cost of consuming grid electricity minus the potential revenue from selling electricity from the CHP back to the grid and the cost of consuming natural gas (including the cost of purchasing CO_2 emission allowances within the European Emission Trading System (EU ETS)). Taxes and other fees for selling power back to the grid are not included in the model. In Eq.(2), $p_{el,\ grid}(t)$ is the electricity price at time *t* in [euro/MWh]. Power flow from the grid to technology *i* is denoted as $P_{gr,i}(t)$ and power flow from technology back to the grid as $P_{i,gr}(t)$. Both are expressed in [MW]. pNG(t) is the cost of using natural gas at time *t* in [euro/MWh]. The quantity of gas consumed per time step is denoted by $NG_{in}(t)$ in [MW].

$$OpEx(t) = p_{el,grid}(t) \cdot \left(P_{gr,i}(t) - P_{i,gr}(t)\right) \Delta t + p_{NG}(t) \cdot NG_{in}(t) \Delta t \tag{2}$$

The CapEx (Eq. (3)) includes the investment required for all newly installed technologies *i* and is a product of their technology cost c_i (in [euro/MW] or [euro/MWh]), their installation factor Inf_i and their size s_i (in [MW] or [MWh]).

$$CaPex = \sum_i c_i \times inf_i \times s_i \times AF_i \tag{3}$$

Since the model only considers one operational year, the investment is annualized using an annualisation factor of the respective technology AFi, which is calculated using Eq.(4). LTi is the lifetime of equipment i, and the discount rate r is set to 10%, as in [20].

$$AF_i = \frac{r}{1-(1+r)^{-LT_i}} \tag{4}$$

The power or heat generation and storage technologies are represented by energy flow balances and the respective technological constraints, as described in section 2.1 of [19]. The CHP in this study is modelled as a combination of a gas turbine, a heat recovery steam generator, and a gas boiler.

Mirroring the situation of the case study, the operational flexibility of the GT is based on the combined operation of two gas turbines, which both have the ability to operate at 60-100% of their capacity. It is assumed that one turbine can be shut down completely. One GT, or 30% of the total GT capacity, has to operate at all times to limit the number of cold starts, which damage the equipment. Therefore, the minimal load of the CHP is assumed to be 30% of its capacity. The heat generation of the CHP is calculated using Eq. (5), where $NG_{GT,in}(t)$ is the amount of natural gas converted in the gas turbine, $\eta_{GT,th}$ the thermal conversion efficiency of the gas turbine, $NG_{GB,in}(t)$ the amount of natural gas going to the gas boiler, η_{GB} the conversion efficiency of the gas boiler and $H_{CHP,out}(t)$ the heat output of the CHP.

$$\left(NG_{GT,in}(t) \cdot \eta_{GT,th} + NG_{GB,in}(t)\right) \cdot \eta_{GB} = H_{CHP,out}(t) \quad (5)$$

The energy conversion of the HP is modelled as stated in Eq. (6), where $H_{HP,out}(t)$ is the heat output of the HP, which is a function of the power input $P_{HP,in}(t)$ and the Ideal, or Carnot, coefficient of performance (COP) COP_{ideal} multiplied by 0.5 because a mechanical closed-cycle HP is expected to operate at 50% of its ideal COP [21, 22]. The ideal COP is calculated using Eq. (7).

$$H_{HP,out}(t) = P_{HP,in}(t) \cdot COP_{ideal} \cdot 0{,}5 \quad (6)$$

The ideal COP is calculated using Eq. (7).

$$COP_{ideal} = T_{sink}/(T_{sink} - T_{source}) \quad (7)$$

All equations of the model are presented in Appendix D.

2.3. Case study

This study explores the electrification of the utility supply for the energy-intensive industry with a highly fluctuating electricity and (high-temperature) heat demand. These conditions are commonly observed in sectors with a large product portfolio, batch processing, and or cleaning-in-place processes such as in the food and beverage, the chemical and pharmaceutical, the textile and the paper and pulp industry. An existing paper mill in the Netherlands with various paper recipes is used as a representative case study for this group of discontinuous processes. Of the considered paper mill, only the heat demand of the drying section was considered, as it requires over 80% of the total heat demand. The heat demand, between 100 ^{0}C and 160 ^{0}C, varies in capacity every 30 minutes. The maximum heat demand is 21.5 MW, the average 13.7 MW and the minimum 1.1 MW. Figure 3 shows the demand duration curve of the process (in blue) and the heat delivered by the CHP when it operates at its minimal load (in orange). For confidentiality reasons, a more detailed description of the underlying demand data cannot be disclosed. Excess heat can be recovered from the drying hood at T = 55 ^{0}C and fed to a HP. Since the HP is required to generate heat at 160^{0}C, the COP of the HP for this paper mill is 2 based on a second law efficiency of 50%. The electricity demand is assumed to be 10% of the heat demand based on information obtained from the plant operator. The grid connection capacity that limits the power flow from or to the local power grid was assumed to be 30 MW based on the capacity of the actual grid connection of the case study plant.

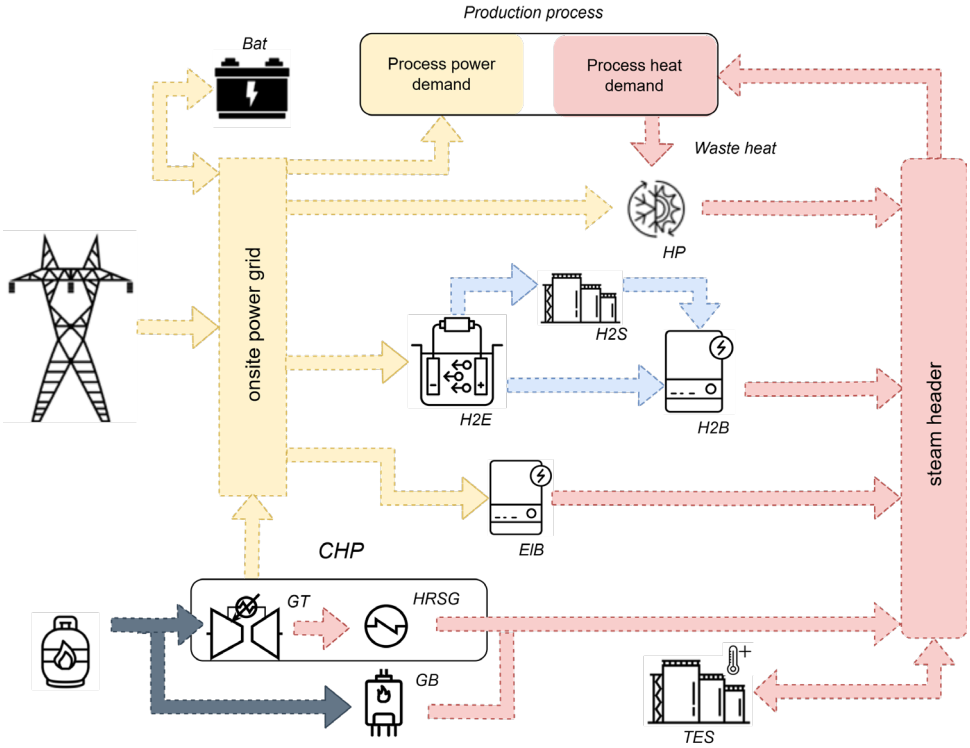

Figure 2 *Potential utility system design including a fossil-based legacy utility system (CHP) consisting of a gas turbine (GT) with a heat recovery steam generator (HRSG) and a gas boiler (GB), and an electric boiler (ELB), a heat pump (HP), and a power-to-gas-to-heat system consisting of an electrolyser (H2E), a hydrogen storage tank (H2S), and a hydrogen boiler (H2B). Energy can be stored in batteries (Bat) and thermal energy storage (TES). Note that the onsite power grid and steam header are used to improve the visualisation. In the model, all interconnections between technologies and from the technologies to the gas or power grid are modelled separately.*

2.3.1 Technical parameters

The parameters used to model the technologies are shown in Tables 1 and 2. Except for the minimal load factor of the CHP, the data is derived from literature. The minimal load factor of the gas turbine is dictated by the equipment installed in the paper mill, and in line with the proposed 50% operational flexibility by Voll et al. [23]. Appendix C shows how the results would look like for more flexible CHPs.

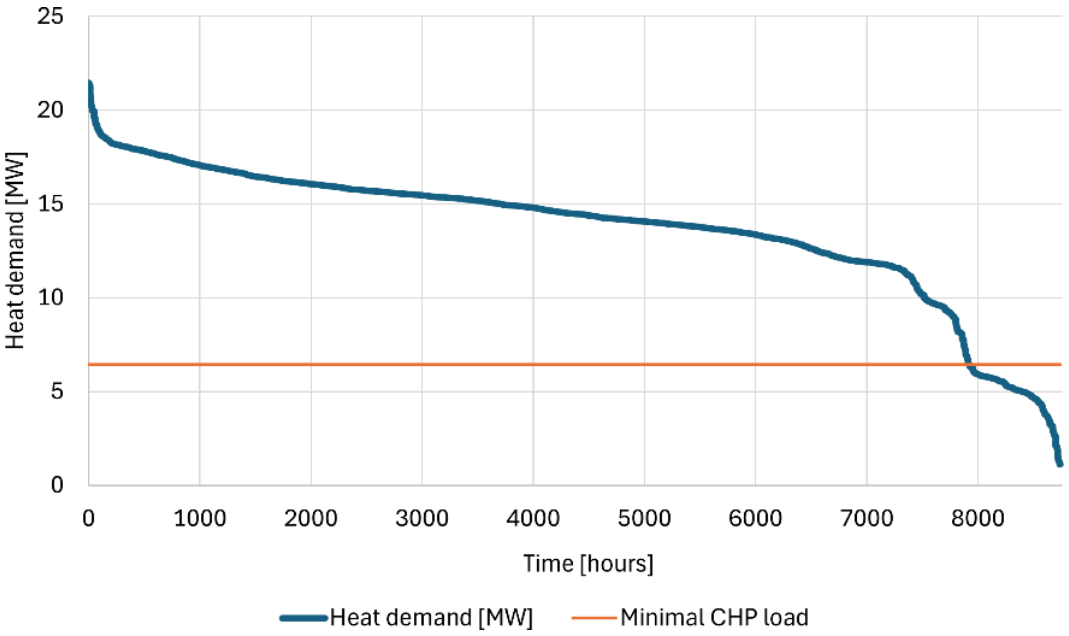

Figure 3 *Heat demand duration curve of the process in the case study and the demand that the CHP supplies at its minimal possible load*

Table 1 Data used to model conversion technologies

	Gas turbine	Gas boiler	El. Boiler	Heat pump	Electrolyser	H_2 boiler
Thermal capacity [MW_{th}]		20% of GT	Decision variable	Decision variable	Decision variable	Decision variable
Electric capacity [MW_e]	-	-				
Efficiency [%]		82	99 [24, 25]	0.5 COP_{ideal}	69 [26]	92 [27, 28]
Minimal load factor [% of max. load]		0	0	0	0	0
Lifetime LT_i (years)	Not included in the model		20 [26]	20 [29]	15	20 (21, 30)

Table 2 *Data used to model storage technologies*

	Battery	TES	Hydrogen tank
Capacity	Decision variable	Decision variable	Decision variable
Efficiency [%]	90 [31]	90 [32]	90 [31]
Max. energy output [% of capacity/Δt]	70 [31]	50 [31]	100
Liftime LT_i [years]	15 [33]	25 [34]	20 [35]

[4] Note: the $\eta_{thermal}$ concerns the generation of heat from natural gas

2.4 Reference utility system

The fossil fuel-based legacy utility system described in 2.1 is the reference system of this study. The reference system's total cost consists of only operational costs. They are calculated according to the cost-optimal operation of the system as described in Eq. (8). The total cost of the reference system is the sum of the costs for grid power and NG use. The cost for grid power use is a function of the electricity price at time t and the difference between electricity consumed by the process $P_{gr,process}(t)$ minus the power generated by the GT and sold to the grid, $P_{GT,gr}(t)$. The cost for NG consumption is a function of the natural gas price at t and the gas used by the gas turbine and the boiler, $NG_{GT,in}(t)$ and $NG_{GB,in}(t)$.

$$Total\ Cost = min \sum_{t=0}^{t=16.000} (P_{el,grid}(t) \cdot \Delta t \cdot \left(P_{gr,process}(t) - P_{GT,gr}(t)\right) \quad (8)$$
$$+P_{NG}\ (t) \cdot \Delta t \cdot (NG_{(GT,in)}\ (t) + NG_{(GB,in)}\ (t)))$$

The same technical parameters and constraints are used as in the optimisation model described in 2.1. All equations used are shown in Appendix D.2.

2.5 Scenarios with differing techno-economic assumptions

The optimisation model is run for a number of energy price scenarios and technology cost (TC) scenarios since the design of an electrified utility system depends on capital and operational costs, and both are subject to uncertainties. The scenario tree containing all explored scenarios is included in the Appendix (Figure A.15).

2.5.1 Energy price scenarios

Three uncertainties have been addressed in this paper, namely 1) The average energy price because of the trade-off between investment and operational cost, 2) energy price variability because of the potential value of flexibility in the utility system, and 3) the electricity-to-gas price ratio (EGR) because PtH technologies compete with existing gas-based technologies. To understand the impact of these uncertainties, several energy price scenarios were designed.

The average electricity price for the 'low mean' scenario is 30 euro/MWh and is based on the average price of electricity on the Dutch day-ahead market in 2020 [36] . The mean electricity price of the 'high mean' scenario is 100 euro/MWh and is based on 2023 data from the same market [36]. The electricity price volatility (its variance) is included via two scenarios, i.e. with a low variance, based on 2019 data, and with a high variance, based on 2023 (Dutch day-ahead market) data [36]. A combination of the two mean and the two variance scenarios leads to four electricity price scenarios. The abbreviations used in the first column of Tables 3 and 4 are based on the mean price and the level of price variance of the respective scenario. The scenario with a low mean price and high levels of price variance, for example, is named 'LMHV' ('Low Mean High Variance').

Two gas price scenarios are added to each electricity price scenario to explore the impact of the EGR. One scenario has cheaper gas than electricity prices, based on the average EGR (including EU ETS allowance price) in 2023 of 1.6 (see data in [36-38]). Note that companies in the Netherlands did not have to pay for all of their CO_2 emissions and that including free allocation rights would result in an EGR of >2 in 2023. For the second scenario, an EGR of 1 was assumed to simulate scenarios with increased gas use prices. The gas price profiles are based on Dutch TTF market data [38] and were adapted to have a mean price matching the desired EGR. To avoid negative gas prices, the gas price is capped at 10 euro/MWh, which aligns with the lowest price in the period 2021 to 2024 (see data in [38, 39]). 17 euro/MWh_{NG} (85 euro/ton_{CO2}) are added to the gas price, mimicking prices in 2023, to include

the cost of purchasing CO_2 emission certificates to the cost of using natural gas (40). This CO_2 price is used in all gas price scenarios.

Tables 3 and 4 provide information about the resulting price scenarios. All price profiles are shown in Figures A.11 to A.14 in Appendix A.

Table 3 *Electricity price and negative price statistics in the energy price scenarios.*

		Electricity Price		Negative Prices	
Scenario	EGR	Mean (Euro/MWh)	Variance (Euro/MWh)^2	Number of hours	Average Value (Euro/MWh)
LMLV	1.6	30	127	30	-6.82
	1	30	127	30	-6.82
LMHV	1.6	30	2,405	1,641	-43.67
	1	30	2,405	1,641	-43.67
HMLV	1.6	100	127	-	-
	1	100	127	-	-
HMHV	1.6	100	2,405	155	-47.46
	1	100	2,405	155	-47.46

Table 4 *Natural gas use cost and hours when the electricity price is lower than the gas cost (including the price for emitting CO_2).*

		Natural Gas Use Cost		Electricity Price < Gas Cost
Scenario	EGR	Mean (Euro/MWh)	Variance (Euro/MWh)^2	Number of hours
LMLV	1.6	35.75	10	6,649
	1	47	10	8,269
LMHV	1.6	35.75	113	4,431
	1	47	113	5,814
HMLV	1.6	79.5	10	121
	1	117	10	8,269
HMHV	1.6	79.5	113	1,945
	1	117	113	5,816

2.5.2. Technology cost scenarios

In this study, the cost for new equipment is the product of technology cost and its installation cost factor. The technology cost was based on a literature review and is shown in Table 5. The installation cost factors were taken from Sinnot and Towler [41]. HPs were considered to be a collection of compressors (2.5) and heat exchangers (3.5), storage technologies miscellaneous equipment (2.5). The hydrogen boiler was considered a gas-fired boiler (2), and the hydrogen storage a pressure vessel (4). For the ElB and the electrolyser, a factor of 1 was used as the technology cost was derived from a reference, which had already included the installation cost. Two technology cost scenarios (TC scenarios) are explored to account for the uncertainty of the TC of Bat, TES, H2E and HP. The technology cost of the ElB, the H2B and the H2S were kept the same for both the high- and low technology cost scenarios, as these technologies are mature and less price development is expected than for the remaining technologies. The first scenario favours installing HPs by assuming low HP costs and high costs for other equipment ('LowHP-HighRest'). In the second scenario, it is the other way around, i.e. HP costs are high, and the cost of the remaining equipment is low ('HighHP-LowRest'). The ranges in technology cost deliberately span a wide range for the purpose of exploring the impact of these cost scenarios on the operation and sizing of the utility system.

Table 5 ***Technology cost scenarios***

Technology	Technology cost per scenario		Reference	Lang Factor
	"HighHP-LowRest"	"LowHP-HighRest"		
ElB	60 [Euro/kW]	60 [Euro/kW]	[22]	1
HP	500 [Euro/kW]	300 [Euro/kW]	[26]	3
Battery	180 [Euro/kWh]	320 [Euro/kWh]	[29]	2.5
TES	15 [Euro/kWh]	40 [Euro/kWh]	[42]	2.5
Electrolyzer	760 [Euro/kW]	980 [Euro/kW]	[26, 43]	1
Hydrogen boiler	35 [Euro/kW]	35 [Euro/kW]	[27]	2
Hydrogen storage	10 [Euro/kWh]	10 [Euro/kWh]	[28]	4

3 Results and discussion

In sections 3.1 to 3.4, the cost-optimal utility systems for the energy price scenarios are presented, and it is discussed how they differ from each other and the respective reference systems.In section 3.5, the sizing of new equipment across scenarios is discussed.

3.1 Cost-optimal utility systems for energy price scenarios with low mean and low variance

This scenario explores the electrification of the utility system if the prices are low and have low fluctuations. Table 6 shows that, while ElB and TES are installed for all values of the EGR and TC scenarios, HPs are only

Table 6 Installed PtH and storage capacities in the energy price scenarios with low mean and variance

EGR	TC scenario	ElB [MW_{th}]	TES [MWh]	HP [MW_{th}]
1.6	HighHP-LowRest	14	24	0
	LowHP-HighRest	6	5	5
1	HighHP-LowRest	14	28	0
	LowHP-HighRest	6	6	5

installed in the 'LowHP-HighRest' scenarios. No HPs are installed in the 'HighHP-LowRest' scenario. Since the same trends in technology choice and sizing can be observed in both EGR scenarios, only the operation of the systems in the 'EGR 1.6' scenarios is discussed in detail.

In the TC scenario with high HP cost ('HighHP-LowRest'), shown in Figure 4a, the CHP operates 97% of the time at its minimum possible load (30% of its capacity) and ramps up to full capacity only when electricity prices are higher than 3 times the average price. The power generated by the CHP is either sold to the power grid when electricity prices are high or directly fed to the paper mill (herein referred to as the process) and the ElB when electricity prices are low. The heat generated by the CHP goes to the process, and excess heat goes to the TES. 6% of the time, when electricity prices are very low, all energy from the CHP goes to the TES (directly or via the ElB). Power and heat are wasted (neither used nor stored) when the electricity price reaches its negative peak, to consume as much electricity as possible with the ElB. The ElB operates 68% of the time and supplies roughly 50% of the total heat demand, as Figure 4a shows. It charges the TES when either heat demand is low enough and excess heat is available, electricity is cheap enough to allow for cost-effective use of the maximum capacity of the ElB, or when electricity prices are negative. Around 25% of the power for the ElB is supplied by the CHP (see Figure 4a). The TES supplies heat to the process during hours with a heat demand exceeding the minimal heat output by the CHP and electricity prices that render using the ElB unfavourable.

When an HP is installed, like in the 'LowHP-HighRest' TC scenario shown in Figure 4b, the CHP still operates at its minimal load 97% of the time. In this scenario, the HP is the main heat supplier next to the CHP, as Figure 4b shows. It operates 94% of the time, mostly at full capacity (its load factor, i.e. the total energy supplied in one operational year over the installed capacity times the number of operational hours, is 92%). Only during peak heat demand and a relatively high electricity-to-gas-price ratio, e.g., 2, is the HP turned off, and the CHP delivers all heat required by the process. This, however, only happens 3% of the time. As Figure 4b shows, the CHP supplies approximately two-thirds of the power the HP requires to run and delivers almost half of the power the ElB uses. The TES supplies heat to the process at peak heat demand. It is charged mainly by the CHP and the HP. The ElB

charges the TES only when electricity prices are very low, and the HP is operating at full capacity, which happens 5% of the time. The ElB operates for a similar amount of hours as in the previous scenario but contributes less to the heat demand of the process than before (compare the two diagrams in Figure 4) as it supplies heat to the process during peak demand when the electricity prices are low, or the TES is empty. The gas boiler is used only 2% of the time and operates for two reasons. Either to supply heat demand exceeding what the ElB, TES, HP and CHP operating at minimal load combined can deliver (maximum 16 MW) and electricity prices or PtH capacities do not allow storing the additional power from the CHP, or it is used instead of the ElB when electricity prices are much higher than gas prices (e.g., 1.5 times higher).

Finally, compared to the reference utility system, less power is sold to the grid in the new systems, as Table 7 shows. The combination of PtH technologies and TES would enable an economically more efficient use of the power generated by the CHP. This is also illustrated by the reduced total use of energy (see Table 7) and the consequent cost savings.

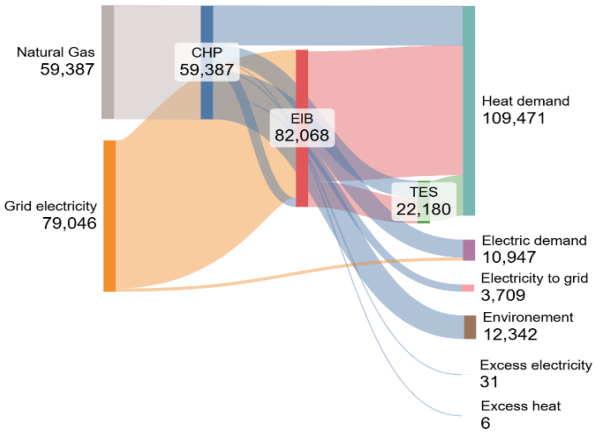

(a) TC scenario 'HighHP-LowRest'

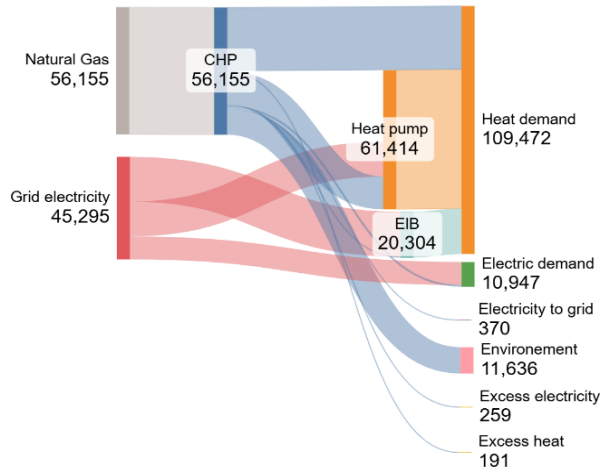

(b) TC scenario 'LowHP-HighRest'

Table 7 Total annual cost (TAC), savings in TAC compared to the reference system, energy consumption including gas and power from the grid, and power sold to the grid in the energy price scenarios with low mean and variance

EGR	System	TC Scenario	TAC [M.Euro]	Savings [%]	NG to system [GWh]	Power Power grid to system [GWh]	System to power grid [GWh]
1.6	Ref.	-	5.9		196.5	0.02	35.1
	New	HighHP-LowRest	4.9	16.9	109.9	43.4	8.6
	New	LowHP-HighRest	4.9	16.9	107.9	21.1	3.8
1	Ref.	-	8.1		195.2	0.02	34.2
	New	HighHP-LowRest	6.1	24.7	105.3	45.7	7.2
	New	LowHP-HighRest	6.1	24.7	105	20.5	2.7

3.2 Cost-optimal utility systems for energy price scenarios with low mean and high variance

As Table 8 shows, only ElBs and TES are installed in the scenarios with low mean and high variance energy prices. The capacities of the installed ElBs come close to the available grid connection capacity of 30 MW to exploit periods of low electricity prices. Note that the lowest price peaks are stronger than in the scenario discussed in the previous section (see 'Negative Price' column in Table 3 and Figures A.11 to A.14). The high price variance also results in TES units from 55 to 112 MWh, a strong increase compared to the TES capacities in the scenarios in 3.1. The cost of the TES has a strong impact on its size as its capacity in the 'HighHP-LowRest' scenarios is about twice as big as in the 'LowHP-HighRest' scenarios.

Scenario 'EGR 1, HighHP-LowRest' is shown in Figure 5 as an exemplary scenario of the energy price scenarios with low mean and high variance. The CHP operates similarly to the 'HighHP-LowRest' scenario in 3.1. The TES enables selling excess power from the CHP to the grid when electricity prices are high, while the CHP operates at its minimum possible load as the TES supplies heat to the process when the demand exceeds what the CHP can generate at minimal load. The TES is either charged by the CHP when demand is lower than the heat generated by the CHP at minimal load or by the ElB when electricity prices are low. Figure 5 shows that the ElB is predominantly used to charge the TES. Table 9 shows that an increase in gas prices leads to a decreased use of the CHP. This explains the slightly larger TES capacities in the 'EGR 1' scenarios compared to those in the 'EGR 1.6' scenarios. The electrified utility systems lead to a higher reduction in TAC than the scenarios with a low price variance (compare Tables 7 and 9). This illustrates that the value of the flexibility to choose the energy carrier is higher than in the scenarios with lower price variance. Since ElB capacity is cheaper than HP capacity, the model chooses to install large over-capacities of ElB combined with large storage capacities to maximise the flexibility of the utility systems. Finally, more power is sold to the grid than in the scenarios with a low variance because the peaks of the electricity price profile are higher (see Table 9).

Table 8 *Installed PtH and storage capacities in the energy price scenarios with low mean and high variance*

EGR	TC scenario	ElB [MW_{th}]	TES [MWh]	HP [MW_{th}]
1.6	HighHP-LowRest	29	103	0
	LowHP-HighRest	28	55	0
1	HighHP-LowRest	29	112	0
	LowHP-HighRest	28	61	0

Table 9 Total annual cost (TAC), savings in TAC compared to the reference system, energy consumption including gas and power from the grid, and power sold to the grid in the energy price scenarios with low mean and high variance

EGR	System	TC scenario	TAC [M. Euro]	Savings [%]	NG to system [GWh]	Power grid to system [GWh]	System to power grid [GWh]
1.6	Reference	-	5.4		207.1	1.9	36.4
	New	HighHP-LowRest	2.6	51.9	134.8	53.5	23.5
	New	LowHP-HighRest	3.1	42.6	139.7	50.6	24.0
1	Reference	-	7.7		201.1	1.9	32.5
	New	HighHP-LowRest	4.0	48.1	115.4	61.7	15.8
	New	LowHP-HighRest	4.5	41.6	117.5	60.2	16.6

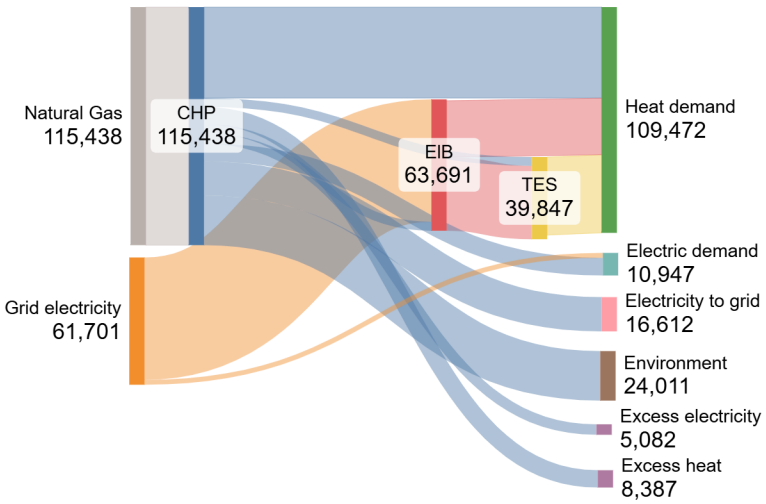

Figure 5 *Energy exchange in [MWh] in the utility systems for the energy price scenario with low mean prices, high variance, EGR 1 and TC scenario 'HighHP-LowRest'.*

3.3 Cost-optimal utility systems for energy price scenarios with high mean and high variance

Table 10 shows the installed technologies for the scenarios with high variance and high average prices. Compared to the scenarios discussed previously, additional investments are made, and the capacities installed show larger differences between the sub-scenarios. HP capacities range from 2 to 9 MW_{th}, TES from 15 to 113 MWh and ElB from 9 to 31 MW_{th}.

The combination of a high HP price and low gas cost in the 'EGR 1.6, HighHP-LowRest' sub-scenario results in the highest consumption of natural gas among all cost-optimal utility systems. The resulting energy flows are shown in Figure 6. The figure shows that most electricity generated by the CHP is sold to the grid, which can be explained by the high electricity prices in this scenario (price peaks reach 470 euro/MWh), which make selling power economically more attractive than storing it in the form of heat for later use. The figure also shows that the ElB supplies more heat than the HP, unlike in other scenarios with ElB and HP instalments, such as the one shown in Figure 4b in 3.1. This is because the combination of ElB and TES allows more flexibility at lower costs than a combination of HP and TES, as explained in the previous section. As a result, only a small HP of 2 MW_{th} is installed. When electricity prices are negative, the ElB operates at full capacity instead of the HP because the ElB is less efficient and consumes more electricity, which is beneficial when prices are negative. The technology portfolio and operation of the utility system in the 'EGR 1, LowHP-HighRest' sub-scenario is very different, as Figure 7 shows. In this scenario, the CHP delivers half of what it did in the HighHP-LowRest scenario depicted in Figure 6, as the thermal output by the ElB doubles and that of the HP nearly triples.

The energy use across the sub-scenarios differs greatly, as shown in Table 11. Even more power is sold to the grid than in the scenario discussed in 3.2, because (mean and peak) electricity prices have increased. In the 'EGR 1.6 HighHP-LowRest' sub-scenario, this results in more power being sold to the grid than consumed. The relative savings in TAC differ by a factor of almost 2 between the EGR scenarios.

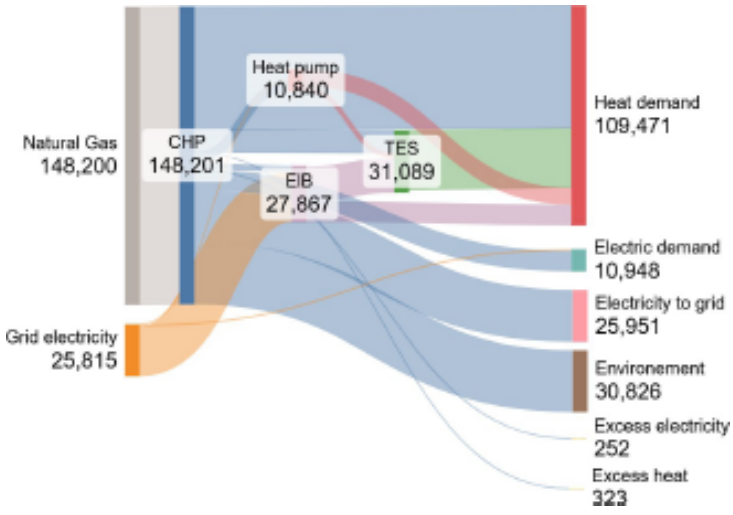

Figure 6 *Energy exchange in [MWh] in the utility systems for the energy price scenario with high mean prices, high variance, EGR 1.6 and TC scenario 'HighHP-LowRest'.*

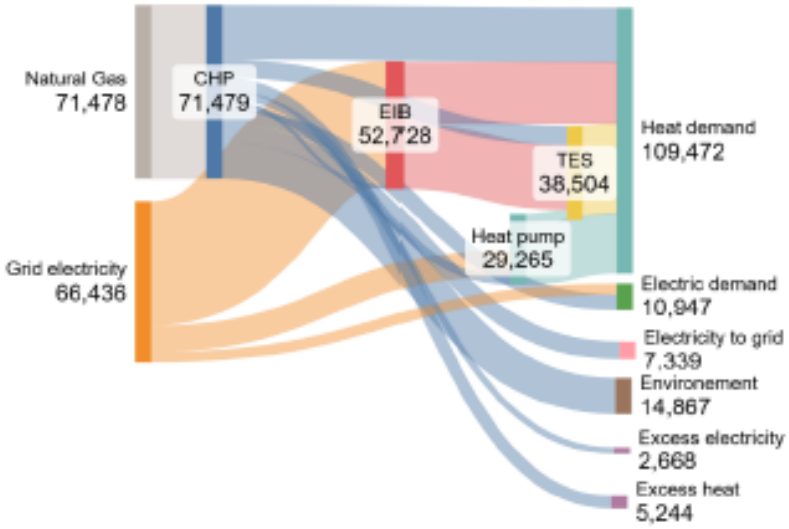

Figure 7 *Energy exchange in [MWh] in the utility systems for the energy price scenario with high mean prices, high variance, EGR 1 and TC scenario 'LowHP-HighRest'.*

Table 10 *Installed PtH and storage capacities in the energy price scenarios with high mean and high variance*

EGR	TC scenario	ElB [MW_{th}]	TES [MWh]	HP [MW_{th}]
1.6	HighHP-LowRest	31	113	2
	LowHP-HighRest	10	15	8
1	HighHP-LowRest	26	97	6
	LowHP-HighRest	9	17	9

Table 11 *Total annual cost (TAC), savings in TAC compared to the reference system, energy consumption including gas and power from the grid, and power sold to the grid in the energy price scenarios with high mean and high variance*

EGR	System	TC	TAC	Savings	NG to system	Power grid to system	System to power grid
		scenario	[M. Euro]	[%]	[GWh]	[GWh]	[GWh]
1.6	Reference	-	11.8		210.5	0.2	45.0
	New	HighHP-LowRest	9.9	16.1	148.2	25.8	26.0
	New	LowHP-HighRest	9.9	16.1	121.0	11.3	26.0
1	Reference	-	19.4		196.8	0.2	34.8
	New	HighHP-LowRest	14.2	26.8	105.5	22.0	3.7
	New	LowHP-HighRest	14.0	27.8	105.2	14.7	4.1

3.4 Cost-optimal utility systems for energy price scenarios with high mean and low variance

In the scenarios with high mean price and low variance, HPs and TES units are installed in all scenarios, with capacities ranging from 7 to 9 MW and 6 to 32 MWh, respectively. ElBs are only installed in scenarios with an electricity-to-gas-price ratio of 1 and their capacity is limited to 2 MW.

The CHP operates at minimal capacity most (i.e. 95-100%) of the time across all sub-scenarios. The heat from the CHP is fed to the process, whereas its power is used to drive the HP, the process itself and the ElB, if installed. When the process demands little heat and power, power from the CHP is sold to the grid because electricity prices are high and storage capacity is limited. The HP operates as a baseload heat supply next to the CHP, as shown for scenario 'EGR 1, HighHP-LowRest' in Figure 8. When heat demand is low, the HP is used to charge the TES. About 8% of the time, the HP is off because the CHP alone provides enough heat. In the 'LowHP-HighRest' scenarios, HP capacity increases while the TES capacity decreases. Since the load factor of the HP in this scenario is up to 10% lower than in the scenario discussed in 3.1, this means that the HP becomes economically viable at high mean electricity prices even when it is not operated at maximum capacity throughout the year. Table 13 shows that in all sub-scenarios, around 3 GWh are sold to the grid, which is less than in all other scenarios and less than one-tenth of the amount sold by the CHP in the reference model. This is due to the use of electricity from the CHP to power the HP. Like in the energy price scenario with high mean and variance (section 3.3), the relative savings in TAC differ by a factor of 2 between the EGR scenarios, reflecting the difference in gas prices. This can be explained by the amount of natural gas consumed, which is relatively similar in both scenarios (see Table 13).

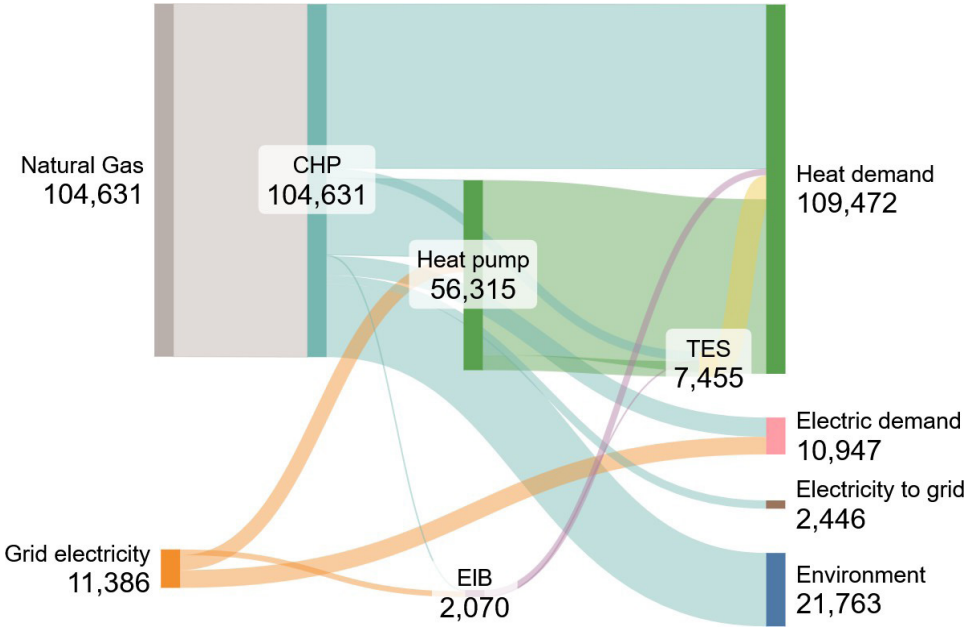

Figure 8 *Energy exchange in [MWh] in the utility systems for the energy price scenario with high mean prices, low variance, EGR 1 and TC scenario 'HighHP-LowRest'.*

Table 12 Installed PtH and storage capacities in the energy price scenarios with high mean and low variance

EGR	TC scenario	ElB [MWth]	TES [MWh]	HP [MWth]
1.6	HighHP-LowRest	0	19	8
	LowHP-HighRest	0	6	9
1	HighHP-LowRest	2	24	8
	LowHP-HighRest	2	7	9

Table 13 *Total annual cost (TAC), savings in TAC compared to the reference system, energy consumption including gas and power from the grid, and power sold to the grid in the energy price scenarios with high mean and low variance*

EGR	System	TC	TAC	Savings	NG to system	Power grid to system	System to power grid
		scenario	[M. Euro]	[%]	[GWh]	[GWh]	[GWh]
1.6	Reference	-	12.0		202.1	0	39.5
	New	HighHP-LowRest	10.7	11.3	109.3	8.5	2.9
	New	LowHP-HighRest	10.2	15.4	107.5	10.1	3.5
1	Reference	-	19.4		195.0	0	34.1
	New	HighHP-LowRest	14.6	24.6	104.6	11.4	2.5
	New	LowHP-HighRest	14.1	27.2	104.6	12.0	3.5

3.5 Equipment sizing

Fig. 9 shows the normalised equipment sizing of the ElBs, the HPs and the TESs in all considered scenarios. The small overlap between the PtH technologies shows that, in most cases, either HPs or ElBs are installed, and rarely both. Large HPs are predominantly installed in scenarios with high mean prices on the left side of Fig.9, and large ElBs are predominantly installed in the case of low and volatile energy prices, depicted on the right side of the figure. The large ElBs are combined with large TES, sized according to equipment cost. The highest HPs are installed when prices are, on average, high and show small fluctuations ('High mean low variance' scenarios). In these scenarios, neither the relative HP cost nor the electricity-to-gas price ratio leads to significant changes in the HP capacity. The large HPs in these scenarios are economically viable despite lower load factors because higher mean electricity prices lead to overall higher operational costs, which in turn leave more room for additional investment that enables operational cost savings.

Figure 9 shows that ElB and HP capacities are combined in the energy price scenarios with a low mean and low variance (LMLV), and with a high mean and a high variance (HMHV). In the LMLV scenarios, HP and ElB capacities are low, as energy prices are too low to justify the investment in HPs and too stable for large ElBs. In the HMHV scenarios, the large positive and negative price peaks lead to a large (26 MW) ElB capacity alongside a 6 MW HP and a 97 MWh TES when the equipment cost of the HP is high ('HMHV HighHP-LowRest'). The HP load factor ranges from 78 to 92%, which means that the HP operates as base load technology next to the CHP and confirms that high mean energy prices are required for the installation of HPs.

When an HP is installed, its size is affected by the EGR when HP capacities are below 5 MW, as seen in Table 10. Higher capacities of the HP are installed when the mean gas price is equal to the electricity price because switching from gas to electricity use leads to higher cost savings than in the scenarios with a lower gas price. The observed threshold of 5 MW can be explained by looking at Figure 10. The curve declines sharply around 12 MW. Since the CHP has to operate at minimal load at all times, the steady heat output of the CHP of around 6.5 MW reduces the heat that is required during around 7000 hours per year to 5.5 MW. HPs that operate above 5.5 MW, therefore, operate with a lower load factor and are only economically viable under HP-favourable conditions, i.e. high mean electricity prices. HPs that operate under those conditions are less sensitive to the EGR.

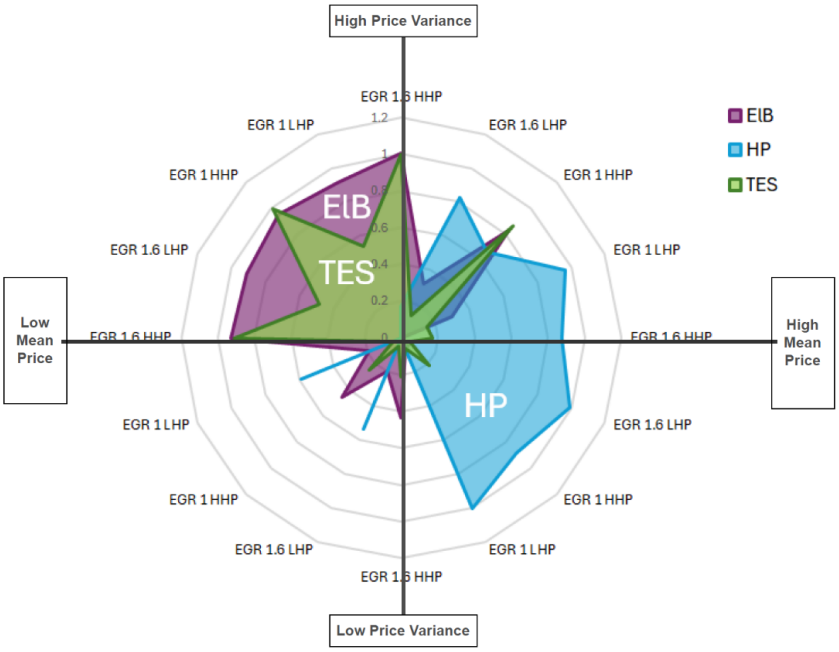

Figure 9 *Overview of normalized installed capacities across all scenarios. The right half of the diagram shows the installed capacities in energy price scenarios with a high mean price and the upper half for scenarios with a high price variance.*

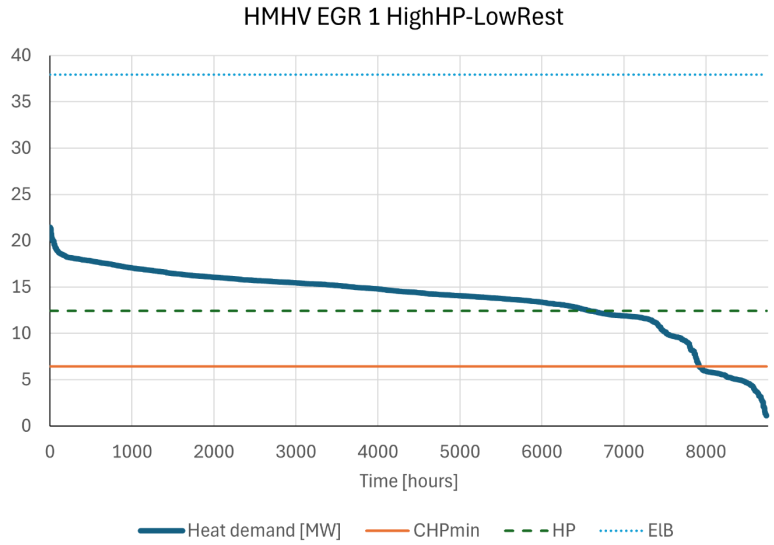

Figure 10 *Heat demand duration curve with the minimal heat output by the CHP and the added capacities by the HP and ElB in the HMHV EGR 1 HighHP-LowRest*

4 Limitations of the study

Though the results provide valuable insights for electrifying utility systems for the energy-intensive industry with fluctuating energy demand, the chosen method, assumptions, and scenarios have limitations. This section addresses them, offering important considerations for interpreting the results of this study.

The selected energy price scenarios are based on the assumption that companies pay for all their CO_2 emissions. Allowing free allocation of CO_2 permits would increase the EGR and likely limit the electrification technologies' economic viability. Additional price scenarios could be added to the analysis to explore "tipping points" for increasing levels of electrification.

Including the cost of energy transport in the model, such as network cost and peak tariffs, is also likely to affect the capacities and may reduce the share of electrification seen in the results. The authors expect that the effect would be more significant for the ElB capacity due to its less efficient use of electricity compared to an HP.

Peak tariffs would likely lead to decreased ElB and TES capacities because they disincentivise the consumption of large amounts of power. However, transport costs would not need to be added to the consumption of power generated by the CHP. Therefore, it would not affect the power exchange between the CHP and the PtH technologies, which is high in the systems presented. Hence, (partial) electrification of utility systems is likely still cost-optimal if grid use costs were included in the model.

The explored energy price scenarios do not account for energy price uncertainty since the system has perfect foresight. Accounting for operational difficulties any system encounters in the real world, where prices might deviate from the forecast, would result in capacities different from those presented, especially those of the storage units. Stochastic programming could be used to explore this aspect in future studies.

The main objective of the model is to minimise the total annual cost of the utility system. While this performance indicator provides valuable insights, other aspects, such as payback time and environmental impact, have not been considered, despite their importance to industry [44]. Including these indicators will likely result in other optimal solutions. The CO_2 emissions related to grid electricity (scope 2 emissions) are currently not considered in the model as they are case-specific and subject to change due to the ongoing decarbonisation of the national power generation. The model could be extended to include multiple objectives to explore the trade-offs between CO_2 emission reduction and TAC. This would likely result in higher PtH capacities, especially HP capacity, because of their conversion efficiency.

The sizing of the HP, ElB and other technologies also depends on the selected discount rate of 10%, and the absence of eventual retrofitting costs for the CHP in the model. A lower discount rate would incentivise investments and lead to larger installed capacities. The need to invest in the CHP due to required maintenance or retrofitting would likely have a similar effect. Larger PtH and storage capacities were also observed in model runs without the constraint limiting the CHP's operation to a minimum of 30% of its capacity. These results and a brief discussion are included in Appendix C. They indicate that more flexible CHPs would likely supply less energy to the process lead to higher levels of electrification in the utility system.

In this study, a CHP exists before electrifying the utility system. Since the results show that PtH and storage technologies use power generated by the CHP, the results would change if the CHP did not exist. The model was used to study the optimal electrification of a utility system for a paper mill with a grid connection capacity of 30 MW, which exists because of the plant's previous role as energy supplier. The size of the grid connection affects the sizing of the PtH technologies. The results show that the ElB is sized to this capacity when energy prices are highly volatile. Hence, a smaller connection capacity would result in a smaller ElB. As a consequence, the TES would be charged less and potentially scaled down. The size of the grid connection is likely to also affect the sizing of the HP, but only in cases when the HP's size exceeds that of the grid connection.

The variable operation of the utility system result in part-load operation of the PtH technologies. While this is not expected to affect the ElB, it would lead to a suboptimal efficiency of the HP. However, a change in the HP's efficiency in part load operation is neglected in the model to decrease its complexity. Accounting for it could lead to changes in HP capacity. Either the capacity would decrease while operation at full capacity would be increased, or the capacities would remain, but the share of heat generation of the HP would increase by reducing the use of any of the other technologies.

Finally, the TES in this study is modelled based on a latent heat storage unit with isothermal operation. This technology was selected based on the isothermal temperature supply by the HP for effective implementation [45]. When multiple TES systems were to be considered, the high-temperature potential of direct electrification could be combined with sensible heat storage that comes at a lower cost than latent heat storage [32]. The option for cheaper TES capacity might lead to higher ElB capacities.

5 Conclusions and recommendations for future work

This study presented an analysis of the influence of energy prices on the electrification of industrial utility systems for processes with highly variable energy demand. To this end, energy price profiles with differing average prices and variances and technology cost scenarios were explored. The analyses were carried out for a paper mill in the Netherlands with an existing utility system comprising a CHP and a connection to the national power grid of 30 MW.

The results show that under the assumed technical and economic conditions (presented in Tables 3, 4 and 5), electrification reduces the total annual cost by between 11 and 52 per cent. The model added heat pumps and/or electric boilers and thermal energy storage to the existing utility system; batteries and hydrogen technologies were not selected. A sensitivity analysis, presented and briefly discussed in Appendix B, shows that the cost for the electrolyser capacity has to decrease by between one and more than three orders of magnitude (depending on the energy price scenario) to become part of the cost-optimal technology portfolio. The difference between the scenarios is likely due to the number of hours with negative electricity prices, which allow the system to generate revenues because of the losses in hydrogen production. The fact that hydrogen is not picked up by the model can thus be explained by the high upfront cost. Therefore, we conclude that for the explored energy price and technology cost scenarios, hydrogen as an energy carrier is not required for cost-optimal electrification, as long as temperature requirements do not exceed what electric boilers and heat pumps can deliver. Using hydrogen might become more interesting when energy prices are high for extended periods of time, and the required storage capacity would become larger, as hydrogen storage costs are lower than the cost for alternative means of energy storage.

The heat supplied by the CHP is reduced to the minimum possible amount in most scenarios and replaced by power-to-heat and storage technologies. By using a large share of the power generated by the CHP to run the power-to-heat technologies, the amount of power sold to the grid is reduced compared to the reference case without power-to-heat and storage technologies.

Heat pumps are sized based on the process's heat demand duration curve, the minimal load of the CHP and the mean energy price. High and stable energy prices lead to the largest installed heat pump capacities. Lower energy prices limit the profitability of the investment-intensive heat pump and result in smaller capacities. The impact of the relative technology cost of heat pumps on their size increases with the variance of energy prices because the heat pump competes with the electric boiler and thermal energy storage, which have a lower cost and are, therefore, the cheaper peak technology.

The size of the electric boiler is mainly defined by the variance of electricity prices and is limited by the size of the grid connection and the thermal energy storage capacity. The operation of all components is a function of the electricity-to-gas-price ratio and the absolute electricity price.

It is recommended to further study utility system electrification. The presented model can serve as a basis for future research, which should explore valuing flexibility by a) assessing different energy markets (e.g., imbalance markets) and b) providing grid services. Moreover, including uncertainty in the analysis would add further understanding of optimal electrification strategies for industries with fluctuating energy demand.

Data availability

The code, selected input data and all results are going to be uploaded to a 4TU repository (DOI: 10.4121/3badc1a4-a0ac-4560-8e1e-2355214331fe) and a GitHub repository (https://github.com/SvenjaBie/ ElectrUtilPapIndOpen) once the article is ready for publication. They can be shared earlier upon request.

List of abbreviations

Bat	Battery
CO2	Carbon Dioxide
CaPex	Capital expenditure
CHP	Combined heat and power plant
COP	Coefficient of performance
EGR	Electricity-to-gas price ratio
ElB	Electric boiler
EU ETS	EU Emissions Trading System
GB	Gas boiler
GHG	Greenhouse gases
GT	Gas turbine
H2	Hydrogen
H2B	Hydrogen boiler
H2E	Electrolyzer
HMHV	High Mean High Variance
HMLV	High Mean Low Variance
H2S	Hydrogen storage tank
HRSG	Heat recovery steam-generator
LMHV	Low Mean High Variance
LMLV	Low Mean Low Variance
NG	Natural gas
OpEx	Operating expense
PtH	Power-to-heat
TAC	Total Annual Cost
TC	Technology Cost
TES	Thermal energy storage
TTF	Title Transfer Facility

Nomenclature of parameters and variables

Symbol	Explanation	Unit
Time-dependent variables (per time step)		
$H_{i,out}(t)$	heat output from technology i	MW
$NG_{in}(t)$	quantity of natural gas consumption	MW
$NG_{i,in}(t)$	quantity of natural gas consumption of technology i	MW
$P_{i,j}(t)$	power flow from technology/system i to j	MW
Sizing variables		
s_i	Sizing of technology i	MW or MWh
Time-dependent variables		
$P_{el,grid}(t)$	Electricity price at time t	Euro/MWh
$P_{NG}(t)$	Natural gas price at time t	Euro/MWh
$H_{dem}(t)$	heat demand of the process at time t	MW
$P_{dem}(t)$	power demand of the process at time t	MW
Constants		
AF_i	Annualization factor of technology i	-
c_i	Capital cost of component i	Euro/unit
COPideal	Carnot Coefficient of Performance	-
Hdem,max	Maximal heat demand	MW
Inf_i	Installation or Lang factor of technology i	-
LT_i	Lifetime of component i	years
r	Discount rate	%
Tsink	Temperature of the heat sink of the heat pump	K
Tsource	Temperature of the heat source of the heat pump	K
Δt	Time step duration	h
η	efficiency	-
$\eta i,therm$	percentage of energy conversion into heat by technology i	-
$\eta i,el$	Electric efficiency of technology i	-

References

[1] Unfccc, "THE PARIS AGREEMENT," techreport 2016. [Online]. Available: https://treaties.un.org/Pages/ViewDetails.aspx?src=TREATY&mtdsg_no=XXV

[2] T. Ministry of the Energy, European overview of GHG emissions.

[3] A. International Energy, "Renewable Energy for Industry From green energy to green materials and fuels," techreport 2017. [Online]. Available: www.iea.org/t&c/

[4] O. Roelofsen, K. Somers, E. Speelman, and M. Witteveen, "Plugging in: What electrification can do for industry," techreport 2020.

[5] H. Son, M. Kim, and J. K. Kim, "Sustainable process integration of electrification technologies with i ndustrial energy systems," Energy, vol. 239, 2022/1//, doi: 10.1016/j.energy.2021.122060.

[6] M. Wei, C. A. McMillan, and S. Can, Electrification of Industry: Potential, Challenges and Outlook. Springer Nature.

[7] B. Zuhlsdorf, "Task 1: Technologies – State of the art and ongoing developments for systems and components," in About High Temperature Heat Pumps, vol. 58. https://heatpumpingtechnologies.org/annex58/task1/: International Energy Agency, 20.

[8] J. Deng, Q. Wei, M. Liang, S. He, and H. Zhang, "Does heat pumps perform energy efficiently as we expected: Field tests and evaluations on various kinds of heat pump systems for space heati ng," Energy and Buildings, vol. 182, pp. 172-186, 2019/1//, doi: 10.1016/j.enbuild.2018.10.014.

[9] J. G. Kirkerud, T. F. Bolkesjø, and E. Trømborg, "Power-to-heat as a flexibility measure for integration of renewable en ergy," Energy, vol. 128, pp. 776-784, 2017, doi: 10.1016/j.energy.2017.03.153.

[10] M. N. I. Maruf, G. Morales-España, J. Sijm, N. Helistö, and J. Kiviluoma, "Classification, potential role, and modeling of power-to-heat and ther mal energy storage in energy systems: A review," Sustainable Energy Technologies and Assessments, vol. 53, 2022/10//, doi: 10.1016/j.seta.2022.102553.

[11] R. Padullés, M. L. Hansen, M. P. Andersen, B. Zühlsdorf, J. K. Jensen, and B. Elmegaard, "Potential for optimal operation of Industrial Heat Pumps with Thermal Energy Storage for emissions and cost reduction," International Conference on Efficiency, Cost, Optimization, Simulation, 2023///, pp. 2194-2205, doi: 10.52202/069564-0198.

[12] H. Son, M. Kim, and J.-K. Kim, "Sustainable process integration of electrification technologies with industrial energy systems," Energy, vol. 239, p. 122060, 2022.

[13] H. Wiertzema, E. Svensson, and S. Harvey, "Bottom–Up Assessment Framework for Electrification Options in Energy-Intensive Process Industries," Frontiers in Energy Research, vol. 8, p. 192, 2020.

[14] J.-K. Kim, "e-Site Analysis: Process Design of Site Utility Systems With Electrifi cation for Process Industries," Frontiers in Thermal Engineering, vol. 2, 2022/4//, doi: 10.3389/fther.2022.861882.

[15] J. V. Walden, M. Bähr, A. Glade, J. Gollasch, A. P. Tran, and T. Lorenz, "Nonlinear operational optimization of an industrial power-to-heat system with a high temperature heat pump, a thermal energy storage and wind energy," Applied Energy, vol. 344, p. 121247, 2023.

[16] S. Trevisan, B. Buchbjerg, and R. Guedez, "Power-to-heat for the industrial sector: Techno-economic assessment of a molten salt-based solution," Energy Conversion and Management, vol. 272, p. 116362, 2022.

[17] N. Baumgärtner, R. Delorme, M. Hennen, and A. Bardow, "Design of low-carbon utility systems: Exploiting time-dependent grid e missions for climate-friendly demand-side management," Applied Energy, vol. 247, pp. 755-765, 2019/8//, doi: 10.1016/j.apenergy.2019.04.029.

[18] C. Reinert et al., "Combining optimization and life cycle assessment: Design of low-carbon multi-energy systems in the SecMOD framework," in Computer Aided Chemical Engineering, vol. 51: Elsevier B.V., 2022, pp. 1201-1206.

[19] S. Bielefeld, M. Cvetkovic, and A. Ramirez. The potential for electrifying industrial utility systems in existing chemical plants [Manuscript submitted for publication].

[20] M. Fleschutz, M. Bohlayer, M. Braun, and M. D. Murphy, "From prosumer to flexumer: Case study on the value of flexibility in decarbonizing the multi-energy system of a manufacturing company," Applied Energy, vol. 347, p. 121430, 2023.

[21] D. M. Bor and C. A. Infante Ferreira, "Quick selection of industrial heat pump types including the impact oft hermodynamic losses," Energy, vol. 53, pp. 312-322, 2013/5//, doi: 10.1016/j.energy.2013.02.065.

[22] G. Oluleye, M. Jobson, and R. Smith, "Process integration of waste heat upgrading technologies," Process Safety and Environmental Protection, vol. 103, no. Part B, pp. 315-333, 2016/9//, doi: 10.1016/j.psep.2016.02.003.

[23] P. Voll, C. Klaffke, M. Hennen, and A. Bardow, "Automated superstructure-based synthesis and optimization of distribut ed energy supply systems," Energy, vol. 50, no. 1, pp. 374-388, 2013/2//, doi: 10.1016/j.energy.2012.10.045.

[24] A. Danish Energy, "Technology Data-Energy Plants for Electricity and District heating gen eration," techreport 2016. [Online]. Available: http://www.ens.dk/teknologikatalog

[25] S. Madeddu et al., "The CO2reduction potential for the European industry via direct electr ification of heat supply (power-to-heat)," Environmental Research Letters, vol. 15, no. 12, 2020/12//, doi: 10.1088/1748-9326/abbd02.

[26] S. Krishnan et al., "Present and future cost of alkaline and PEM electrolyser stacks," International Journal of Hydrogen Energy, 2023, doi: 10.1016/j.ijhydene.2023.05.031.

[27] X. Wang, W. Huang, W. Wei, N. Tai, R. Li, and Y. Huang, "Day-Ahead Optimal Economic Dispatching of Integrated Port Energy Syste ms Considering Hydrogen," IEEE Transactions on Industry Applications, vol. 58, no. 2, pp. 2619-2629, 2022, doi: 10.1109/TIA.2021.3095830.

[28] H. Yang, X. Lin, H. Pan, S. Geng, Z. Chen, and Y. Liu, "Energy saving analysis and thermal performance evaluation of a hydroge n-enriched natural gas-fired condensing boiler," International Journal of Hydrogen Energy, vol. 48, no. 50, pp. 19279-19296, 2023/6//, doi: 10.1016/j.ijhydene.2023.02.027.

[29] B. Zühlsdorf, "IEA High-Temperature Heat Pumps Task 1-Technologies Task Report Operat ing Agent," techreport. [Online]. Available: https://heatpumpingtechnologies.org/annex58/wp-content/uploads/sites/70/2023/09/annex-58-task-1-technologies-task-report.pdf

[30] Arup and kiwa, "Industrial Boilers. Study to develop cost and stock assumptions for op tions to enable or require hydrogen-ready industrial boilers," techreport 2022/12//. [Online]. Available: https://assets.publishing.service.gov.uk/government/uploads/system/uploads/attachment_data/file/1123264/External_research_study_hydrogen-ready_industrial_boilers.pdf

[31] M. Fleschutz, M. Bohlayer, M. Braun, and M. D. Murphy, "From prosumer to flexumer: Case study on the value of flexibility in d ecarbonizing the multi-energy system of a manufacturing company," Applied Energy, vol. 347, p. 121430, 2023/10//, doi: 10.1016/j.apenergy.2023.121430.

[32] A. International Renewable Energy, Innovation outlook thermal energy storage.

[33] Nrel, Utility-Scale Battery Storage.

[34] L. Council, McKinsey, and Company, "Net-zero heat Long Duration Energy Storage to accelerate energy system decarbonization Contents," techreport 2022. [Online]. Available: www.ldescouncil.com.

[35] I. Petkov and P. Gabrielli, "Power-to-hydrogen as seasonal energy storage: an uncertainty analysis for optimal design of low-carbon multi-energy systems," Applied Energy, vol. 274, 2020/9//, doi: 10.1016/j.apenergy.2020.115197.

[36] E. Entso, ENTSO-E Transparence Platform.

[37] Ember, Carbon Price Tracker.

[38] investing.com, Dutch TTF Natural Gas Futures Historical Data.

[39] Ice, Dutch TTF Natural Gas Futures.

[40] Statista, Daily European Union Emission Trading System (EU-ETS) carbon pricing f rom 2022 to 2024 (in euros per metric ton).

[41] G. Towler and R. Sinnott, "Chemical Engineering Design: Principles, Practice and Economics of Pla nt and Process Design, Second Edition," techreport.

[42] Bves, "Technology: Solid Medium Heat Storage GENERAL DESCRIPTION Mode of ener gy intake and output," techreport 2024. [Online]. Available: https://iea-es.org/wp-content/uploads/public/FactSheet_Thermal_Sensible_Solids.pdf

[43] Ispt, "A One-GigaWatt Green-Hydrogen Plant. Advanced Design and Total Install ed-Capital Costs," techreport 2022.

[44] C. s. reporting, "Financial Services Directorate-General for Financial Stability and Capital Markets Union.." [Online]. Available: https://finance.ec.europa.eu/capital-markets-union-and-financial-markets/company-reporting-and-auditing/company-reporting/corporate-sustainability-reporting_en.

[45] I. Sarbu and C. Sebarchievici, A comprehensive review of thermal energy storage. MDPI.

SECTION 4

CONCLUSIONS

CHAPTER 7
CONCLUSION

This dissertation presents the development of design methods that support the deployment of heat pump solutions in a transitioning industrial sector. These are developed by addressing potential changes in production processes, heat pump configurations, integration with other utilities and energy storage units, energy prices, and equipment costs. These methods will support decision-making processes because the deployment of heat pumps is often hindered by challenges such as identifying the right process connections, identifying economically feasible solutions, and integrating heat pumps with other power-to-heat and storage technologies. By addressing these aspects, this thesis aims to foster the deployment of heat pump technologies in industry and thereby decarbonize its heat demand, which accounts for about 75% of industrial greenhouse gas emissions.

Section 7.1 presents the research outcomes of this study. Section 7.2 discusses the overall limitations and section 7.3 presents the overarching conclusions. Section 7.4 closes this dissertation with recommendations for future research.

1 Research outcomes

The development of design methods that support the deployment of heat pump solutions for industrial processes in the context of the energy transition is based on the answers to the research sub-questions presented in Chapter 1. This section presents the answers to each of these questions.

Question 1: *How does the deployment sequence of a heat pump and other industrial CO_2 mitigation measures influence their combined CO_2 reduction potential?*

A state-of-the-art review conducted in Chapter 2 showed that in decarbonization pathways currently proposed in the literature, potential interactions between mitigation measures that could affect the overall performance are not explicitly addressed but are often assumed to be covered by choosing conservative estimates and working with ballpark figures [1, 2]. However, some authors, like Johanson et al. [3], indicate that while this might be sufficient for changes to core processes, it may be inadequate for heat integration measures. In this thesis, the impact of the deployment sequence on the combined CO_2 reduction potential was studied by exploring future plant layouts using a biodiesel production process as a case study. These layouts were developed based on a literature review of CO_2 mitigation measures with a Technology Readiness Level (TRL) of at least 8 as the focus was on technologies that could be implemented in the short and medium term. For each future plant layout, consistent energy and mass balances were constructed and used in a pinch analysis to estimate the performance of the heat pump. Subsequently, all possible sequence variations were compared to assess their impact on total CO_2 mitigation potential.

The results show that heat pumps, as a heat integration measure, are particularly sensitive to changes in process conditions. This sensitivity is illustrated in the extreme case presented in the decomposition graph in Fig. 1. This figure shows that although the heat pump could significantly reduce direct (scope 1) CO_2 emissions of the plant (from 4.6 to 1.1 kt/a), this reduction will be largely canceled out by the sequential deployment of the divided-wall column (+2.2 kt/a), as the required temperature of its reboiler was deemed too high for the heat pump and therefore steam from natural gas was needed to reach the required temperature. The later addition of a membrane reactor would not significantly affect the total mitigation potential.

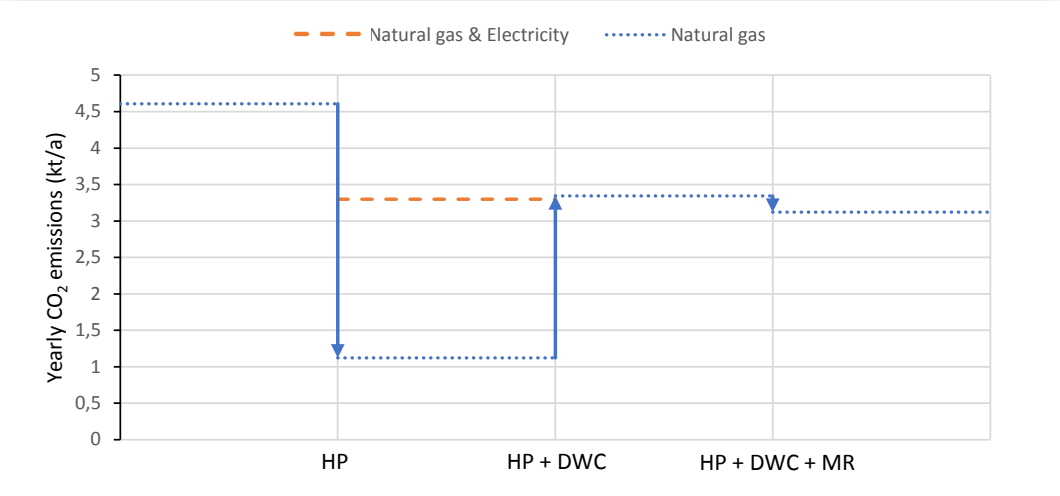

Figure 1 *Decomposition graphs of a deployment sequence, where changes in the amount of CO_2 emissions from natural gas combustion and electricity generation are presented in the curve. A heat pump (HP) is deployed at the first step on the x-axis, thereafter a divided wall column (DWC), and a membrane reactor (MR).*

The mutual exclusivity between the heat pump and the divided wall column highlights the risk of lock-in. This risk is especially apparent when considering heat integration measures, like heat pumps, at the outer rings of the Douglas onion-diagram. The deployment of mitigation measures belonging to the inner rings of the onion, such as the reactor and separation sections, seemed to have less effects on each other. When such mitigation measures are considered, a conservative estimation of the reduction potential is likely to provide a good enough representation of the combined CO_2 mitigation potential.

Hence, the study presented in Chapter 2 shows that when heat pumps are considered in the portfolio of mitigation options, the combined CO_2 reduction potential cannot be estimated as the sum of individual measures. In the case study, only 58% of the expected combined CO_2 reductions would be achieved in the deployment sequence with the highest CO_2 reduction, where the combination of a membrane reactor and a divided wall column enable the use of a heat pump. The deployment sequence, thus, determines the combined CO_2 reduction potential of a set of technologies, especially when heat integration measures such as heat pumps are considered, as it can exclude other technologies from being effective, reduce the effectiveness of existing processes, or enable new opportunities for to-be-installed technologies. Careful consideration of interactions between measures is, therefore, essential to maximize the effectiveness of industrial CO_2 mitigation strategies and achieve deep decarbonization.

***Question 2**: How to identify CO_2 mitigation measures that improve the performance of an already installed heat pump?*

Heat pumps are a promising option to decarbonize industrial heat demand, as they can use a surplus of heat existing within a given process to meet heating requirements. This requires placing the heat pump across the pinch point and thereby connecting a region with a net surplus of heat to a region with a net heat demand. However, additional CO_2 mitigation measures are likely to be needed to meet CO_2 reduction goals, for instance, processes may need to change. These process changes might affect the location of the pinch point and, therefore, the performance of the heat pump.

In Chapter 3, the impact of process changes on the location of the pinch point and the performance of the heat pump was studied by using Process Change Analysis. In this approach, streams of interest, such as heat pump connections, are extracted from the rest of the process to study how those streams relate to the pinch point formed by the remaining (background) process. In this chapter, the method was extended by including the concept of exergy to examine how process changes affect the work requirements of a heat pump. By extending this approach with exergy analysis, it was possible to assess the impact of deploying CO_2 mitigation measures on the pinch point of the rest of the process and, consequently, on the heat pump's work targets. This approach was used in two case studies: a biodiesel production plant and a vinyl chloride monomer purification process.

The split- Exergy Grand Composite Curve of the biodiesel production plant showed that the performance of the heat pump was limited by a 40 kW pocket that resulted from the heat pump connections being above the pinch point of the background process. Lifting the pinch point of the background process would therefore improve the plant-level coefficient of performance (COP) of the heat pump. The pinch point was lifted by replacing the wet water washing column with a membrane separation unit, which resulted in a reduction of heating requirements from 0.9 MW to 0.3 MW, whilst increasing the plant-level COP of the heat pump from 4.0 to 4.1.

The split-grand composite curve of the vinyl chloride monomer purification process showed that the heat source of the heat pump could provide heat in several ways with regard to the pinch point of the background process. Heat could be extracted at a higher temperature whilst crossing the background pinch, or from a lower temperature whilst extracting heat from below the background pinch, as depicted in Fig. 2. Extracting heat from the top-end minimized work requirements, but resulted in a penalty due to the inappropriate placement. Extracting heat from the bottom-end would avoid this penalty, but it requires more work. Extracting heat over the entire temperature range, a split heat extraction achieved the highest plant-level COP by extracting heat at a higher temperature without incurring a penalty. This split heat extraction led to a 6.5 % increase in COP compared to the top-end extraction approach.

In conclusion, when selecting CO_2 mitigation measures that are to be placed alongside an already installed heat pump, their impact on the pinch of the background process and its relation to the connections of the heat pump is vital. Chapter 3 shows that a combination of Process Change Analysis and a Split-Exergy Grand Composite Curve can assist in this process, as it not only visualized the relation between the pinch of the background process and the heat pump connections, but also the work requirements by the heat pump.

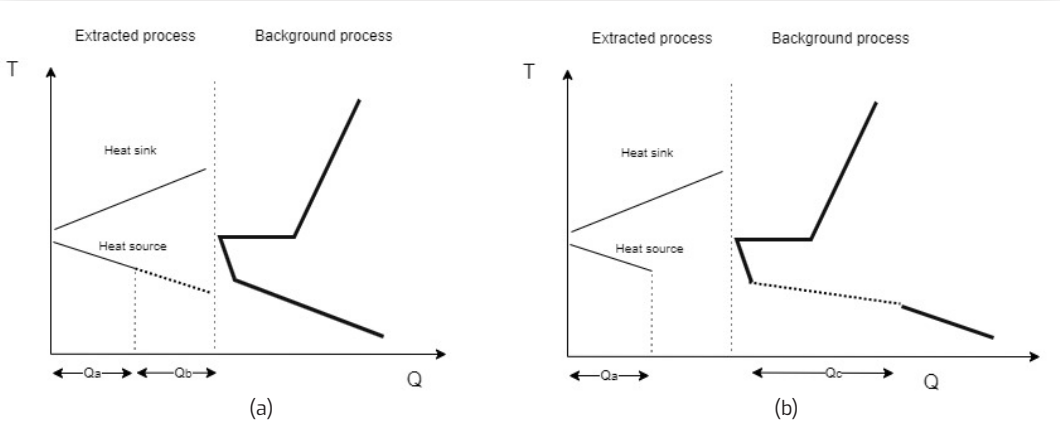

Figure 2 *Split grand composite curve. a) A split grand composite curve for a given process, where heat pump connections are extracted from the background process. The heat source of the heat pump is split into two sections; Q_a and Q_b, representing the top and bottom end of the stream, respectively. b) A split grand composite curve of the same process, where a heat pump is extracted, but the bottom-end of the heat available in the heat source is transferred back into the background process, forming Qc in the process.*

Question 3: *How to identify the optimal techno-economic heat pump configuration in case of high temperature lifts?*

Irreversibilities cause the subcritical single-stage (SS) cycle, Fig. 3.a, to become uneconomical at higher temperature lifts, leading to increased operational costs. Advanced heat pump configurations aim to minimize these irreversibilities, reducing the work required by the compressor and thus increasing the COP. While many advanced configurations are discussed in the literature for specific sink temperatures and temperature lifts, they are often benchmarked against each other or based on new ideas. However, we lack a) a systematic approach to develop an SS cycle into an advanced cycle for specific applications, and b) a thorough understanding of how the heat sink temperature and temperature lift impact the contributions of these changes.

In Chapter 4, both energy and exergy-based cost minimization were used to identify the origin of the operational cost in a heat pump cycle. Energy use by the compressor was used as the main metric for the energy-based analysis. For the exergy-based analysis, the flow rate of exergy destruction was used to calculate the cost flow rate at a component level, as all exergy destruction had to be compensated by additional work requirements at the compressors drive. Both approaches were illustrating by optimizing the techno-economic performance of a steam-generating heat pump that produced 10 tonnes per hour of 2 bar steam from 50 kg/s wastewater at 80 °C.

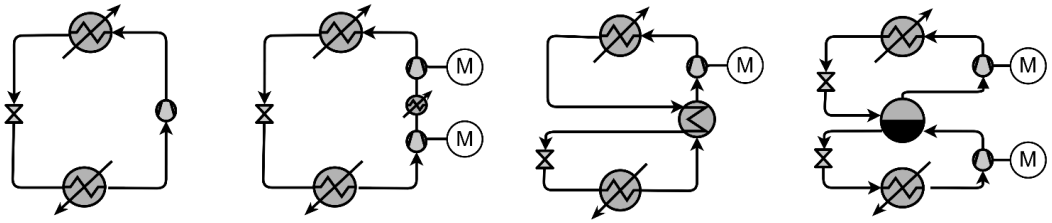

Figure 3 *Overview of advanced HP configurations.*
a) Subcritical single-stage (SS) cycle,
b) two-stage compression and intermediate cooler (2IC) cycle;
c) Internal heat exchanger (IHX) cycle, and
d) two-stage compression with a flash vessel (2FV) cycle.

The results of the energy-based analysis showed that the compressor was the cause of most operational losses for a steam-generating SS cycle heat pump. Intermediate compression, as in Fig 7.3.b, was used to improve the compressor's efficiency and reduce operational cost. Contrary, the exergy-based analysis pinpointed the expansion valve as the main source of operational cost. Therefore, an internal heat exchanger (IHX), as shown in Fig 7.3.c, or a two-stage compressor with a flash vessel (2FV), as shown in Fig 7.3.d, were introduced to reduce exergy destruction in the expansion valve and its related operational cost. Opposed to the introduction of the intermediate cooler that reduced the COP by 0.1 and increased the total cost of ownership (TCO), the exergy-based changes resulted in both a higher COP and a lower TCO after five years. Under the assumed equipment cost and energy price, the addition of the internal heat exchanger showed the largest improvement on the techno-economic performance (it increased the COP from 2.3 to 2.8 and lowered the TCO from 9.2 M€ to 8.7 M€ after five years).

In addition, Chapter 5 shows how the performance of heat pump cycles is affected by changes in the sink temperature and the temperature lift. In this chapter, an exergo-economic analysis was used to compare heat pumps at a cycle-level and explain these differences by mapping declines in exergy efficiency at a component-level. Moreover, advanced exergy analysis was used to identify the origin of the decline in exergy efficiency by separating component-level exergy destruction into destruction caused by inefficiencies of the component itself (endogenous) from the exergy destruction caused by interactions and inefficiencies of other components (exogenous).

Chapter 5 explored the hourly cost rate, composed of the hourly levelized cost of investment and the cost of exergy destruction of a single stage subcritical cycle (SS), the internal heat exchanger cycle (IHX), the ejector cycle (EJ), and the cycle with a two-stage compressor and flash vessel (2FV). The key results of this study are depicted in Fig. 4 for a heat source of 50 °C. The figure shows that the hourly cost rate of the SS cycle is the lowest at a sink temperature of 80 °C, and the highest at a sink temperature of 140 °C. Moreover, the graph shows that the rate of decrease in the cost of exergy destruction differs between cycles. This is due to the different decline rates of exergy efficiency, as depicted in Fig. 5. In this figure, the decline rate of the SS cycle (Fig. 5.a) is much higher than the rate of the 2FV cycle (Fig. 5.b). The advanced exergy analysis further identifies the origin of this decline. At low temperature lifts, the exergy destruction was evenly distributed between endogenous (50%) and exogenous (50%) sources. However, at higher temperature lifts for the SS cycle, it shifts to 80% endogenous and only 20% exogenous. Similar trends are apparent for the other cycles. For these cycles, it holds that the addition of components improves the exergy efficiency at component-level, but also introduces a new source of exergy destruction. Nonetheless, the new sources in the 2FV and IHX cycle add the least amount of new exergy destruction, which makes them the preferred cycle at high temperature lifts. Chapter 5 also explores the option of an open cycle and a mechanical vapor

recompression (MVR) system. The MVR system is preferred when a heat source can directly produce steam at a pressure that meets the MVR's minimum pressure requirement. This preference is due to its low equipment cost. Moreover, the results show that for higher sink temperatures above 130 °C, the MVR has a marginally better economic performance than the considered closed-cycles when combined with an SS cycle that produces steam at 80 °C. In the range between being able to directly produce steam from a heat source and a sink temperature of 130 °C, closed-cycles are preferred under the used economic assumptions. However, the closed-cycle that is preferred shifts with nearly each temperature step and is the outcome of a constant trade-off between reducing operational expenses and increasing the investment cost. Nonetheless, chapters 4 and 5 show that the economic viability of a heat pump can be significantly improved by systematically assessing the exergy destruction within the cycle.

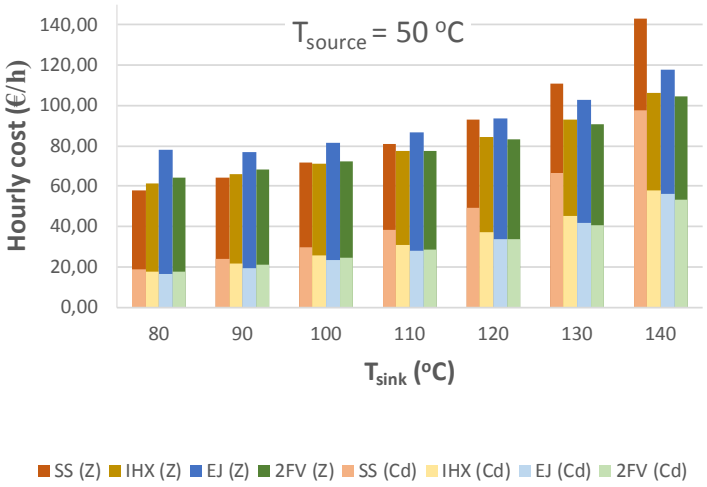

Figure 4 *Comparison of the total hourly levelized cost of investment ($\dot{z}$) and the cost of exergy destruction ($\dot{C}d$) of closed SGHP cycles, namely the single stage subcritical cycle (SS), the internal heat exchanger cycle (IHX), the ejector cycle (EJ), and the cycle with a two-stage compressor and flash vessel (2FV). The subfigures depict the hourly cost with a source temperature of 50 °C*

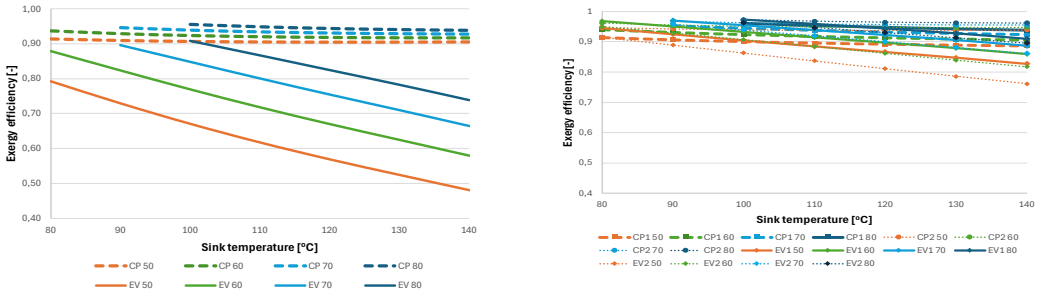

Figure 5 *The development of component-level exergy efficiency with increasing sink temperatures. The temperatures in the legend indicate the source temperature.*
a) subcritical single-stage (SS) cycle and
b) two-stage flash vessel (2FV) cycle.

In summary, the study presented in Chapter 4 shows that exergy analysis provides a better bases for identifying improvements to the configuration of a heat pump cycle than energy analysis as it pinpoints the origin of additional work requirements for the compressor. Hence, the work illustrates why exergy analysis should be the basis for improving heat pump configurations. Chapter 5 shows that the economically preferred heat pump configuration changes with the required temperature lift and sink temperature, which is due to a trade-off between investment and operational cost. The latter strongly depends on the cycle configuration and becomes increasingly important with rising temperature lifts and temperature sinks. The figures, such as those provided on the cycle-level exergo-economic comparison in Chapter 5.3.1, can be used to identify interesting configurations for a specified source and sink temperature. The impact of, for example, changes in the electricity prices can be deduced from the exergy efficiency plots in Chapter 5.3.2. Together, they will assist in identifying the techno-economically optimal heat pump configuration.

Question 4: *How do energy prices and technology costs affect the deployment of heat pumps and other power-to-heat and storage technologies in the electrification of utility systems?*

Heat pumps are a crucial technology for enhancing energy efficiency by utilizing waste heat and enabling electrification through the switching of energy carriers. When deployed, they are often combined with other power-to-heat (PtH) and storage technologies to maximize economic benefits from fluctuating renewable energy sources. These energy sources can lead to periods of low electricity prices when abundant and high prices when scarce. The impact of these price variations on the optimal sizing and operation of electrified utility systems, including heat pumps, is however not well understood.

Chapter 6 presents a mixed integer linear program (MILP) model aiming to minimize the total annual cost (TAC) of an electrified utility system for a process with highly volatile heat demand. The model includes options for: 1) direct electric power-to-heat conversion using an electric boiler; 2) indirect electric power-to-heat conversion via hydrogen using an electrolyser, a storage tank, and a hydrogen boiler, and 3) electrification by upgrading waste heat in a heat pump. Power to or heat from these technologies can be stored in an electric battery or thermal energy storage, as depicted in Figure 6. The study examines additions to an existing fossil-based utility system under different energy prices and equipment cost scenarios, exploring three key uncertainties: average energy price, price fluctuations, and the electricity-to-gas price ratio based on manipulated data of the day-a-head market on a hourly basis.

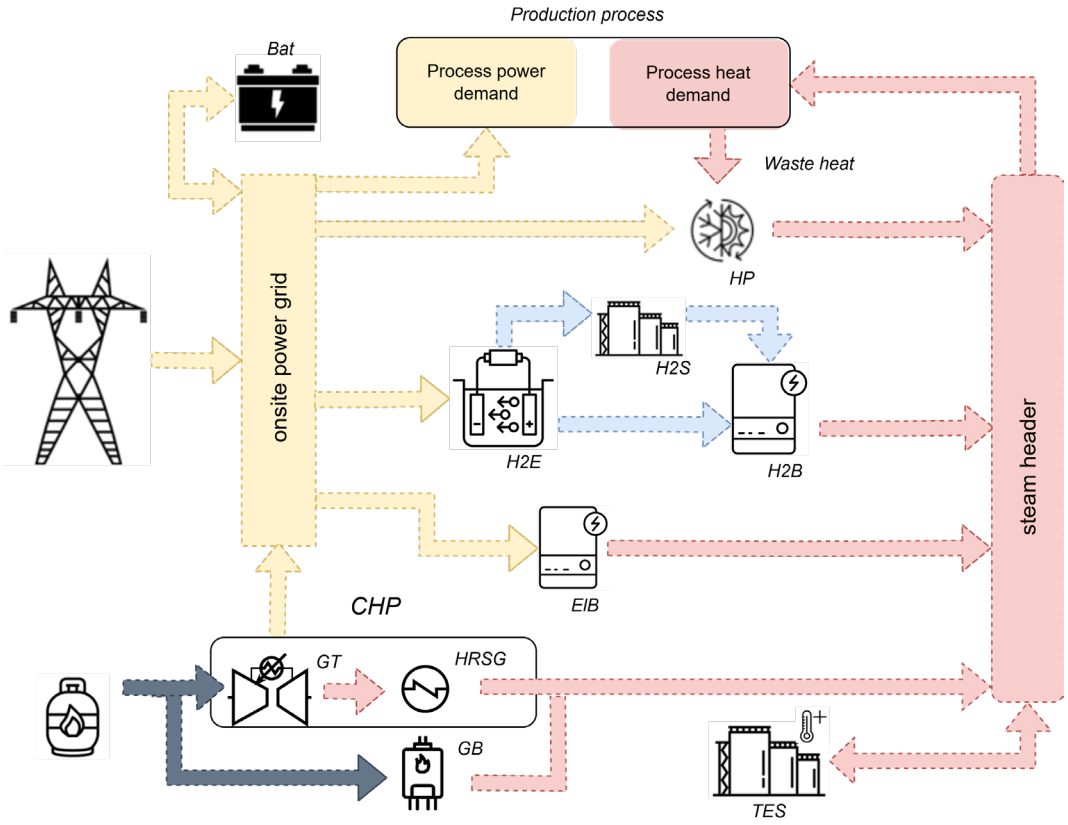

Figure 6 *Electrified fossil utility model consisting of the original combined heat and power (CHP) unit consisting of a gas turbine (GT), a heat recovery steam-generator (HRSG) and a gas boiler (GB), and three potential electrification routes: 1) direct electricity to heat conversion by an electric boiler (ElB); 2) indirect electricity of heat conversion via hydrogen (H2) with an electrolyser (H2E), a storage tank (H2S), and a hydrogen boiler (H2B), and 3) electrification by upgrading waste heat in a heat pump (HP). Power or heat from these technologies can either be stored in an electric battery (Bat) or a thermal energy storage (TES) unit.*

The results show that electrification of existing utility systems is economically viable under the considered energy and equipment prices. In all scenarios, either an electric boiler, a heat pump, or a combination of both is installed. Indirect electrification via hydrogen or power storage in batteries is not selected by the model as an economically attractive option due to its high upfront cost and low conversion efficiency, although thermal energy storage is utilized. The model sizes the heat pump based on the process's heat demand curve, the heat supply by the combined heat and power unit, and the mean energy price. The combined heat and power operates at a minimum load in most scenarios. High and stable electricity prices lead to the largest installed HP capacities, allowing for an economically viable solution with a lower load factor. Under these conditions, the heat pump serves as a baseload heat supply, consuming most of the power from the gas turbine. The impact of equipment cost on the sizing of the heat pump is limited under high and stable electricity prices.

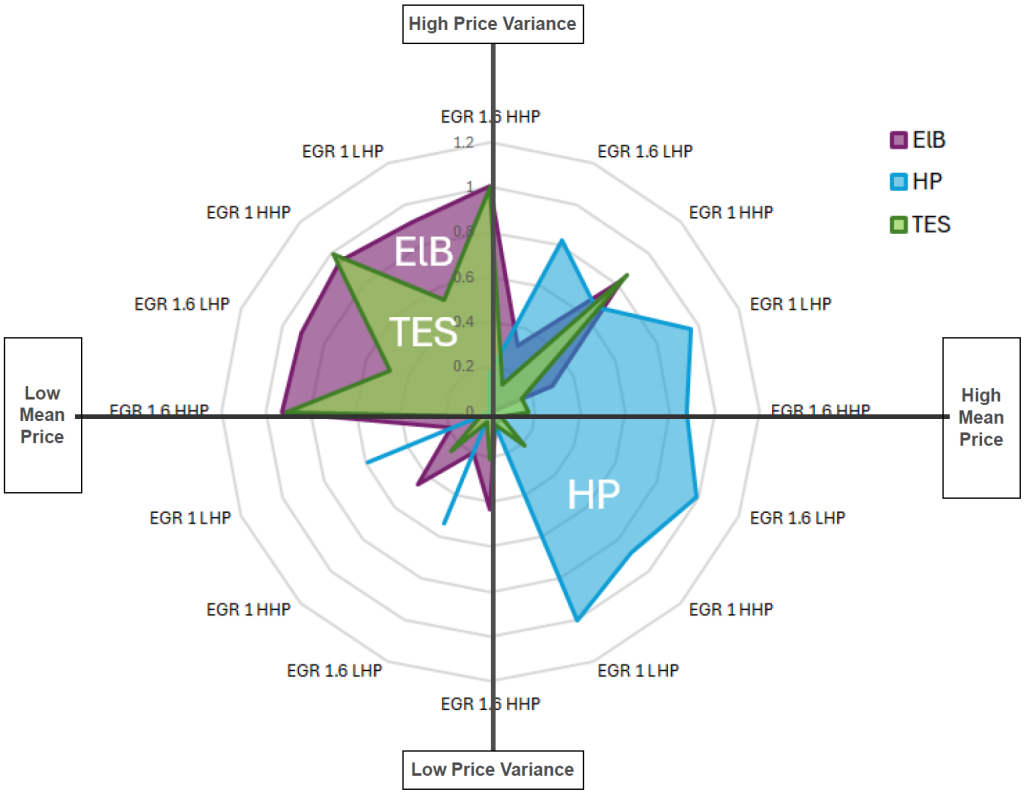

Figure 7 *Radar diagram of unitized installed power-to-heat and storage technology capacities for a range of scenarios with changing levels of price variance, average (mean) values, electricity-to-gas price ratios and equipment cost scenarios (LHP stands for Low equipment cost heat pump scenario; and HHP for high equipment cost heat pump scenario).*

With higher price volatility, the model favored the use of electric boilers combined with large thermal energy storage and the export of power from the gas turbine when electricity prices were high and the electricity-to-gas price ratio was favorable. In such scenarios, the size of the electric boiler was defined by the grid connection capacity (30 MW in the case considered), as maximizing its use during low or negative price hours provided the best economic performance. Consequently, the size of the heat pump varied from 2 to 9 MW, and the size of the electric boiler ranged from 9 to 31 MW, depending on equipment costs. Competition from the electric boiler was even stronger at low mean prices. Under these conditions, heat pumps were only installed in scenarios with low equipment costs and low energy price volatility. When energy price volatility was high, no heat pumps were installed. Hence, the efficient but high investment cost of the heat pump provides a different type of solution than the low investment but low efficiency electric boiler, as depicted in Fig. 7.

In conclusion, this work shows that both energy prices and grid connection capacity play a crucial role in determining the deployment and operation of heat pumps and other power-to-heat and storage technologies in electrifying utility systems. High and stable electricity prices favor the installation of heat pumps, while high price variations and lower electricity prices make electric boilers and thermal energy storage more attractive. The electricity-to-gas price ratio further influences the choice and sizing of technologies, with lower ratios promoting electrification. Low equipment cost prices have a similar effect.

2 Limitations

Due to limited time-resources, only a limited number of technical interactions between the heat pump and modifications to the production plant could be assessed, which used simplified process models and plant layouts (e.g. Chapters 2 and 3). The extent to which these simplifications may not capture all interactions between technologies was not explored. It should also be noted that the emphasis of this study was on the design of utility systems and not on core production processes. Nonetheless, process change analysis extended with the Split-Exergy Grand Composite Curve, as shown in Chapter 3, can be used to study the impact of all possible heat related modifications.

The work in this thesis did not include the impact of operational dynamics on the performance of a heat pump. These include the impact of a system start-up, a shut-down, or other forms of off-design operation. Insights from such analysis might, for example, advocate for less process-integrated heat pumps that are less dependent on process conditions elsewhere in the production process and can operate regardless of local process fluctuations.

Finally, it is worth highlighting that the accuracy of cost estimates in this exploratory stage of technology solutions is limited due, amongst others, a limited knowledge about the cost of integration, actual equipment cost and the future cost of energy (use). Especially the latter two aspects are notoriously difficult to predict, due to the sharp increase in renewable variable electricity in the grid, regulatory changes, and geopolitical developments. Although Chapter 6 explores the impact of changes in the mean energy price and its fluctuations, these changes were based on simplified assumptions as it was not possible to include actual developments within the power sector, such as the exemption of for example grid-fees and an exploration of different types of "energy markets and services" (e.g. the automated frequency response reserve). The inclusion of these aspects will likely favor more flexible solutions.

3 Overarching conclusions

The aim of this work has been to develop design methods that support the deployment of heat pump solutions in a transitioning industrial sector. To achieve this, the impact of both technical changes to the production process and the heat pump configuration as well as changes in energy prices and equipment cost on the techno-economic viability of an industrial heat pump have been studied. The main research question has been:

How to identify optimal techno-economic heat pump solutions for industrial processes in the context of the energy transition?

To answer this question, the following aspects have been considered: 1. the relation between heat pumps and other process changes, 2. the components that make up the heat pump configuration, and 3. the relation between a heat pump and alternative power-to-heat and energy storage technologies in the context of fluctuating energy prices.

The relation between the heat pump and other process changes needed to meet the CO_2 reduction goals is of the utmost importance as their deployment sequence determines the combined CO_2 reduction potential of the technologies. This is especially the case when heat integration measures such as heat pumps are considered. The deployment of a technology can result in the exclusion of other technologies, reduce the effectiveness of existing processes, or enable new opportunities for

to-be-installed technologies. When selecting CO_2 mitigation measures that are to be placed alongside an already installed heat pump, their impact on the pinch of the background process and its relation to the connections of the heat pump is vital. A combination of Process Change Analysis and a Split-Exergy Grand Composite Curve can assist in this process, as they not only visualize the relation between the pinch of the background process and the heat pump connections but also the heat pump's minimal work requirements.

The techno-economically optimal heat pump configuration balances the goal of achieving these minimal work requirements with the required investment. Exergy-based economic analysis should be used to identify which improvements to the configuration of a heat pump cycle are needed based on the cost of exergy destruction by a certain component. The exergy destruction depends on the heat pump's sink temperature and required temperature lift. As a result, the economically preferred heat pump configuration changes with them, as the optimal result is a trade-off between minimizing investment and operational cost. The latter strongly depends on the cycle configuration and becomes increasingly important with rising temperature lifts and temperature sinks. At higher temperatures and or lifts, investments in additional components become justified and more complex configurations are economically preferred. The figures, such as those provided on the cycle-level exergo-economic comparison in Chapter 5.3.1, can be used to identify interesting configurations for a specified source and sink temperature. The impact of, for example, changes in the electricity prices can be deduced from the exergy efficiency plots in Chapter 5.3.2. Together, they will assist in identifying the techno-economically optimal heat pump configuration.

The role of such a heat pump in an electrified utility system heavily depends on both energy prices and grid connection capacity. Both play a crucial role in determining the deployment and operation of heat pumps and other power-to-heat and storage technologies. High and stable electricity prices favor the installation of a heat pump as the predominant heat supply. However, high price variance and lower electricity prices make electric boilers and thermal energy storage more economically attractive due to their capacity to utilize low cost electricity prices and avoid power consumption during price peaks. The electricity-to-gas price ratio further influences the choice and sizing of technologies, with lower ratios promoting electrification. Low equipment cost prices have a similar effect. Dynamic optimization is needed to optimize the configuration of the electrified utility system over time, seeking the optimal sizing for changing energy prices whilst providing process heat demand.

In conclusion, the optimal techno-economic heat pump solutions are identified when 1. its interactions with other process changes are assessed with Process Change Analysis and the Split-Exergy Grand Composite Curve, 2. its configuration is improved according to the results of (advanced) exergo-economic analysis, and 3. its sizing is based on dynamic optimization of its contribution to an electrified utility systems alongside other power-to-heat and energy storage technologies under various energy and equipment price scenarios.

4 Recommendations for future research

The energy transition not only demands an increase in energy efficiency and a shift to low-carbon energy carriers, but also a time-dependent alignment between power generation, transportation capacity and end use. This alignment is a key aspect of the efficiency on a system-level. The results of the techno-economic optimization presented in Chapter 6 highlight this by showing that it is economically beneficial to add less efficient technologies with low-cost peak capacity. This is in contrast to the studies of chapters 2-5, where the most energy efficient technologies were preferred due to the assumption of constant energy prices. Future research should look into methods to integrate the valuable insights from pinch and exergy analysis with the needed time-dependent alignment.

Moreover, the literature reviews the role of integration cost in Chapters 4 and 5 and the study of the impact of equipment costs on the sizing of the heat pump in Chapter 6 indicate that highly integrated heat pumps, as in Chapters 2 and 3, come with a disadvantage when energy prices and heat demand are fluctuating. In addition to a lower installed cost and more constant operation, a less process-integrated heat pump would also allow for easier integration with thermal energy storage. This argument also further strengthens the case for steam-generating heat pumps and/or mechanical vapor recompression systems. Further research should look into economic and operational "tipping points" that indicate an appropriate heat pump process-integration level.

On top of that, future studies should look into the impact of part-load efficiencies. In the results of Chapter 6, the heat pump was operated at a load factor of more than 80%, and part-load performance was of limited interest. However, the electric boiler was in some scenario's only operated 10% of the time. A (very) low cost mechanical vapor recompression system may have a similar style of operation and part-load efficiency will be of interest in identifying the optimal sizing. Future studies should provide insights into how such mechanical vapor compression systems should be operated and how energy storage should be included to realize optimal techno-economic performance.

References

[1] C. M. Nwachukwu, C. Wang, and E. Wetterlund, "Exploring the role of forest biomass in abating fossil CO2 emissions in the iron and steel industry–The case of Sweden," Applied Energy, vol. 288, p. 116558, 2021.

[2] E. Yáñez, A. Ramírez, A. Uribe, E. Castillo, and A. Faaij, "Unravelling the potential of energy efficiency in the Colombian oil industry," Journal of Cleaner Production, vol. 176, pp. 604-628, 2018/03/01/ 2018, doi: https://doi.org/10.1016/j.jclepro.2017.12.085.

[3] D. Johansson, J. Rootzén, T. Berntsson, and F. Johnsson, "Assessment of strategies for CO2 abatement in the European petroleum refining industry," Energy, vol. 42, no. 1, pp. 375-386, 2012.

APPENDICES

Appendices

A.1 Considered technologies for each section of the production plant and their expected energy savings per section

Sections	Technology	Expected reduction in heating requirement	Expected overall reduction in heating requirements	Ref.
Reaction	Replace the current homogeneous base catalyst with a homogeneous sour catalyst.	(+) there is no production of soap which results in a slightly higher conversion rate (--) Requires higher methanol: oil ratio by a factor of 5, thereby increasing heating requirements (-) operational temperature increases from 58 °C to 110 °C, which is above the pinch and thus increases overall heat demand	--	[1-4]
	Replace the current homogeneous base catalyst with a heterogeneous catalyst basic.	(+) catalyst (solid) separation via filtration, reduces the amount of water required for washing (--) Increased methanol: oil ratio by a factor of 3, thereby increasing heating requirements	-	[5, 6]
	Replace the current homogeneous base catalyst with a heterogeneous catalyst sour.	(+) catalyst (solid) separation via filtration, this reduced the required amount of water for washing (--) Increased methanol: oil ratio by a factor of 3, thereby increasing heating requirements (-) the operational temperature increases to 110 °C, which is above the pinch and thus increases overall heat demand	--	[6, 7]
	Replace the ambient pressure CSTR with a supercritical reactor.	(+) pre-treatment can be omitted which reduces total heat consumption by 5%. (-) increases operation temperature (270-300 °C), which is above the pinch, and thus increases overall heat demand	0	[8]
	Replace the ambient pressure CSTR with a membrane reactor with methanol-recycling.	(+) higher conversion rate (about 3%), lower specific heat consumption (+) purer downstream products, therefore, requiring less separation (++) about 75% less methanol of the methanol-rich stream must be recovered as it can be recycled	++	[9, 10]

Separation	Replacing the sedimentation tanks with a membrane separation unit.	(0) Speed up separation, but as sedimentation has no heating requirement, there are no impacts on the heat balance	0	[11]
	Replacing the water washer with a membrane separation unit.	(+) Requires no water from water washing thereby avoiding drying requirements (expected reduction 100% reduction of local heating requirements, about 5% of total heating requirement)	+	[2, 12-16]
	Integrate the methanol recovery and the glycerol drying column in a single divided wall column.	(++) Integration of methanol and glycerol recovery reduces reboiler loads (expected reduction of 30% of local heating requirements, about 20% of total heating requirement)	++	[17-19]
Power	Switch the boiler feed from natural gas to low carbon fuels.	(--) increased heating requirements above the pinch for reforming and separation processes	--	[20, 21]
	Replace the gas fired boiler with an electric one.	(+) lack of primary energy being lost to flue gasses increases overall heat requirement by about 5%	+	[22]
	Recycle process gas from the anaerobe water cleaning to the gas fired boiler.	(+) reduced need for natural gas (1% of total heating requirements) (-) increased heating demand due to the need for scrubbing	0	[23]

References

[1] S. H. Y. S. Abdullah et al., "A review of biomass-derived heterogeneous catalyst for a sustainable biodiesel production," Renewable and Sustainable Energy Reviews, vol. 70, pp. 1040-1051, 2017.

[2] I. Atadashi, M. Aroua, and A. A. Aziz, "Biodiesel separation and purification: a review," Renewable Energy, vol. 36, no. 2, pp. 437-443, 2011.

[3] I. Atadashi, M. Aroua, A. A. Aziz, and N. Sulaiman, "The effects of catalysts in biodiesel production: A review," Journal of industrial and engineering chemistry, vol. 19, no. 1, pp. 14-26, 2013.

[4] P. P. Oh, H. L. N. Lau, J. Chen, M. F. Chong, and Y. M. Choo, "A review on conventional technologies and emerging process intensification (PI) methods for biodiesel production," Renewable and Sustainable Energy Reviews, vol. 16, no. 7, pp. 5131-5145, 2012.

[5] N. U. Soriano Jr, R. Venditti, and D. S. Argyropoulos, "Biodiesel synthesis via homogeneous Lewis acid-catalyzed transesterification," Fuel, vol. 88, no. 3, pp. 560-565, 2009.

[6] W. Roschat, T. Siritanon, B. Yoosuk, and V. Promarak, "Biodiesel production from palm oil using hydrated lime-derived CaO as a low-cost basic heterogeneous catalyst," Energy Conversion and Management, vol. 108, pp. 459-467, 2016.

[7] J. Gupta, M. Agarwal, and A. Dalai, "An overview on the recent advancements of sustainable heterogeneous catalysts and prominent continuous reactor for biodiesel production," Journal of Industrial and Engineering Chemistry, 2020.

[8] R. E. Gumba, S. Saallah, M. Misson, C. M. Ongkudon, and A. Anton, "Green biodiesel production: a review on feedstock, catalyst, monolithic reactor, and supercritical fluid technology," Biofuel Research Journal, vol. 3, no. 3, pp. 431-447, 2016.

[9] P. Cao, M. A. Dubé, and A. Y. Tremblay, "Methanol recycling in the production of biodiesel in a membrane reactor," Fuel, vol. 87, no. 6, pp. 825-833, 2008.

[10] M. Dubé, A. Tremblay, and J. Liu, "Biodiesel production using a membrane reactor," Bioresource technology, vol. 98, no. 3, pp. 639-647, 2007.

[11] J. Saleh, A. Y. Tremblay, and M. A. Dubé, "Glycerol removal from biodiesel using membrane separation technology," Fuel, vol. 89, no. 9, pp. 2260-2266, 2010.

[12] I. Atadashi, M. K. Aroua, A. A. Aziz, and N. Sulaiman, "Refining technologies for the purification of crude biodiesel," Applied energy, vol. 88, no. 12, pp. 4239-4251, 2011.

[13] H. Bateni, A. Saraeian, and C. Able, "A comprehensive review on biodiesel purification and upgrading," Biofuel Research Journal, vol. 4, no. 3, pp. 668-690, 2017.

[14] M. C. S. Gomes, N. C. Pereira, and S. T. D. de Barros, "Separation of biodiesel and glycerol using ceramic membranes," Journal of Membrane Science, vol. 352, no. 1-2, pp. 271-276, 2010.

[15] H. He, X. Guo, and S. Zhu, "Comparison of membrane extraction with traditional extraction methods for biodiesel production," Journal of the American Oil Chemists' Society, vol. 83, no. 5, pp. 457-460, 2006.

[16] M. L. Savaliya, B. D. Dhorajiya, and B. Z. Dholakiya, "Current trends in separation and purification of fatty acid methyl ester," Separation & Purification Reviews, vol. 44, no. 1, pp. 28-40, 2015.

[17] A. Kiss, J. Segovia-Hernández, C. Bildea, E. Miranda-Galindo, and S. Hernández, "Innovative biodiesel production in a reactive dividing-wall column," in Computer Aided Chemical Engineering, vol. 30: Elsevier, 2012, pp. 522-526.

[18] A. A. Kiss and C. S. Bildea, "A review of biodiesel production by integrated reactive separation technologies," Journal of Chemical Technology & Biotechnology, vol. 87, no. 7, pp. 861-879, 2012.

[19] A. A. Kiss and R. M. Ignat, "Enhanced methanol recovery and glycerol separation in biodiesel production–DWC makes it happen," Applied Energy, vol. 99, pp. 146-153, 2012.

[20] I. IEA, "Energy technology perspectives 2017," Catalysing Energy Technology Transformations, 2017.

[21] E. Rubin and H. De Coninck, "IPCC special report on carbon dioxide capture and storage," UK: Cambridge University Press. TNO (2004): Cost Curves for CO2 Storage, Part, vol. 2, p. 14, 2005.

[22] M. Marsidi, "Electric Industrial Boiler - Technology Factsheet (TNO)," 21-12-2018 2018.

[23] D. Klarenbeek, "Personal communications," 13-10-2020 2020.

A.2 Energy price and technology cost scenarios

To study the impact of changes in the energy and technology cost on the results of the model sixteen scenarios were formulated. Figures A.2.1 to A.2.4 show the energy price profiles in these scenarios, presented in 2.3.1. Figure A.11 depicts the energy prices in the LMLV scenario. It clearly shows the difference in volatility between the electricity prices (EP) and the gas prices (GP). Moreover, it shows how the two gas prices differ in the EGR scenarios, with the 'EGR 1' being the scenario with the highest average price. The ratio between the GP in EGR 1 and the GP in EGR 1.6 is the same in Figures A.2.2 to A.2.4. Figure A.2.5 shows how the different energy price scenarios are combined with the technology cost scenarios.

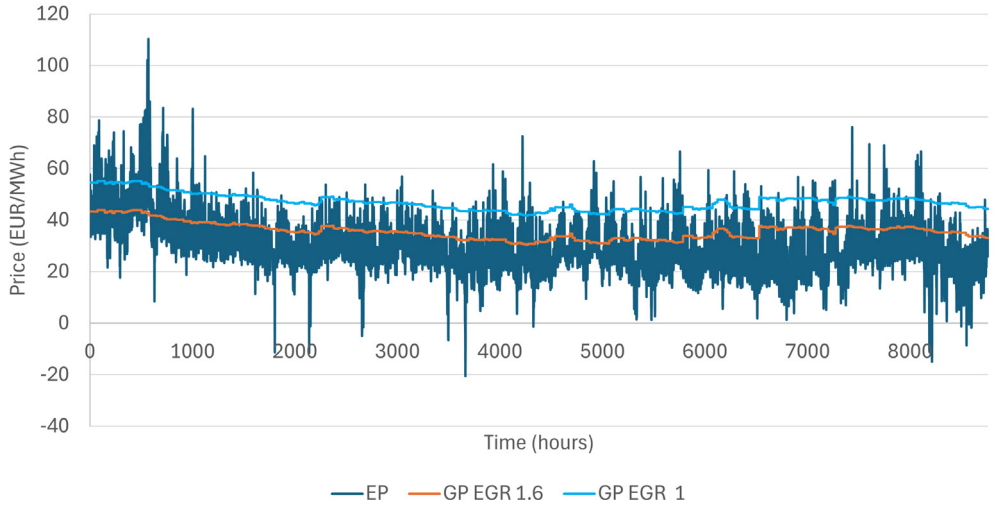

Figure A.2.1: *The electricity (EP) and gas (GP) prices for the electricity-to-gas ratio (EGR) of 1.6 and 1 for the 'Low Mean Low Variance' scenario*

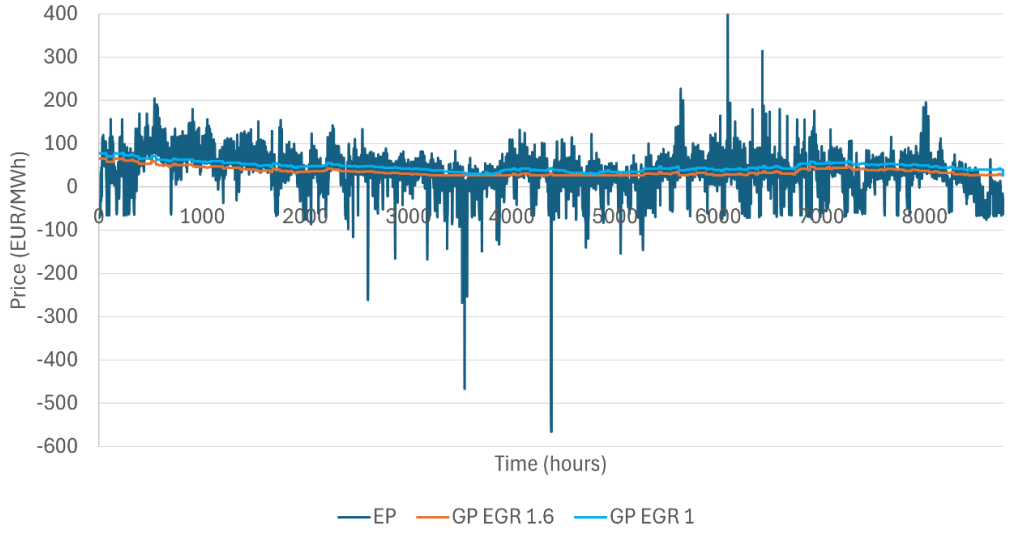

Figure A.2.2: *The electricity (EP) and gas (GP) prices for the electricity-to-gas ratio (EGR) of 1.6 and 1 for the 'Low Mean High Variance' scenario*

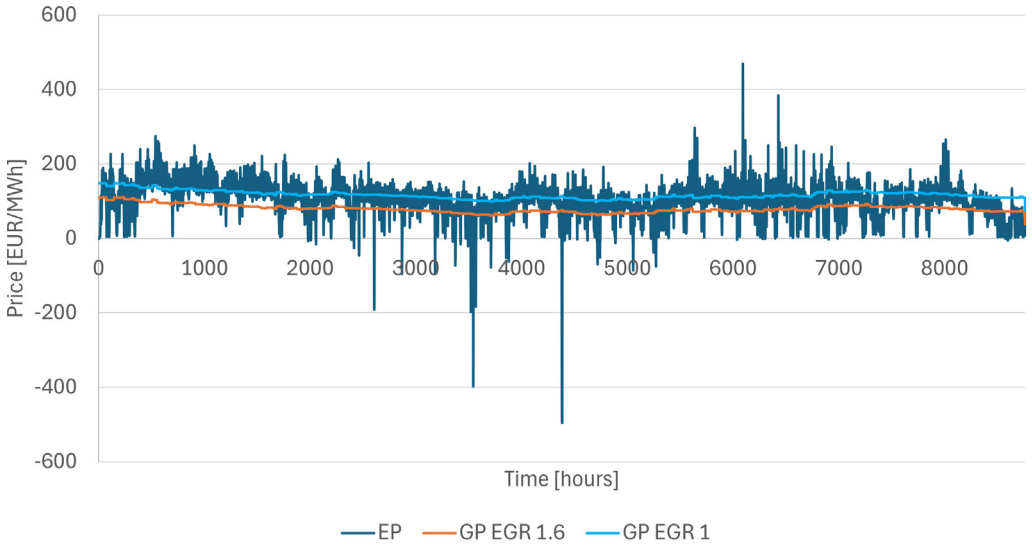

Figure A.2.3: *The electricity (EP) and gas (GP) prices for the electricity-to-gas ratio (EGR) of 1.6 and 1 for the 'High Mean High Variance' scenario*

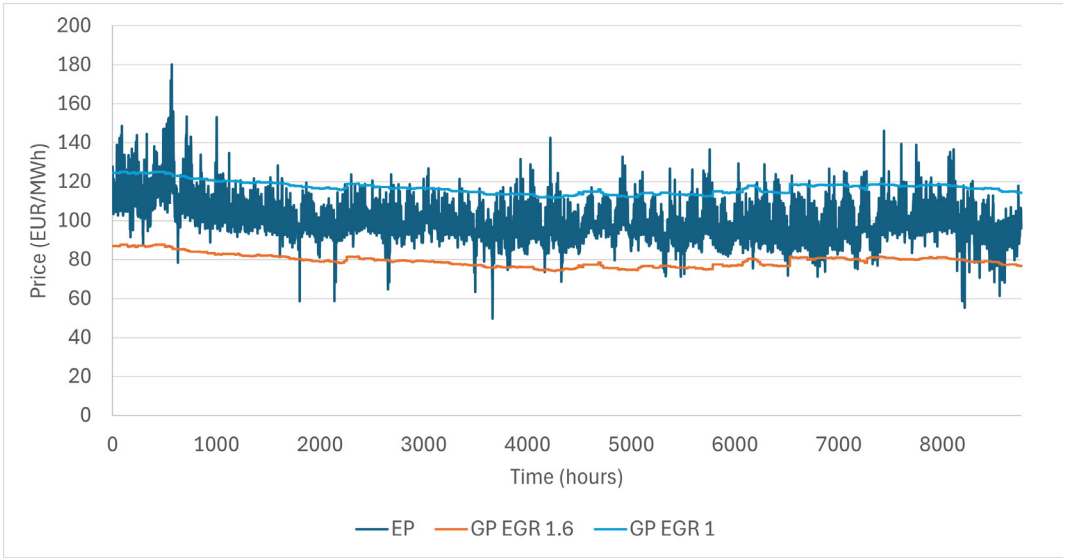

Figure A.2.4: *The electricity (EP) and gas (GP) prices for the electricity-to-gas ratio (EGR) of 1.6 and 1 for the 'High Mean Low Variance' scenario*

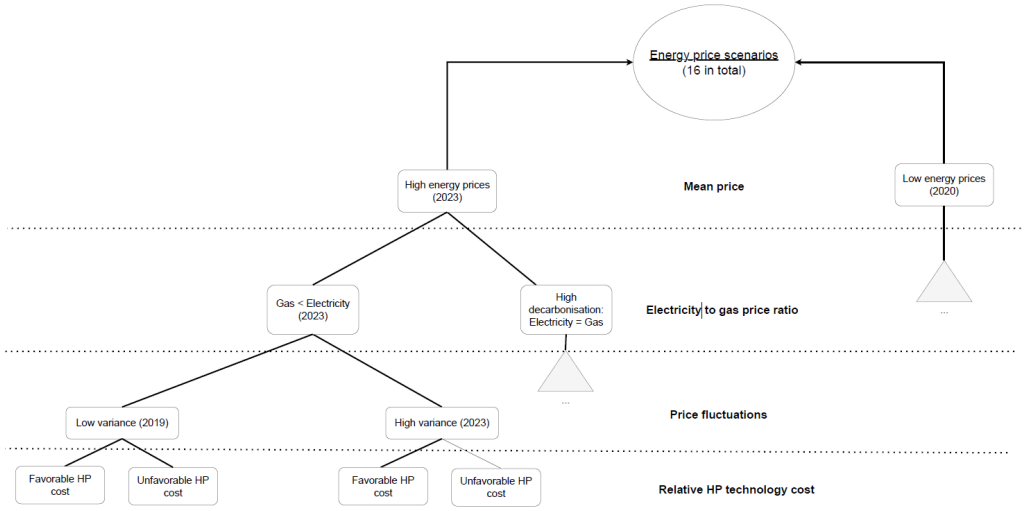

Figure A.2.5: *Scenario tree considering the mean energy price, the electricity-to-gas price ratio, the energy price fluctuations and the technology cost*

A.3 Results without the minimal load constraint of the CHP

Tables B.14, B.15, B.16 and B.17 show the technology portfolio of the cost- optimal utility system if the CHP operation is not constrained and can shut down completely. Omitting this constraint and accepting it, though not accounting for the increase in maintenance cost, results in the following changes to the sizing and operation of the PtH technologies. For low and stable electricity prices more PtH technologies are installed. The size of the HP increases with the previous minimal capacity of the CHP. The combined capacity of TES and ElB increase by a factor of 2. When price fluctuations increase, the change in capacities is limited as the size of ElB and the TES were already limited by the grid connection capacity of the system. Nevertheless, less natural gas is consumed overall. When the mean energy price increases, the size of the ElB reduces, the capacity of the TES remains the same, and the size of the HP increases compared to the scenario with the CHP constraint. Reducing price fluctuations whilst maintaining the high mean energy price results in the same increase in HP capacity, whilst the capacities of the TES and ElB remain relatively unchanged. Though the total natural gas consumption is reduced in all scenarios when the CHP is allowed to shut down completely, complete electrification is only cost-optimal in the scenario with high mean prices, low price fluctuations and a low electricity-to-gas-price ratio.

Table B.14 Installed PtH and storage capacities in the energy price scenarios with low mean and variance

EGR	TC cost scenario	ElB [MW_{th}]	TES [MWh]	HP [MW_{th}]
1.6	HighHP-LowRest	24	42	0
	LowHP-HighRest	6	5	11
1	HighHP-LowRest	25	49	0
	LowHP-HighRest	6	6	12

Table B.15 Installed PtH and storage capacities in the energy price scenarios with low mean and high variance

EGR	TC cost scenario	ElB [MW_{th}]	TES [MWh]	HP [MW_{th}]
1.6	HighHP-LowRest	29	103	0
	LowHP-HighRest	28	62	0
1	HighHP-LowRest	29	113	0
	LowHP-HighRest	28	68	0

Table B.16 *Installed PtH and storage capacities in the energy price scenarios with high mean and high variance*

EGR	TC cost scenario	ElB [MW_{th}]	TES [MWh]	HP [MW_{th}]
1.6	HighHP-LowRest	24	94	8
	LowHP-HighRest	7	15	14
1	HighHP-LowRest	22	96	13
	LowHP-HighRest	6	18	15

Table B.17 *Installed PtH and storage capacities in the energy price scenarios with high mean and low variance*

EGR	TC cost scenario	ElB [MW_{th}]	TES [MWh]	HP [MW_{th}]
1.6	HighHP-LowRest	0	19	14
	LowHP-HighRest	0	6	15
1	HighHP-LowRest	2	22	14
	LowHP-HighRest	2	6	16

Table C.18 *Installed PtH and storage capacities in the energy price scenarios with low mean and high variance*

EGR	TC cost scenario	ElB [MW_{th}]	TES [MWh]	HP [MW_{th}]
1.6	HighHP-LowRest	29	103	0
	LowHP-HighRest	28	62	0
1	HighHP-LowRest	29	113	0
	LowHP-HighRest	28	68	0

Table C.19 Installed PtH and storage capacities in the energy price scenarios with high mean and high variance

EGR	TC cost scenario	ElB [MW_{th}]	TES [MWh]	HP [MW_{th}]
1.6	HighHP-LowRest	24	94	8
	LowHP-HighRest	7	15	14
1	HighHP-LowRest	22	96	13
	LowHP-HighRest	6	18	15

Table C.20 Installed PtH and storage capacities in the energy price scenarios with high mean and low variance

EGR	TC cost scenario	ElB [MW_{th}]	TES [MWh]	HP [MW_{th}]
1.6	HighHP-LowRest	0	19	14
	LowHP-HighRest	0	6	15
1	HighHP-LowRest	2	22	14
	LowHP-HighRest	2	6	16

Curriculum Vitae

Brendon de Raad was born on December 21, 1990, in Rotterdam. In 2008, he completed his senior general secondary education and began his Bachelor's degree in Mechanical Engineering at the Rotterdam University of Applied Sciences. After graduating in 2012 with a focus on waste heat recovery using organic Rankine cycles, he joined the university's thermodynamics department as a lecturer.

In 2014, Brendon pursued a Master's degree in Sustainable Energy Technology at Delft University of Technology, specializing in "Energy and Industry". He graduated in 2017 with a thesis on the stochastic optimization of integrated climate assessment models. In 2015, he also received his basic qualification in teaching skills from the University of Amsterdam.

Following his graduation from TU Delft, he continued his work at the thermodynamics department at the Rotterdam University of Applied Sciences and joined their research institute for Sustainable Port Cities as a researcher in power-to-heat systems. In 2019, Brendon received an internal scholarship to start a Ph.D. research project on methods to assist in the deployment of heat pumps in the industrial sector. In 2020, he was appointed head of the thermodynamics department. For his contributions to industrial practice, he was awarded the Blue Sky Pro Young Professionals award by the Confederation of European Paper Industries in 2023 and the Global Blue Sky Young Professional Innovation award in 2025 by the International Council of Forest and Paper Associations.

Acknowledgements

The goal of my project has been to develop practical engineering tools to foster the implementation of heat pumps. My love for practice-oriented research stems from a childhood in a family where the TÜV dictated the law and the German Master-apprentice structure of learning in practice was seen as the ultimate form of education. A strive for the German "Grundlichkeit". However, despite not being born in Germany and being much of a traveler, I did have the opportunity to learn under various Masters of the Arts.

The first master I encountered was Emile Jackson, who introduced me to the field of thermodynamics. His lessons changed me from a so-called straight-six student with the attitude of minimizing time within academia (the plan was to leave academia after two years), to someone who started dreaming of an academic career and obtaining a master's degree. However, this plan was somewhat delayed by my inability to put myself into topics that did not resonate with me at that age. Sorry, Tijmen and Leo for failing your classes. Not being able to switch universities after my first year resulted in a greater appreciation for applied engineering/research, as I got to experience it for another three years. Years, in which my second master, Andrea Blankenstein, awakened my love for modeling and gave me the confidence to take the "big" step to Delft.

During my time at Delft, I always kept a strong foot in Rotterdam, as a research-driven thermodynamics teacher specializing in waste heat recovery technologies. An interest, that my next master, Marit van Lieshout, allowed me to follow in my next endeavor, my Ph.D. project. I vividly recall our first sessions together with Sowande Boksteen at the library where we researched possible research angles and tried to find our role as an applied research group. Your suggestions, thinking and bridging academia with industry have had a profound impact on my life. Just as your ways of sharpening ideas and methods, confidence and art of negotiation. No matter what life threw at us (e.g. being closed doors from industry, a pandemic, personal troubles) you were always there and made me feel at home. I am truly grateful for helping me to realize my Ph.D.-dream and will forever be indebted.

My collaboration with Marit led me to the Department of Engineering Systems and Services at the Technology, Policy, and Management faculty. Specifically, the Low Carbon Systems and Technologies group led by Andrea Ramírez Ramírez. A second master! With Andrea, I found a place where I could work on the questions that I had in mind and bridge practice with theory. Working with you has been a real joy and honor. I often speak proudly about your global contributions and achievements and I find it very admirable how you always try to make time for the person behind the email/table/project, despite your infeasible agenda. My favorite characteristic of your supervision style is that the true meaning behind your suggestions may take months to truly resonate and that you allow a student to take that time. I truly am happy that you were willing to supervise me in this journey.

At the end of one of my exploratory conversations with Andrea, I mentioned the concept of "Exergy". Andrea's eyes drifted a bit and she asked me to follow her. A little stroll brought me to the door of my third master in the last years, Lydia Stougie. Lydia really helped me to get my ideas and arguments across. This included rigorous feedback on my writing (she asked me to save all the feedback so she could staple it together at the end, though I do not think you could staple a tree). As a (Ph.D) student, you of course always fear feedback to some extent. But, especially when Lydia mentioned her proverbial "comb", my eyes widened a bit. However, I am forever grateful for this journey. Speaking of journeys, I would also like to thank you for introducing me to the ECOS-network and accompanying me to Copenhagen, Las Palmas and Paris. These were truly formative events.

Furthermore, I would like to thank the "Best Boss group" and the faculty of Technology Policy and Management. From leaving post-its on my monitor with kinds greetings to elaborate lunch discussions, I enjoyed it all. You are all very special and it was amazing to be part of a team that will truly enable change. I would like to specifically mention Svenja, who endured to be my research partner for the last two years. I don't know how many hours we worked together, but my sons daily question is: "Will you call with Svenja today?". I could not have done this work without you. Thanks for being so open and being a mirror to my own process towards an independent researcher.

Lastly, I would like to thank all those who have been supporting me throughout this journey. From the MT who believed in me, my colleagues who had to deal with me being absent all the time and being flooded with weird ideas and philosophical questions, my students who had to endure weird new concepts that I came across, and friends & family who had to deal with me being even more absent minded than before. Rein and Veer, I'm sorry. I think I can now be normal again.